NTNU – Trondheim
Norwegian University of
Science and Technology

Analysis of Compact Separation Systems and Experimental Study of Centrifugal Separation in Helically Coiled Pipes

Sverre Andre Engvik
Jonas Vidnes

Subsea Technology
Submission date: June 2015
Supervisor: Olav Egeland, IPK
Co-supervisor: Sigbjørn Sangesland, IPT
Tor Berge Gjersvik, IPT

Norwegian University of Science and Technology
Department of Production and Quality Engineering

NTNU – Trondheim
Norwegian University of
Science and Technology

Analysis of Compact Separation Systems and Experimental Study of Centrifugal Separation in Helically Coiled Pipes

Jonas Vidnes and Sverre A. Engvik

June 2015

MASTER THESIS

Master of Science in Subsea Technology

Department of Production and Quality Engineering

Norwegian University of Science and Technology

Supervisor 1: Professor Sigbjørn Sangesland

Supervisor 2: Professor Tor Berge Gjersvik

Preface

This thesis concludes our 2-year Master's Degree Programme in Subsea Technology at NTNU's Department of Production and Quality Engineering. This project was conducted during the spring semester of 2015, in cooperation with the Department of Petroleum Engineering and Applied Geophysics, which provided supervisors and facilities.

The project concerns compact separation systems related to hydrocarbon production. Our supervisors, Professor Sigbjørn Sangesland, and Professor Tor Berge Gjersvik, gave the idea of this project.

Trondheim, 2015-06-12

Jonas Vidnes

Sverre A. Engvik

Acknowledgement

We would like to thank the following persons from the Department of Petroleum Engineering and Applied Geophysics for their great contributions during the work with this project.

For providing equipment and helping with assembly of the experimental setup of this project, we are grateful to both Håkon Myhren and Åge Sivertsen.

For guidance and help with challenges related to the analysis, we are grateful to Milan Edvard Wolf Stanko.

For providing the idea of this project, along with motivational and constructive feedback during the entire semester, we are grateful to both our supervisors, Professor Sigbjørn Sangesland and Professor Tor Berge Gjersvik.

J.V. and S.A.E.

Summary

The offshore petroleum industry is experiencing challenges as exploration and production are forced towards remote and deeper reservoirs, combined with high cost-efficiency demands. Topside facilities struggle with limited space, and use of subsea processing equipment is increasing. Here, separation systems play an important role and has potential for improvement. Cyclonic separators are often referred to in association with compact separation systems. However, other types of separators have the potential of achieving compact designs.

In order to meet rising challenges in the industry, this project involves an analytical- and experimental study, seeking alternative or improved compact separation solutions. To define the state of existing technology, the analysis involved studies of fluid dynamic theory, gravitational and centrifugal separation principles, and "state-of-the-art" separators and concepts. The objective with the experimental study was to investigate separation capabilities for a less common centrifugal principle, using helically coiled pipes.

The results of the analytical study implied that most compact systems utilise the centrifugal principle. Factors promoting the helical coil principle were defined. This included a simple pipe structure, excellent pressure-containment abilities, and previous helical coil experiments showed promising phase distributions. However, achieving stable phase distributions to allow separation seemed sensitive to variations in flow rate and coiled pipe geometry.

The experimental study featured an air-water flow in a helically coiled pipe. The flow in the coiled pipe was photographed for a range of air and water flow rates, different numbers of loops, and different curvature radii. Images indicated that above certain air flow rates, the coiled pipe caused transition from stable to unstable phase distribution. Unstable phase distributions were typically recognised as plug or slug flow. The effect of having more than one loop in the coil reduced the air flow rate at which unstable flow developed. The effect of shortening the curvature radii increased the air flow rate that caused unstable flow. In other words, the helical coil achieved best results for short curvature length, either by minimising the number of loops or reducing the curvature radius. These measures indirectly caused a higher flow rate, because shorter curvature length reduces the frictional pressure loss. In addition, shorter curvature radius and higher flow rate increase the centrifugal effects.

A different observation was that despite maintaining a favourable phase distribution throughout the coiled pipe, an instant transition to unstable flow could occur at coil outlet. This indicated that the stable distribution may not sustain downstream of the coil. The level of similitude between the experimental flow and a hypothetical full-scale gas-liquid flow was analysed. The analysis indicated that the experiment could suffer from scale-effects, because viscous- and surface tension forces become significant at small scales.

The experimental study gave indications on separation capabilities, as achievement of stable phase distribution was possible for certain coil configurations and flow rates. However, the narrow operating range, and possible errors in the experiment, brought uncertainties to whether a full-scale helical coil could achieve phase separation. Hence the results in this thesis could neither prove nor disprove the helical coil as a phase separator. More comprehensive research is required to determine the separation capabilities. Recommendations for further work include larger experimental dimensions to reduce scale-effects, and using fluids that improve similarities to hydrocarbon flows.

Sammendrag

Petroleumsindustrien står overfor nye utfordringer når leting og produksjon rettes mot fjerntliggende og dypere reservoarer, kombinert med strenge kostnadseffektiviseringskrav. Plattformer sliter med begrenset plass, samtidig som bruk av subsea prosesseringsutstyr øker. Separasjonssystemer spiller en viktig rolle i prosesseringen og har potensiale for forbedringer. Syklonseparatorer blir ofte nevnt i forbindelse med kompakte separasjonssystemer, men andre separatortyper kan ha potensiale for å oppnå kompakte design.

For å møte de økende utfordringene i bransjen, involverer dette prosjektet en analytisk- og et eksperimentelt studie med mål om å finne alternative eller forbedrede kompakte separasjonsløsninger. For å definere hvor langt utviklingen av eksisterende teknologi var kommet, ble det utført studier på fluiddynamikk, gravitasjonsseparasjon og sentrifugalseparasjon, og "state-of-the-art" separatorer og konsepter. Målet med det eksperimentelle studiet var å undersøke hvorvidt strømning i spiralformede rør hadde egenskaper egnet for separasjonsformål.

Den analytiske delen av prosjektet gjorde det forstått at de fleste eksisterende kompakte separasjonssystemer benytter sentrifugalprinsippet. Videre ble det definert faktorer som fremmet bruk av spiralformede rør som separatorer. Deriblant enkel rørkonstruksjon, evner til å tåle høye trykkforskjeller, og at tidligere studier hadde oppnådd lovende fasefordeling i spiralformede rør. Men det ble understreket at gunstig fasefordeling kun var mulig innenfor små variasjoner av strømningshastigheter og for visse spiralgeometrier.

Det eksperimentelle forsøket gikk ut på å føre en vann-luftstrømning i et spiralformet rør. Strømningen i røret ble fotografert for varierte luft- og vannstrømningshastigheter, forskjellig antall spiraler, og forskjellige krumningsradier. Bildene viste at for luftstrømning over et visst nivå kunne spiralen forårsake overgang fra stabil til ustabil fasefordeling. Ustabil fasefordeling ble gjenkjent som vekslende luftlommer og vannplugger. Effekten av å øke antall spiraler var at ustabilitet oppstod ved lave luftstrømningshastigheter. Effekten av å redusere krumningsradien gjorde at det krevdes høyere luftstrømningshastigheter for at ustabile strømningsmønstre skulle oppstå. Dermed ble best fasefordeling oppnådd for korte spiralrør, enten ved å minimere antall spiraler eller ved å redusere krumningsradien. En bieffekt av konfigurasjonen med kort spirallengde var høyere total strømningshastighet, fordi kortere spirallengde gir lavere

friksjonstrykktap. I tillegg gir kortere krumningsradius og høyere strømningshastighet større sentrifugalkrefter.

Det ble også observert at stabile strømningsmønstre som ble opprettholdt gjennom hele spiralen, likevel kunne forandres til ustabile mønstre umiddelbart etter spiralen. Dette indikerte at stabil strømning i spiralen ikke nødvendigvis vedvarer nedstrøms. Til slutt ble det analysert i hvor stor grad den eksperimentelle luft-vannstrømningen kunne forestille en hypotetisk fullskala gass-væskestrømning. Resultatene antydet at eksperimentets kvalitet kunne lide av skaleringseffekter, hovedsakelig på grunn av at viskøse krefter og overflatespenninger blir betydelige i små rør.

Det eksperimentelle studiet gav indikasjoner på om spiralformede rør hadde egnede egenskaper. Oppnåelse av stabil fasefordeling var mulig for bestemte spiralkonfigurasjoner og strømningshastigheter. Men det smale suksessområdet, og mulig innvirkning av skaleringseffekter, bringer tvil om hvorvidt en fullskala spiral kan oppnå ønsket fasefordeling. Dermed kan dette prosjektet verken bevise eller motbevise potensialet for det spiralformede røret som en faseseparator. Det kreves mer omfattende forskning for å avgjøre spiralprinsippets egenskaper. Ut fra dette prosjektets erfaringer anbefales det å gjennomføre eksperimenter med større dimensjoner for å redusere innvirkning av skaleringseffekter. I tillegg kan andre fluider utnyttes for å forbedre strømningens sammenliknbarhet til fullskala gass-væskestrømninger.

Nomenclature

Symbol	*Description*	*Unit*
a	Centrifugal acceleration	m/s^2
A	Cross-sectional area	m^2
d	Pipe inner diameter	m
De	Dean number	–
Fr	Froude number	–
g	Gravitational acceleration (9.81 m/s^2)	m/s^2
p	Pressure	$bara$
q_l	Liquid flow rate [litres per minute]	l/min
q_g	Gas flow rate [litres per minute]	l/min
q_{tot}	Total flow rate [litres per minute]	l/min
r	Radius	m
Re	Reynolds number	–
R	Curvature radius	cm
T	Temperature	°C
U	Terminal velocity	m/s
v	Velocity	m/s
$\overline{v}$	Average flow velocity	m/s
v_{sl}	Liquid superficial velocity	m/s
v_{sg}	Gas superficial velocity	m/s
x	Particle diameter	m

Greek symbol	*Description*	*Unit*
α	Void fraction	–
δ	Curvature ratio	–
κ	Dean number (other defintion)	–
λ	Linear scale ratio	–
μ	Viscosity	cP
ρ	Density	kg/m^3
ρ_s	Density of soild(s)	kg/m^3
ω	Angular velocity	$1/s$

Table of Contents

List of Figures

List of Tables

Chapter 1

Introduction

1.1 Background

Challenges arise when separators are utilised in the petroleum industry. Offshore topside facilities struggle with limited space, subsea developments encounter difficulties when reaching ultra deep depths, and marginal fields require cost-efficient solutions. Conventional gravity settling separators are of inconvenient size, heavy weight, and high cost. These factors make them unattractive for developments with limited space, high ambient pressure, and low total revenue.

The need for compact separation systems is present. Several compact separation systems have been developed, where the majority utilise high centrifugal forces to separate fluids, so-called cyclonic separators. The cyclone principle is proven in the field for a variety of applications, although there is potential for improvement.

Possible benefits with subsea separation systems are increased total recoverable reserves, enhanced flow assurance, and being one step closer to elimination of surface host facilities. However, issues like ambient pressure, maintenance, and extensive intervention have to be addressed. This is where compact separation technologies have their advantages, featuring simple, small-sized, pressure-robust structures, which may require less maintenance and ensure simple intervention.

A less common solution for separation purposes is the helical coil principle. Helically coiled pipes can apply high centrifugal forces to flowing fluids. The question is whether the helical coil can achieve phase separation, similar to the cyclone separators. Research on the princi-

ple exists, and results indicate that it has potential, yet no commercial products utilise helical coils for separation. The indications from existing research, and possible benefits as a compact separator, form the background for including helically coiled pipes in this project.

Problem Formulation

In order to contribute to the development of compact separation systems, the project group should investigate "state-of-the-art" systems. This includes existing technologies, patents, and developing solutions. To enhance the analysis of found systems, basic physics of fluid behaviour and separation principles should be addressed. A small number of studies examine the principle of utilising helical coils for separation purposes. It is desired to assess the state of the helical coil principle, especially related to its potential as a compact separation system. In addition to the analysis, an experimental study on small-scale helical coils can be conducted. The experimental study may reveal additional indications of whether helical coils are able to achieve phase separation.

1.2 Objectives

The main objectives of this Master thesis are

1. Analyse existing compact separation systems
2. Evaluate the motivation and potential for helical coils as separation systems
3. Perform an experimental study of gas-liquid separation capabilities for helically coiled pipes
4. Evaluate similarities between the experiment and genuine full-scale hydrocarbon flows

1.3 Limitations

The research on separation systems in this thesis is limited to gravitational and centrifugal separation principles.

This being a one-semester project, requires a certain level of simplicity to the experimental study. The experiments are therefore limited to air-water two-phase flow. The study is limited to observation of phase distribution in the pipes, supported by flow measurements. Solutions for extracting one of the phases from the coil are discussed, but were not a part of the experimental study.

1.4 Structure of the Report

The structure of the report after the Introduction is as following.

- Chapter 2 presents theory related to basic fluid dynamics and is meant to support the understanding of fluid flow discussions in the following chapters
- Chapter 3 concerns separation principles, the gravity settling principle and the centrifugal separation principle. State-of-the-art separation systems are presented, along with relevant helical coil flow and separation research. Assessment on the helical coil principle as a compact separator is conducted
- Chapter 4 presents the experimental study on the helical coil principle. This includes the motivation for the research, description of the experimental setup, how the results were obtained, and presentation and discussion of the results
- Chapter 5 presents a study on the level of similitude between the experiments and genuine full-scale scenarios. The study includes similarity requirements, as superficial velocity, geometric-, kinematic-, and dynamic similarity
- Chapter 6 includes the main conclusions of the project and recommendations for further work

Chapter 2

Basic Definitions in Fluid Dynamics

This chapter presents theory related to basic fluid dynamics. The sections in this chapter are meant to help understand concepts within fluid flow problems, and highlight phenomena's that are discussed in other chapters in this thesis.

2.1 Compressible and Incompressible Flow

Liquids are often considered as incompressible fluids, where it cannot be much variation in volume (and density) on variation of pressure and temperature. Gas and vapours are often considered as compressible fluids, showing changes in volume (and density) on variation of pressure and temperature.

Classification on whether a fluid is compressible or incompressible cannot only be taken on the type of fluid. It should be taken on what type of process the fluid is undergoing, as liquids in reality act as compressible fluids for high pressure and temperature variations (Balachandran, 2006).

In chapter 4 regarding the experimental study, neither air nor water is assumed to undergo significant variations in pressure and temperature. However, in chapter 5 regarding similarities between experimental and full-scale hydrocarbon flows, both the gas and liquid phase in a hypothetical hydrocarbon flow are considered compressible.

2.2 Laminar and Turbulent Flow

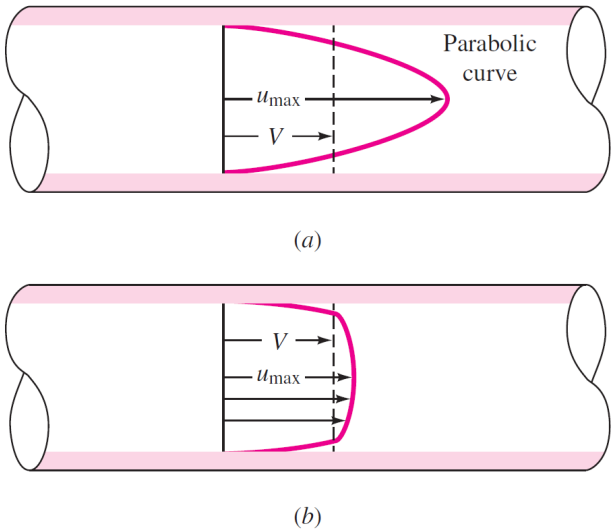

Figure 2.1: Laminar (a) and turbulent (b) flow velocity profiles, where V is the mean flow velocity, and u_{max} is the maximum flow velocity (White, 2011).

Laminar flow is often characterised by low flow velocities. The flow produces streamlines that run parallel to the axis of the tube, and the fluid particles mainly moves in the axial direction of the flow. Figure 2.1 illustrates a typical laminar velocity profile for no-slip conditions, i.e. flow velocity is zero at the pipe wall. The no-slip condition is a requirement that is based on the fact that *"All liquids essentially are in equilibrium with the surfaces they contact"* (White, 2011). This means that the fluid particles being in contact with the pipe wall, try to achieve momentum and energy equilibrium with the surface. Hence the velocity of the fluid is equal to the velocity of the pipe surface, which is zero.

Turbulent flow is often characterised by higher flow velocities. The streamlines observed for laminar flow become increasingly unstable, and fluctuate from the axial flow direction. At some point the fluctuations occur continuously, indicating that *fully turbulent* flow is achieved (White, 2011). Figure 2.1 shows a typical turbulent velocity profile, where the mean flow velocity is close to the maximum velocity.

The shift from laminar to fully turbulent flow is called *transitional* flow. In the transitional flow there is a period with unpredictable fluctuations back and forth between laminar and tur-

bulent flow.

Most practical cases, including the experiments in chapter 4 and actual hydrocarbon production, are characterised by turbulent flow. A result of turbulent flow is a high level of mixing within the fluid (Zamir and Zamir, 2000), which could be a disturbing factor for separation quality in multiphase flows. Whether a flow is laminar or turbulent is commonly determined by the value of the *Reynolds number*, which is explained in the next section.

2.3 Developing and Fully Developed Flow

"The flow is fully developed when it no longer varies with axial position". (Berger et al., 1983)

The concept of developing and fully developed flow can partly be explained by the illustration in Figure 2.1. For a fully developed flow, either laminar or turbulent, the velocity profile of the flowing fluid is independent on the axial position in the pipe. Hence, the velocity profile does not change over time. This imply a constant velocity profile, a constant wall shear, and a linear pressure drop along the axial position (White, 2011).

For a developing flow, the velocity profile, wall shear, and pressure drop, are all changing along the axial position of the flow. The term developing length, or entrance length, describes the required axial length a developing flow must travel until it becomes a fully developed flow.

The explanation above regards single-phase flows, and the effect of multiphase flows on developing lengths are not elaborated in this thesis. However, in chapter 4, the flows that are observed upstream, inside, and downstream of the helical coil are assumed to be developing flows. This is because of non-constant orientation of the pipe upstream the coiled section, and the relatively short axial length from the commingling point of air and water to the coiled pipe section.

2.4 Reynolds Number

Osborne Reynolds research on the flow characteristics in the 19th century gave the discovery that turbulent flow not only depends on the average flow velocity $\overline{v}$, through a tube. Properties like density ρ, viscosity μ, and tube diameter d, plays an equal role in determining the flow

characteristics. The onset of turbulent flow does not depend on one of the properties individually, but the non-dimensional combination of them, the so-called Reynolds number as shown in Equation (2.1).

$$Re = \frac{\rho \bar{v} d}{\mu} \tag{2.1}$$

White (2011) defines the *"qualitative ratio of effects"* of the Reynolds number as the ratio of inertial forces to viscous forces, acting in the flowing fluid. The higher Reynolds number, the more dominant are the inertial forces compared to the viscous forces. Zamir and Zamir (2000) states that Reynolds numbers below a value of 2000 characterises a laminar flow, and that the transition to turbulent flow may vary upon factors as pipe roughness and pipe entrance disturbances on the flow. White (2011) provides some approximate ranges of Reynolds number and flow types, though stating that they may vary dependent on flow geometry, surface roughness, and inlet (entrance) fluctuations. Values below 3000 are generally laminar, but flow in circular pipes has an accepted limit of about 2300. Above these values and up to 4000 are transitional flows, while values above 4000 is considered as turbulent flows.

In this thesis, the Reynolds number is used mainly for characterising, and ensuring, the level of turbulent flow achieved in the experiments. In addition, the Reynolds number acts as an important parameter in the similarity analysis in chapter 5.

2.5 Dynamic Viscosity

Viscosity is an essential fluid property when analysing fluid flow in a pipe, and is generally a measure of the fluids resistance to flow. The term viscosity is, in most cases, more specifically referring to the *dynamic viscosity* of a fluid, not to be confused with the *kinematic viscosity*.

Vogel (1996) explains the property dynamic viscosity by looking at the fluid as *"a large stack of very thin sheets of paper"*, where relative movement between the sheets are the same as fluid shear rate. Then the dynamic viscosity acts as a parameter describing the resistance of which the sheets move relative to each other, or as a friction factor between the sheets. The higher dynamic viscosity, the larger force is required to obtain relative movement at a certain velocity between the sheets. Dynamic viscosity has the symbol μ, and the units cP (centi-Poise) or $mPa \cdot s$.

Kinematic viscosity, ν, is the ratio between dynamic similarity and density, and its practical significance is not elaborated in this thesis.

Temperature has strong effects on viscosity of liquids and gases. Increased temperature for air increases its dynamic viscosity. Unlike air, increased temperature for water decrease its dynamic viscosity (Vogel, 1996).

The importance of viscosity in this project is mainly related to chapter 5. Here, similarities between experimental air-water flow and full-scale gas-liquid flows at both standard and non-standard temperatures and pressures, are addressed. Additionally, in a separation scenario where one of the phases has high viscosity, the other phase would require long residence time to allow separation. This is due to the large flow resistance for droplets/bubbles to settle/rise in the more viscous phase.

2.6 Velocity and Superficial Velocity

Assuming no-slip conditions at the fluid boundaries, the velocity of a single-phase fluid in a pipe varies from zero at the pipe wall, to maximum at the centre of the pipe. Due to this phenomenon, it is convenient to work with an average flow velocity. The average velocity equals the total volumetric flow rate divided by the cross-sectional pipe area. This average velocity is constant for an incompressible fluid flowing along a pipe with constant cross-sectional area (Massey and Ward-Smith, 1998).

In order to describe the velocity of a multiphase flow, the term *superficial velocity* is introduced. The superficial velocity is the velocity that each phase would have if it were the only fluid flowing in the pipe. The superficial velocities are related to the average total flow rate of the current phase, and are calculated as shown in Equation (2.2) and (2.3). However, it does not describe the actual velocity at which the phase moves inside the pipe. This is because the actual flow velocities of each phase in a multiphase flow are largely dependent on the distribution of the phases, i.e. flow regime. If gas bubbles are dispersed in a liquid dominated flow, forming a bubbly flow, then the gas bubbles follow the liquid and have the same actual velocity. Still, the gas superficial velocity is much lower than for the liquid (Palmer and King, 2008).

$$v_{sl} = \frac{q_l}{A} \tag{2.2}$$

$$v_{sg} = \frac{q_g}{A} \tag{2.3}$$

In chapter 5, superficial velocities are used to calculate full-scale gas-liquid volumetric flows, with equal superficial velocities as air and water in the experiment.

2.7 Flow Regimes

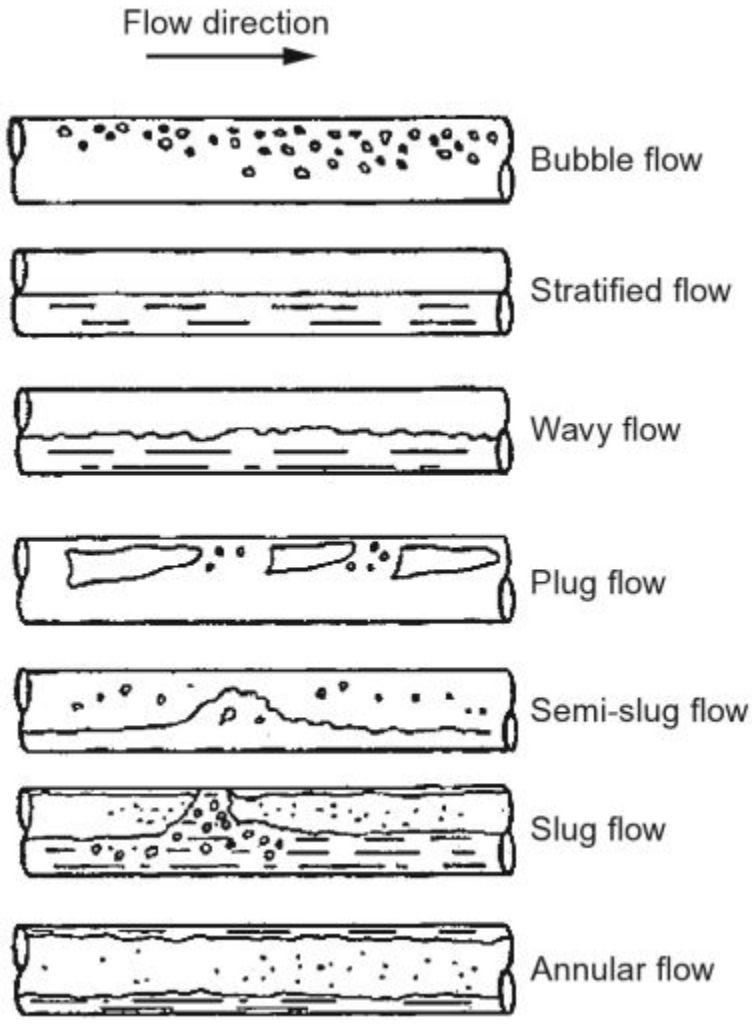

Figure 2.2: Typical two-phase gas-liquid flow regimes in horizontal pipes (Falcone et al., 2009).

Several factors affect the phase distribution, i.e. flow regimes that can be observed in a two-

phase flow. The main factors are phase flow rates, surface tension, wetting, dispersion, coalescence, body forces, and heat flux effects (Falcone et al., 2009). Despite the number of factors, one can differ between the most common gas-liquid flow regimes by a few main categories. The flow regimes typically found in horizontal pipe flow are illustrated in Figure 2.2. It is expected that helical coil flow regimes, where the coil axis is vertical and the coil pitch is small, can be recognised in Figure 2.2. This is based on the small vertical elevation compared to horizontal flow length. The *bubble flow* consists of large liquid fraction with gas bubbles dispersed in the liquid. Buoyant forces elevate the majority of the bubbles to the upper pipe region. The *stratified flow* illustrates that the two phases are completely separated as a result of gravitational forces. One large horizontally oriented interface can be observed. This flow regime seems preferable for a case where extraction of one of the phases, or phase splitting, is desired. The *wavy flow* has equal phase distribution as the stratified flow, but irregularities on the gas-liquid interface similar to waves is observed. The occurrences of waves are usually related with higher gas than liquid flow rates. The *plug flow* is recognised by bullet-shaped air bubbles or pockets. Similar to the smaller bubbles in bubble flow, the air phase tends to accumulate in the upper pipe region, as a result of buoyancy. The *semi-slug flow* appear as large frothy liquid waves that does not reach the top of the pipe. This regime will cause irregular liquid fraction along the pipe. The *slug flow* is characterised by occurrence of frothy liquid waves, called slugs, that occupy the whole pipe cross-section. In between the slugs, the flow regime can sometimes appear as wavy or annular. The *annular flow* has the gas phase occupying the core of the pipe, while the liquid flow along the pipe wall as a film. The liquid film is usually thicker in the lower pipe region due to gravity.

Falcone et al. (2009) adds that the difference between plug, semi-slug, and slug flow regime can be hard to distinguish, hence those three regimes can be categorised as *intermittent flow*.

In chapter 4, all experimental measurements are given a flow regime characterisation determined from images. The flow regimes mentioned in chapter 4 are recognisable with the regimes presented in this section.

2.8 Pressure loss in pipes

Fluid in motion through a pipe will encounter shear forces working tangential to the surface on which the fluid it acts. The fluid will suffer loss of energy as dynamic viscosity counteracts the shear forces, resulting in a decrease of pressure (Massey and Ward-Smith, 1998).

The *head loss* is the sum of change in pressure, and hydrostatic pressure, over a given length. Besides elevation changes, the main contributor to pressure loss are viscous forces in the fluid, initiated by shear forces between the fluid and the pipe surface (White, 2011).

The so-called Darcy-Weisbach equation is a common method to estimate the head loss in a pipe flow, and is shown in Equation (2.4). For a pipe flow without elevation change, the head loss is dependent on horisontal pipe length, L, pipe diameter, d, mean flow velocity, $\overline{v}$, and a *friction factor*, f.

For turbulent flows, the friction factor is dependent on Reynolds number and *relative roughness*. The relative roughness is the ratio of the surface roughness height to the pipe diameter. A smooth pipe surface, gives lower roughness height, and hence reduces the friction factor.

$$h_f = f\frac{L}{d}\frac{(\overline{v})^2}{2g} \tag{2.4}$$

Fluid flowing through a bend or other curvatures will suffer larger pressure losses than straight pipe flows. The flow encounters "separation" from the inner wall of the curved pipe, and swirling secondary flow as a result of centrifugal forces. In this case, flow separation means that the fluid tends to leave the inner pipe wall, causing a low-pressure drag zone. Secondary flow is explained in section 2.8.

The losses due to flow separation and secondary flow increase for lower R/d, as this increase curvature effects. The losses due to friction increase with R/d, as this increase the total length of curved pipe (White, 2011).

In thesis, no quantitative analysis was made on fluid pressures. However, it was assumed that the value of the discussions in chapter 4 is enhanced with a basic understanding of pressure losses, especially related to curved pipe flows.

2.9 Secondary Flow

Berger et al. (1983) states that *"Secondary flow appear whenever fluid flows in curved pipes or channels"*. The secondary flow pattern is recognised by looking at velocity profiles in a plane perpendicular to the primary (axial) flow direction. In Figure 2.3 the secondary flow pattern is seen as two counter-rotating vortexes.

The secondary flow pattern initiates because the axial fluid velocity profile is highest in the centre of the pipe, and zero at the pipe wall. Assume a fluid particle in the centre of the pipe in Figure 2.3. High axial velocity cause the particle to be affected by higher centrifugal force than the surrounding particles, hence it is forced outwards. When the particle approaches the outer pipe wall, the velocity is reduced as a result of the no-slip condition. The centrifugal force acting on the particle is reduced, allowing it to move inwards along the upper or lower vortex. The inward movement is supported by the pressure distribution in the cross-sectional plane, induced by the centrifugal force, where the outer region has higher pressure than the inner region.

In Figure 2.3, the two counter-rotating vortexes are symmetric around a horizontal and vertical centre line. This only represents the secondary flow pattern for low velocity laminar flows. For higher axial flow velocities, the two vortexes are biased in the horizontal direction towards the outer pipe wall, loosing their vertical symmetry.

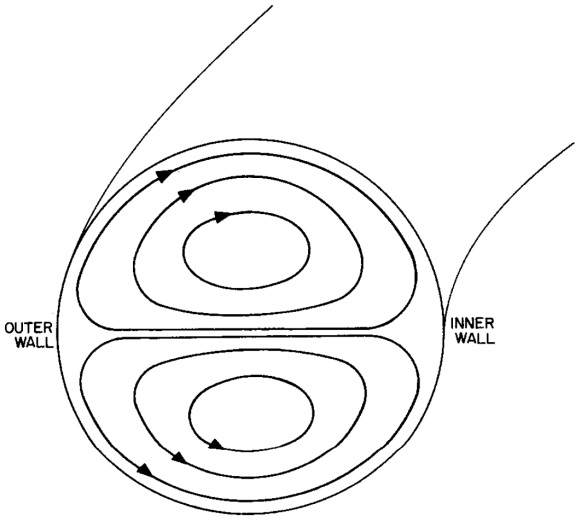

Figure 2.3: Secondary flow pattern for a laminar flow (Truesdell and Adler, 1970).

Secondary flow developing length

Developing length for straight pipes are mentioned in section 2.4. The same principle regards curved pipe flows, where a certain length of constant curvature is required to achieve fully developed flow. Vashisth and Nigam (2009) published a study on two-phase flow in coiled tubes addressing the curved pipe developing length of secondary flow. Their study included examination of several correlations for estimation of developing length, and a two-phase developing length correlation was suggested. Results from the study indicated that shorter curvature radii required longer developing length, because of small curvature and increased centrifugal effects.

The secondary flow developing length is not further elaborated in this thesis. However, in the discussions in chapter 4 the phenomenon is mentioned.

2.10 Dean Number

Two important parameters that characterises fluid flow in bends are the curvature ratio and the Dean number (Berger et al., 1983). The curvature ratio is defined by Equation (2.5), where r equals the inner pipe radius and R is the curvature radius.

$$\delta = \frac{r}{R} = \frac{d}{2R} \tag{2.5}$$

Berger et al. (1983) states that the qualitative meaning of the Dean number describes the ratio of centrifugal-, inertial-, and viscous forces, as shown in Equation (2.6). He further states that secondary flow initiates mainly as a result of centrifugal and viscous forces, and that the Dean number is a measure of the magnitude of secondary flow.

$$De = \frac{\sqrt{Centrifugal \times Inertial}}{Viscous} \tag{2.6}$$

Berger et al. (1983) highlighted that a variety of Dean number definitions was used in different reports, but suggested Equation (2.7) to be used in future studies. Be aware that in Equation (2.7), the Reynolds number was defined as $Re = (\rho \overline{v} r)/\mu$, and Dean number was denoted as κ[1].

[1] To distinguish different Dean equations, denotation was adopted from Berger et al. for this definition of Dean number

$$\kappa = 2 \times \sqrt{\delta} \times Re = 2 \times \sqrt{\frac{r}{R}} \times \frac{\rho \overline{v} r}{\mu} \tag{2.7}$$

For the common definition of Reynolds number in circular pipe flow, $Re = (\rho \overline{v} d)/\mu$, the Dean number becomes as in Equation (2.8), denoted as *De*. This is the Dean number used in this report.

$$De = \sqrt{\delta} \times Re = \sqrt{\frac{d}{2R}} \times \frac{\rho \overline{v} d}{\mu} \tag{2.8}$$

In chapter 5, the Dean number is used as a similarity parameter between the experimental helical coil, and a hypothetical full-scale helical coil.

2.11 Similarities

This section briefly present the concept of similarity, used to relate experimental models to prototypes or full-scale scenarios. Three types of similarity are described, including geometric, kinematic, and dynamic similarity. In chapter 5, the similarities are investigated further, with relation to the experiments in chapter 4.

Geometric Similarity

"A model and prototype are geometrically similar if and only if all body dimensions in all three coordinates have the same linear scale ratio". (White, 2011)

As the statement above indicates, all dimensions of a geometrical shape must be scaled with the similar parameter. This means that for a rectangular shape, the width, length, and height is individually multiplied with the same scale ratio from model to full-scale. It is further required for geometric similarity that the shape of the model is equal to the full-scale, hence all angles must be unchanged between them. In other words there are several homologous points in the model shape that, by geometric similarity, are related with the linear scale ratio in the full-scale shape. For fluid mechanic cases, the requirements of the model shape also regard the fluid geometry. Additionally, White (2011) states that all directions of the fluid flow are preserved.

Kinematic Similarity

"The motions of two systems are kinematically similar if homologous particles lie at homologous points at homologous times". (White, 2011)

White (2011) states that to achieve kinematically similarity the model and prototype must have the same length scale ratio, and the same time scale ratio. To have the same length scale ratio would require having geometric similarity.

For frictionless low-speed flows, White (2011) say that flows with no free surface can be kinematic similar only by defining independent (different) length and time scale ratios. For free-surface flows, kinematic similarity is obtained with length and time scale ratios described by equality of Froude number, because effects of gravity are dominating.

Dynamic Similarity

"Dynamic similarity exists when the model and the prototype have the same length scale ratio, time scale ratio, and force scale (or mass scale) ratio". (White, 2011)

To achieve dynamic similarity, first of all geometric similarity must be ensured. Then dynamic similarity, together with kinematic similarity, is obtained for the following flows and requirements. *Compressible flow* requires equal Reynolds number, Mach number, and specific-heat ratio. *Incompressible flow with no free surface* requires equal Reynolds number. *Incompressible free-surface flow* requires equal Reynolds number, Froude number, and possibly Weber number and cavitation number.

Regarding modelling of fully enclosed (pipe) flows Chanson (2004) states that the effect of viscosity at solid boundaries as pipe walls are important, hence Reynolds number equality is the dominating parameter when modelling such flows.

Chapter 3

Study of Separation Principles

This chapter presents the physics and theory behind gravity settling separation and centrifugal separation systems, and state-of-the-art compact separation systems. The majority of the existing systems are products from well-known subcontractors of the petroleum industry. Publications regarding multiphase flow in helically coiled pipes and the use of coiled pipes as centrifugal separators, are presented. The separation techniques are discussed towards subsea applications.

3.1 Philosophy of Separation

"A separator is a pressure vessel designed to divide a combined liquid–gas system into individual components [...] for subsequent disposition or processing" (Stewart and Arnold, 2008).
Well streams are typically characterised by a multiphase turbulent flow, with various fractions of gas, oil, water, and solids. A separation process is thus required in order to exploit the different petroleum phases individually.

Production of oil and gas into a separator carries a certain amount of mass fraction from associated components. The components will then either be in the vapour phase or if not in the liquid phase. The multiphase flow behaves differently dependent on temperature and pressure. Phase diagrams are developed to understand these behaviours. To accomplish these conclusions the equilibrium vapour-liquid ratio has to be identified. Factors like pressure and temperature play an essential role on this value. Additional factors as the composition of the pro-

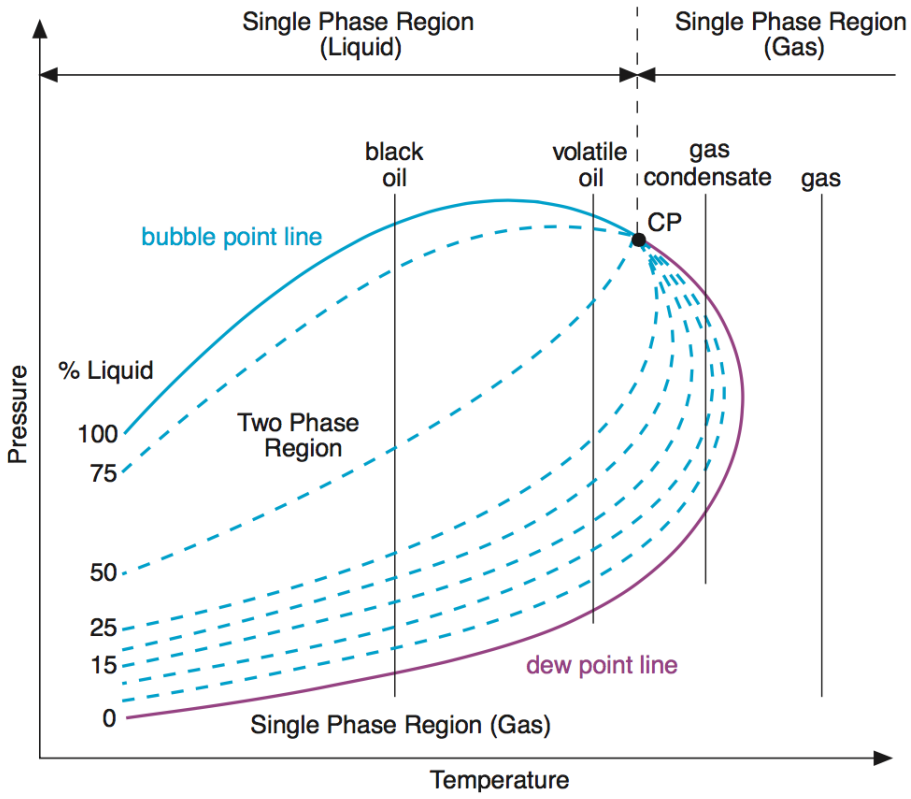

Figure 3.1: Pressure-temperature phase envelopes for main hydrocarbon types - showing initial conditions relative to the phase envelope only (Jahn et al., 2008)

duced hydrocarbon fluid plays a key role, as there is interaction of the various components in the system. The basic separation process is similar for both oil and gas production, although the relative amounts of each phase will be different. (Jahn et al., 2008).

A typical P-T phase diagram is illustrated in Figure 3.1. The phase diagram describes the various conditions of the phases considering temperature and pressure differences. The bubble point line describes the line of 100% liquid. Going above this line means 100% liquefied oil, while below this line leads to the first release of ethane vapour bubbles. Moving from the bubble-line to the dew-line indicates a gradual process of decreasing liquid, or increasing gas fraction. The dew point line is where the last drop of liquid is vapourised. Below this point only gas remains, and the gas volume is determined by its compressibility. The two lines meet at the critical point (CP) where one is no longer able to make a distinction between compressed gas and liquid. Located inside the envelope is the two-phase region, a mixture of gas and liquid phase. From a phase diagram the separator can be designed to uphold the desired pressure and

temperature for maximising the separation efficiency (Jahn et al., 2008).

The single-stage separator (one separator vessel) will have an optimum working pressure, this yields the maximum quantity of oil and minimises the transport of heavy components into the gas phase. Additional separators in a process train can increase the oil yield, but the incremental yield of oil will decrease with each separator added in the train. Adding of more separators in the process train increase the capital and operating costs, meaning that a balance between increased oil yield and cost has to be made. One- or two-stage separation is most common in the industry. The economics rarely supports more than three stages of separation. Low pressure may constrain the multistage separation process. The actual separation process includes a rather significant pressure drop, and low inlet pressures will result in a smaller scope for separation (Jahn et al., 2008).

3.2 Gravity Settling Separation

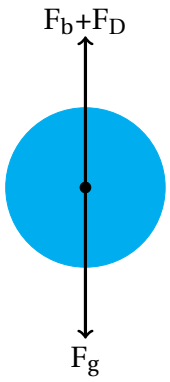

Figure 3.2: Forces acting on droplet surrounded by a fluid.

The most common separation solution for topside facilities is the gravity settling principle. The principle utilises a given duration for the fluids to settle into different layers as a result of their different densities.

To understand the principle, one can consider a spherical droplet entrapped by another fluid, whereas the density of the droplet varies from the surrounding fluid. If the droplet is more dense, it would descend through the fluid. The descending droplet is affected by gravitational-, buoyant-, and drag forces, as shown in Figure 3.2. Yamaguchi (2008) says that at some point the droplet will obtain a constant velocity, the so-called terminal velocity, where the sum of the buoyant (F_b)- and drag (F_D) force equals the gravitational force (F_g). Stewart and Arnold (2008) states that flow around oil droplets in water and water droplets in oil is laminar, hence Stokes' law for fluid drag force is valid. For an oil-water separation scenario, the force balance at terminal velocity can be expressed by Equation (3.1) and (3.2). Here d is droplet diameter, ρ_s is sphere density, ρ is fluid density, μ is fluid viscosity,

U is the terminal velocity, and g is the gravitational constant.

$$F_b + F_D - F_g = 0 \tag{3.1}$$

$$\frac{\pi}{6} d^3 \rho g + 3\pi\mu d U - \frac{\pi}{6} d^3 \rho_s g = 0 \tag{3.2}$$

Equation (3.2) can be isolated for the terminal velocity, U, as shown in Equation 3.3.

$$U = \frac{d^2 g(\rho_s - \rho)}{18\mu} \tag{3.3}$$

The terminal velocity can be used to estimate the time required for a droplet with a given size to settle at the bottom of a tank. Among other factors, the terminal velocity can be used for design of gravity separators.

Separator Design

The design of the inlet section of a separator is intended to separate most of the liquid phase, e.g. large slugs or droplets, from a multiphase flow. The design leads the multiphase flow down towards the liquid at the bottom of the vessel. This causes segregation of the flow while avoiding a mist formation (Jahn et al., 2008).

Some small droplets that still remain in the gas phase require handling of extraction systems. To prevent these from following the gas stream, demisting sections are installed to recover the liquid mist. Large liquid droplets will fall out of the gas under the act of gravitational forces, while small liquid particles are intercepted by impinging the demister section before the outlet of gas phase. Wire mesh or metal plates are traditionally used for constructing these systems. The droplets that are intercepted coalesce and move downward by gravity into the liquid phase (Jahn et al., 2008).

As liquid is prevented in the gas phase, gas must also be prevented in the liquid phase. Entrapped gas bubbles in the liquid phase must be given the required residence time to escape from the liquid under forces of buoyancy. The liquid viscosity affects the process at which the

small gas bubbles escape. Higher viscosity requires longer residence time. Typical residence times can vary from 3 minutes (light crude) to 20 minutes (very heavy crude). Three main factors determine the separator sizing; gas velocity (minimise liquid mist in gas phase), viscosity (residence time), and surge volume allowances (up to 50% over normal operating rates) (Jahn et al., 2008).

Separator Types

Jahn et al. (2008) states that the basic separator types can be characterised in two ways; firstly by their main function (bulk or mist separation), and secondly, by orientation (vertical or horizontal).

Knockout vessels are the most typical kind of basic separators in the industry. The removal of droplets from the gas stream is poor as there are no internals installed in the vessel. These are utilised in dirty service conditions, i.e. well streams containing sand, water, and corrosive products, and work well.

Demister separators are applied where small liquid particles remaining in the gas phase create problems. Sometimes liquid recovery is less important than eliminating liquid particles from the gas stream, especially when feeding gas to an eventual compression system.

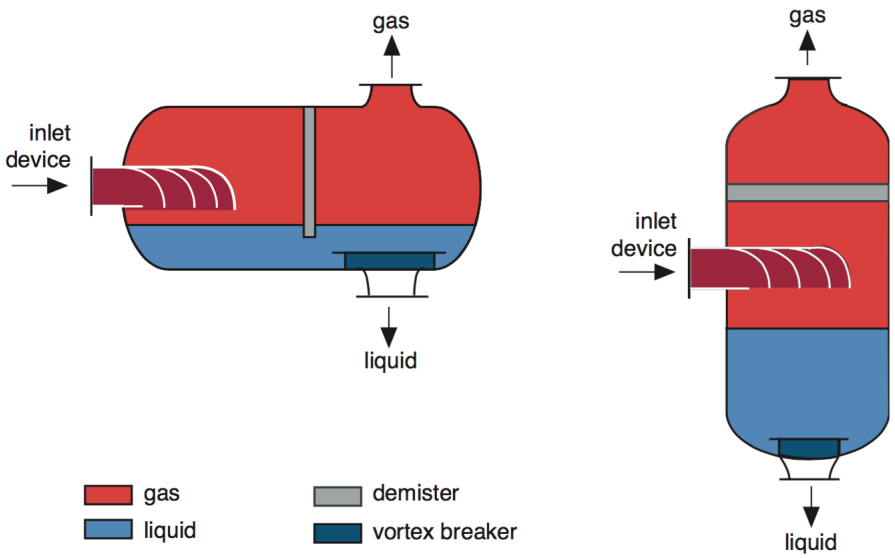

Figure 3.3: Horizontal and vertical demister separators (Jahn et al., 2008)

The separators can be constructed vertically or horizontally. Figure 3.3 briefly show examples of the horizontal and vertical demister separator design. Vertical separators are usually preferred when high oil capacity and the requirement of large surge volume is present. However, degassing may generate an issue if liquid viscosity is high, as this slows the escape of gas bubbles. The horizontal separators can deal with high gas volumes and foaming crude. These are usually put in action when facing high flow rates and high gas-liquid ratios (Jahn et al., 2008).

Conventional Gravity Separator

The characteristic of a conventional gravity separator is a huge pressure vessel. The separator occupies large areas on process facilities which already have limited space, i.e. offshore processing. Application of this technology entails high capital and operational expenditures. These separators are applied to separate both two-phase and three-phase production. This technique is associated with thorough and final separation. Figure 3.4 illustrates a typical three-phase horizontal separator vessel, where the layers are facilitated by gravitational forces. The size of the vessel depends on the required residence time for the phases to separate and settle.

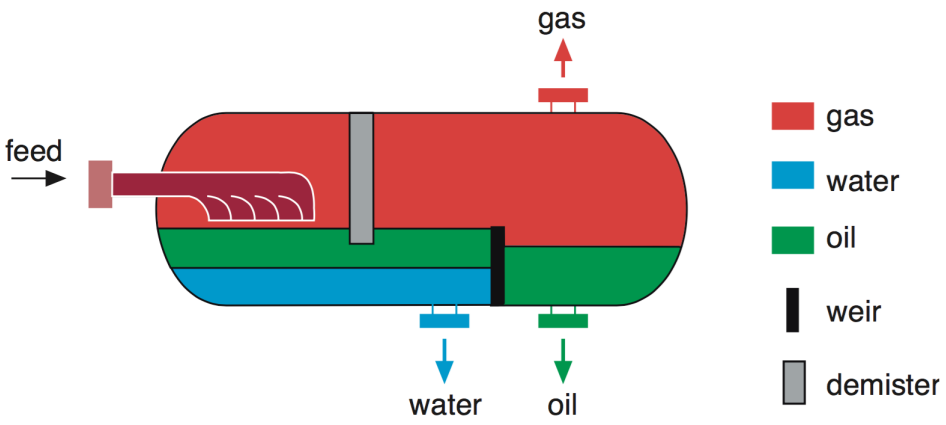

Figure 3.4: A basic three-phase separator (Jahn et al., 2008)

The horizontal technique is suited with low level of liquid, this level should be kept as constant as possible. Losing liquid level can imply gas entering liquid drain, this can also occur if the liquid drain produces a swirl. High sand production is unwanted as this may cause clogging and increases the need for intervention. Measurements for avoiding these factors are usually included in the construction.

3.3 Centrifugal Separation

Centrifugal separators utilise the effect of radial forces induced on fluids moving in a circular motion. This force is commonly referred to as the centrifugal force. Depending on the separator design, the induced centrifugal force can be of magnitudes up to 500 000[1] times the gravitational force.

Equation (3.4) shows the relationship between centripetal acceleration, a, tangential velocity, v, and the curvature radius, R, for uniform circular motion.

$$a = \frac{v^2}{R} \tag{3.4}$$

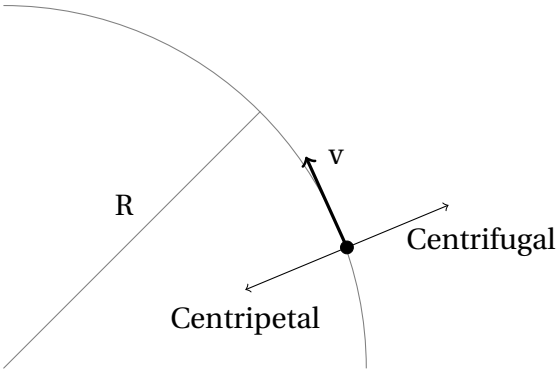

Figure 3.5: Uniform circular motion: a particle moving along a constant radius, at constant tangential velocity.

Centripetal force is the force acting perpendicular to the tangential velocity of the particle, pointing towards the centre of rotation, causing a circular motion. Without the centripetal force the particle would move in a straight line.

Centrifugal force is the force acting perpendicular to the tangential velocity of the particle, but in the opposite direction of the centripetal force. It is a reactive force of the centripetal force. When the two forces are at equilibrium, the circular movement is constant, i.e. the particles circular motion neither sharpens nor straightens.

Holdich (2002) describes buoyancy with the following; *"if a particle floats, rather than sinks, then it will move inwards in a centrifugal field. Particles denser than the fluid will move outwards.*

[1] The higher value is only obtainable for gas streams. An example is the Twister® Supersonic Separator.

The centrifugal field acts like an enhanced gravitational field and is usual to speak in terms of the equivalent 'g' force: i.e. centrifugal acceleration / 9,81 m/s^2 "

$$\frac{dr}{dt} = \frac{x^2(\rho_s - \rho)r\omega^2}{18\mu} \tag{3.5}$$

In a centrifugal motion, particles travel radially and the radial position is affected by the force of circular motion. The particles will then accelerate throughout its movement in the radial direction. Meaning, to express the position of the particle as a function of time, integration is necessary. In the definition of physical forces acting on a particle in circular motion, the centripetal force and not the centrifugal force should be considered. If the centripetal force was abruptly eliminated, an uncontrolled particle would exit its orbit tangentially. This is the ideal situation for particles separated from gases in cyclones. In reality, the particle will move in changing orbits, not exit tangentially from one orbit, and gradually travel outwards in the radial direction (given that the surrounding phase is less dense than the particles). To describe this travel mathematically, Equation (3.5) can be used (Holdich, 2002).

Cyclone Separator

The petroleum industry has started to replace the conventional gravity separators with the cyclonic separation technology, which indicates the growing influence it has on the field. The compact separation vessel and efficient gas-liquid separation makes it advantageous. Similar to gravity separators the cyclones can be constructed to deal with large volumetric concentrations of liquid. The cyclone principle allows for separation of both liquid and solid particles (Hoffmann et al., 2003).

Cyclone is termed as a special separator, utilising large centrifugal forces to enhance the separation process. This includes elimination of liquid droplets (condensate) in a gas phase stream. The inlet stream is forced in a circular motion generating the centrifugal force. The liquid being the denser phase is forced against the wall of the vessel by the centrifugal force. This is either obtained by forcing the fluids around the outer wall using inlet vanes, or directing gas into several smaller cylinders acting as small cyclones. In both cases the liquid is collected at the bottom of the vessel. In some cases the gas phase flows through a settling area before

leaving the vessel at the top (Kidnay et al., 2011).

The cyclones are very effective when operating with high gas rates. They efficiently sort out droplets with diameters larger than 10 μm. However, their efficiency falls rapidly when the inlet flow rate decreases. This set limitations to the technology as it narrows the operating range. In addition, the cyclones are recognised to have a rather high pressure drop, and it also face challenges when operating with liquid slugs. The technology is attractive for applications where the gas and liquid flow does not vary much. The cyclones are frequently applied in power plants, where it removes the condensate in steam systems. On the other hand, they are less frequently used for natural gas processing due to the fluctuating flow rates and liquid slugging (Kidnay et al., 2011).

Hydrocyclone Separator

Hydrocyclones (also sometimes referred to as cyclones) are based on nearly the same technique and principle as the cyclones mentioned above. Variation in the cyclones operating conditions can lead to drastic losses in separation efficiency. These conditions are usually inlet flow rate, viscosity, temperature, and liquid/gas characteristics. The term hydrocyclones are based on the liquid being the primary phase, where solids or gas are separated from a liquid flow. This includes separation of water from oil, so-called liquid-liquid separators. The hydrocyclone, like the mentioned cyclone, is a more coarse separation technique as opposed to the conventional gravity settling method.

Jahn et al. (2008) states that *"Hydrocyclones have become common on offshore facilities and rely on centrifugal force to separate light oil particles from the heavier water phase. As the inlet stream is centrifuged, the heavier water phase is 'spun' to the outside of the cyclone whilst oil particles move to the centre of the cyclone, coalesce and are drawn off upwards. The heavier water is taken out at the bottom"* .

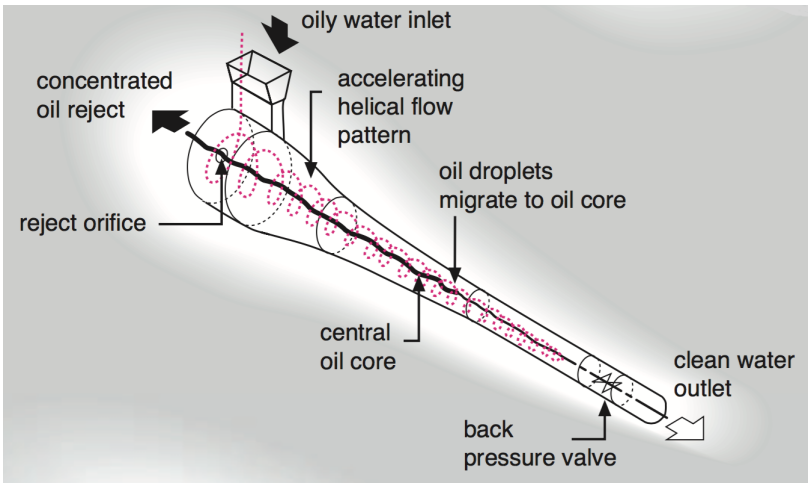

Figure 3.6: Hydrocyclone for oil-in-water removal (Jahn et al., 2008)

Figure 3.6 illustrates the hydrocyclone features, where the feed enters tangentially into the vessel. The feed mixture is separated and forced towards opposite axial directions, i.e. the two outlets at each end of the vessel.

The tangential inlet forces the incoming flow to enter a rotational motion. This eliminates the need for rotating the wall of the device mechanically, e.g. centrifuge. Hence, the vesssel contains no rotating parts. However, the device requires a "prime mover" to ensure separation, e.g. a pump or a high-energy well stream. Inside the hydrocyclone the flow pattern is rather complex, and three velocities need to be accounted for. The tangential velocity is critical for the operation of the cyclone, as it ensures separation of particles subjected by the centrifugal force. Tangential velocities of oil, water, and solids may reach as high as 20 m/s. The radial velocity is much lower, typically less than 0.1 m/s. There is a radial net flow of oil (lighter particles) inside the vessel directed towards the centre, and a radial net flow of water or solids (heavier particles) directed outwards to the wall. This makes it essential to differentiate between the radial flows of the separate phases. The third velocity is in the axial direction, where the hydrocyclone has two outlets. The outlets continuously send out the different phases into two separate streams. This means that the axial flow velocity has to be evaluated continuously to ensure that the intended phase exits the correct outlet. The hydrocyclone operates as a thickener, i.e. concentrates a suspension, and a classifier, i.e. selects particles of a specific size. Whereas one outlet has the diluted flow from the feed (finer particles), and the other outlet has a thickened flow, coarser particle distribution (Holdich, 2002).

Helical Coil Separator

A different technique utilising high centrifugal forces to separate different phases, is the helical coil principle. The principle involves a mixed feed entering a pipe of helical shape, with one or several loops, where the denser phase gets 'slung' to the outer region of the pipe cross-section. In the case of gas and liquid flow, the liquid phase is thought to distribute at the outer region of the curved pipe. Hence, the gas will be located at the inner region closer to the centre of the loop. The technique cannot separate the phases into two different streams on this basis, although it will force a more distinct interface between them. A possible method to draw one phase from the other, is to drain one of them from the main stream.

The technology is not applied to any practical separation applications, and is rather uncommon. However, research and experiments on the technique has been conducted. da Mota and Pagano (2014) studied phase segregation in one looped helical pipes with multiphase flow, to examine its potential for flow conditioning. Murai et al. (2006) investigated the effect of centrifugal acceleration on flow regime with air-water flow in five looped coils. Mujawar and Rao (1981) study flow patterns, holdup, and pressure drop, on gas-liquid two-phase flow in helical coils. Zhang et al. (2006) investigated oil/water separation mechanism inside helical pipes, where the system contained several loops and drainage holes for extracting one phase from the other. At last, Al-Yazdi (1991) patented a method for separation of water from crude oil, where the system contains a vertical spiral separator unit with drainage. These researches are elaborated in more detail later in this chapter.

3.4 Subsea Separation

The use of subsea separation systems are still in a developing phase. Although, several applications are installed and have proved their potential, there are still issues to address in order to achieve confidence in the concept. The benefits of subsea separation lies in its ability to increase the total production, improve reservoir recovery, and enhance the total revenue. The enhancement of reservoir recovery essentially results in prolonging the plateau length of the field. Reduction in capital expenditure is especially targeted towards deep-water applications (Hannisdal et al., 2012)

Subsea separation is seen as an enabler for exploiting deep water and Arctic resources, as well as producing from marginal fields. Developments in these areas have traditionally been referred to as uneconomical, or too challenging because of the remote locations, harsh environments, low energy reservoirs, or long tieback requirements due to no existing infrastructure (Hannisdal et al., 2012).

Subsea separation can reduce the unnecessary heavy transportation of water and solids to topside facilities, increasing production rates. Typically low energy reservoirs require artificial lift to overcome pressure drops between reservoir and process facility. Gas lift is a viable option, although its applicability is not always present as it requires high gas-oil ratios. A second viable option is the use of subsea pumps, whereas subsea separation can improve the boosting efficiency. This is a result of the separation feature, where it can control the magnitudes of gas and liquid in the flow (Hannisdal et al., 2012). This implies possibilities of exploiting single-phase pumps and compressors, which provides higher hydraulic efficiency and increased differential pressure for the processed phases.

Subsea separation and boosting provides cost efficient flow assurance opportunities. Given that the separation provides separate pipelines for gas and liquid, it enables hydrate management possibilities. In addition, it ensures a reduction of glycol requirements for the gas line, and prevents Joule-Thomson cooling in the liquid line. Subsea separation and pumping can reduce flow assurance issues related to slug flow, especially in risers going to topside facilities (Hannisdal et al., 2012).

Applying systems subsea require modularised constructions. This means that sections of the construction can be retrieved from the seabed, excluding the whole structure and foundation. The actual defect module can then easily be replaced, without the need of larger intervention vessels. Having smaller modules implies that these can be stored at nearby facilities. Intervention then becomes more agile and efficient. However, due to the reduction in maintainability as for installing equipment subsea, Hannisdal et al. (2012) states that, *"the reliability of a subsea station is expected to be high, for example with target availability of 97.5 %, so a minor drop in availability makes a large impact on the overall business case. It is therefore essential to find a good compromise between the realised reduction in overall capital expenditure and the reduced robustness to fluctuating conditions, when making separators smaller"*.

Functions performed subsea instead of topside brings advantages in form of the boundaries for the installations. Limited space topside is an issue for large separation vessels usually associated with the conventional gravity separators. Applying more equipment subsea ensure simplifications to topside facilities, eventually it could imply complete subsea factories, eliminating the current topside strategy.

Concerns related to subsea applications are sand removal, flow assurance, reliability, durability, maintainability and power distribution. Sand handling systems are required to reduce wear due to erosion. Sand accumulation is therefore a concern for the installations, and its removal is of utmost importance. Pipelines located at the seabed may experience difficulties related to flow assurance, induced by phenomenons as hydrates and asphalts. Mapping and sampling of the seabed foundation is essential to level and secure the installed equipment. Durability for the subsea applications is vital for minimising the required maintenance, typically the equipment is designed to endure about 25 years of service. However, the experience is that some components are more critical towards failure and require intervention more regularly. In cases like these the components should be modularised as mentioned above. Challenges may occur when distributing power to the subsea applications through umbilical cables, as very long cables can delay the response time. If hydraulics, electricity, and signal cables are wined into the umbilical they quickly become large and expensive. The most power consuming subsea modules are often related to pump and compressor stations.

Gravity Settling Principle

The gravity settling principle has been exploited subsea, in fields like Pazflor, Tordis and Troll. The construction becomes more complicated than for topside applications. The large and inconvenient structures are associated with an expensive application and operation (Hannisdal et al., 2012).

The size and shape of these separators makes them unsuitable for deep subsea operation. The stress applied on the vessel structure is a result of ambient pressure acting on the vessel surface. This cause complications for vessels with large surface areas, where a solution is to increase the vessel wall thickness. This generates a huge construction of heavy weight, increasing material costs, and is unattractive for intervention and maintenance.

Separation efficiency is directly related to residence time, requiring a certain vessel size. When deeper waters imply smaller vessels, it is clear that that efficiency decrease with increase of water depth. In addition, requiring a certain residence time for the phases to settle, could impact the productivity and cause a holdup for the production. Another consequence of a time-consuming separation process, could be loss of temperature resulting in hydrate formation in pipes.

Centrifugal Principle

The centrifugal principle provides the opportunity to construct compact subsea separation applications. The technique utilising high centrifugal forces is not dependent on large gravity settling vessels. Despite that subsea fields essentially have unlimited space, smaller vessels are still desired. Stresses induced by ambient pressure on the vessel structure can be reduced with reduction of vessel surface area, enabling deep water applications. The technology requires little maintenance as there are no moving parts. Depending on the sand handling solution, issues are mostly related to erosion, and not sand accumulation. As the centrifugal principle requires a certain flow velocity to be efficient, it requires a prime mover for the flow. Initially, the well flow energy can be sufficient, but this energy drops over time of production.

The centrifugal separation technology becomes more ideal where the phases to separate have large density difference, deeper waters (more than 1200 m), and Arctic applications. The reduction in weight and size enables intervention with a variety of commercial vessels, eliminating the need for specially designed and large intervention vessels.

The helical coil technique utilising the centrifugal principle is an interesting concept for a subsea application. Like the cyclones the technique can be classified as compact, and includes no moving parts. The geometry of a helical coil separator is ideal for containing high pressures, and taking high ambient pressures, due to essentially being a circular pipe. Depending on length of curved pipe to achieve separation, the flow through a helical coil may not experience critical pressure loss. With respect to modularisation, the helical coil could be a module that is easily replaceable, whereas the connection to inlet and outlet to the coil would be disconnected. The helical coil exposed to the high velocity flow would, however, be affected with erosion and become a critical module.

3.5 Existing Technologies

This section presents existing compact separation systems. The systems are based on both centrifugal and gravitational separation principles.

3.5.1 In-line Cyclone Separation

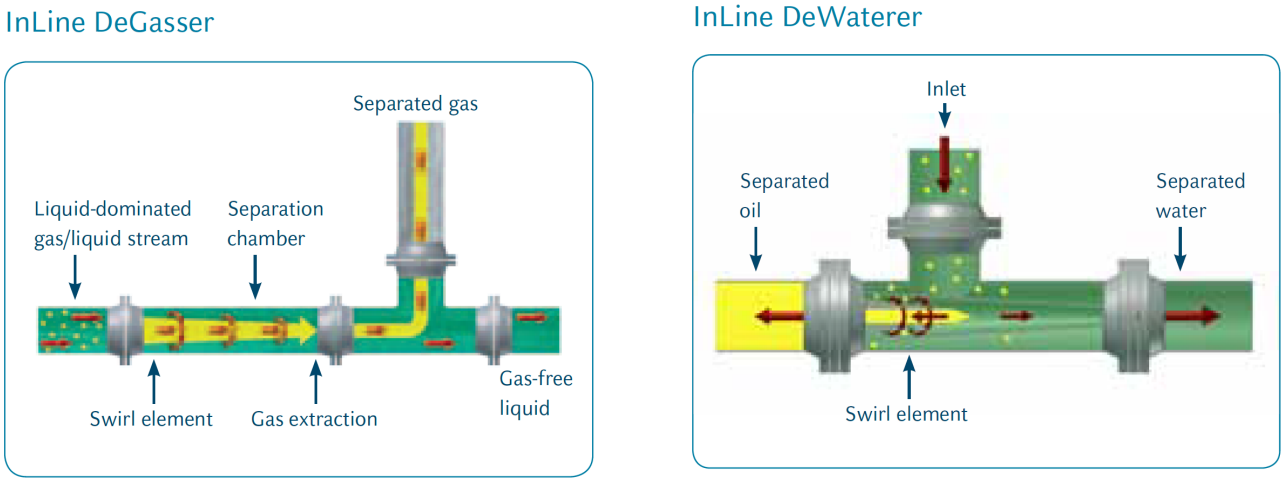

Figure 3.7: InLine separators

Seeking towards compact separation solutions, *in-line* systems have been developed. FMC Technologies deliver several types of in line solutions, including both gas-liquid and liquid-liquid separation. Field-testing of the solutions started in 2003 and the technology has proven to be reliable.

Figure 3.7 shows two of the products that FMC offer. The InLine DeGasser comprises a straight pipe section with a swirl element that induce cyclonic flow pattern in the pipe. As the denser liquid is forced outwards to the pipe wall, the less dense gas occupies the centre of the pipe. A certain length downstream of the swirl element a gas extraction device is found. The gas extraction device leads the gas out of the pipe into a gas pipe. FMC says the InLine DeGasser is mainly designed for separation of gas from high liquid content flows. The Statfjord B platform has had an InLine DeGasser installed since 2003.

The InLine DeWaterer is one of the liquid-liquid separators that FMC offers. The design is shown in Figure 3.7, comprising a T-pipe with a swirl element. The inlet fluid is forced into a cyclonic flow pattern, accumulating the lower density phase in the centre. The low density phase is extracted from a centred outlet while the high density phase is extracted from the outer region. The InLine DeWaterer has operating range of up to 50 % oil in water and 50 % gas volume fraction at inlet. Within this operating range the water removal efficiency can reach up to 95 % (FMC Technologies, a). The InLine DeWaterer system was field tested at Gullfaks C in 2010 with good results. FMC Technologies (a) claims that the system is being developed as a subsea separation solution.

FMC has developed a three-phase separator test skid comprising only in-line separation technology. According to FMC the skid shall be tested offshore on a well stream. Depending on the results, the skid may be taken further for development of a full-scale subsea separation system. The skid includes One CDS Gasunie inlet cyclone, two stages with InLine DeWaterer, and one stage of HydroCyclone for "water polishing". The system utilise a water recirculation loop to enhance separation efficiency.

3.5.2 CDS-Gasunie Cyclone Scrubber

Figure 3.8: CDS-Gasunie Cyclone Scrubber (FMC Technologies, b).

The Cyclone Scrubber uses optimised blade geometry to rotate the multiphase flow entering the vessel. Solid particles and liquid accumulates towards the wall as a result of being exposed to the centrifugal force, and descend to the bottom of the Scrubber. The gas gathers at the centre and flows out the centre pipe connected to the gas outlet nozzle at the top. Baffles at the bottom of the vessel stops the heavy phase from rotating further. A blocking plate prevents liquid being entrained with the gas, avoiding both gas carry-under and liquid carry-over. The technology can handle liquid/gas volume ratios of up to 10%. The vessel does not contain any moving parts making it maintenance friendly. The small size and weight makes it attractive for offshore applications, it has excellent slug handling capabilities, and high turn-down (FMC Technologies, b).

The scrubber can be used to separate liquid (water, hydrocarbon, glycol, etc.) from gases (natural gas or other). The technology can also be applied for protection of downstream equipment like compressors, gas turbines, and flow meters. Similar to liquid separators, this technology can separate solid particles (dust, sand, etc.). This makes the scrubber suitable as a gas wellhead separator (FMC Technologies, b).

3.5.3 Supersonic Separator

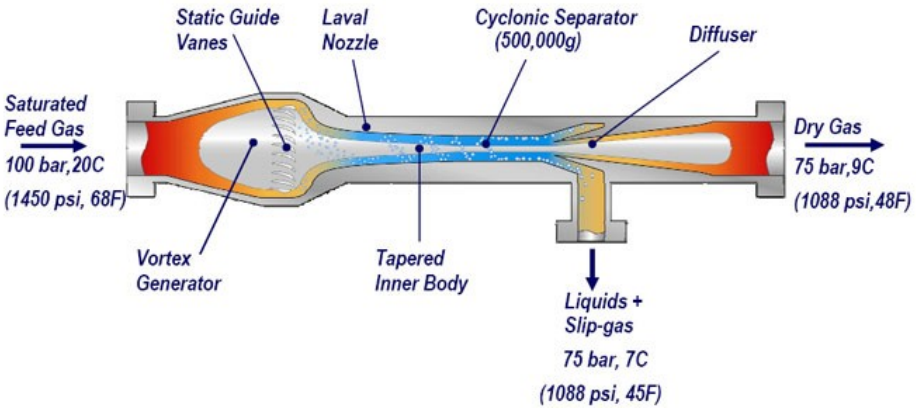

Figure 3.9: Twister® Supersonic Separator (Twister BV)

The Twister Supersonic Separator is a device for gas conditioning, utilising cyclonic separation together with gas condensation. Figure 3.9 show the separator design and working principle. The compact flow duct and the guide vanes in the vortex generator convert the high pressure energy into kinetic energy. The gas obtains supersonic velocity and the pressure decrease causes temperature decrease. This enable condensation of water and hydrocarbons, creating droplets that are forced to the outer pipe. Denser fluids are extracted to a compact de-liquidiser, where slip-gas is re-injected to the dry gas flow. The strong cyclonic effect is capable of causing up to 500 000 g. A total pressure loss of 15-20 % can be expected (Twister BV)

3.5.4 ASCOM Spherical Separator

Figure 3.10: ASCOM Spherical Separator (ASCOM Separation)

The spherical separator is a concept utilising the gravity settling principle. The concept is being developed for gas/liquid- and liquid/liquid separation, sand handling, and produced water treatment. Testing and verification of the technology is being planned, and the concept is thought to handle depths down to 3000 m. The size and shape of the spherical separator makes it a compact unit compared to a conventional horizontal separator. ASCOM Separation states that their high performance special internals makes the technology just as efficient as a conventional horizontal separator. However, conventional spherical separators have less efficiency than the conventional horizontal separators. Additional benefits of this spherical system, is the reduction in footprint, weight, capital expenditure, simplification in fabrication, ultra deep subsea applications, and seabed installations (ASCOM Separation).

3.6 Publications on Two-Phase Flow in Helical Coils

This chapter presents content and results from studies and patents on flow in helical coils. The studies are aimed towards investigation of flow characteristics, or for separation purposes, in helically coiled pipes.

3.6.1 *Simulation and experimental study of phase segregation in helical pipes: A new method for flow conditioning*

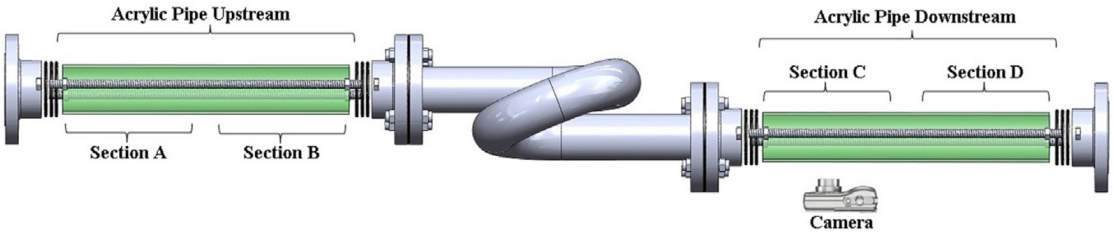

Figure 3.11: Top view of the experimental helical coil setup (da Mota and Pagano, 2014).

The report *Simulation and experimental study of phase segregation in helical pipes: A new method for flow conditioning* (da Mota and Pagano, 2014) investigate multiphase flow in helical pipes. The main goal with the report was to study multiphase behaviour in helical coils and the use of a helical coil as flow conditioner. A one-loop helical coil with horizontal coil axis was investigated, as shown in Figure 3.11. Numerical simulation was conducted with CFD-software. The simulation was based on the Euler-Euler multiphase model, with oil as primary phase. Water and gas was considered as droplets and bubbles in the oil.

In the numerical simulation, the influence on phase segregation by changing pipe inner diameter, gas and liquid flow rates, helical curve radius, number of loops, and gas bubble diameter was tested.

An inner diameter of 25.4 mm (1 inch) was expected to increase fluid velocity and also increase the centrifugal force. Still, the results showed phase segregation with a more distinct gas-liquid interface for a 50.8 mm (2 inch) inner diameter pipe. It was noticed that further increase of inner diameter would again reduce the quality of phase segregation.

At constant liquid flow rate of 2 kg/s, increasing the gas flow rate from 0.0035-0.5 kg/s seemed to improve the segregation up to 0.01 kg/s. Above this value the gas volume fraction increased significantly. At constant gas flow rate of 0.0035 kg/s, increasing the liquid flow rate from 0.5-8.0 kg/s did not seem to improve segregation. Below 0.1 kg/s the gravitational force overcame the centrifugal halfway through the coil.

Increasing the curvature radius gave reduced centrifugal force. This affected the flow es-

pecially at the highest point of the coil. Here the gravitational force became larger than the centrifugal, and reduced the phase segregation effect.

The number of loops was increased, showing just small changes in the gas-liquid interface distinction. The results from the simulations showed that after about one quarter of the helical coil loop a stratified type of flow could be recognised, including a clear gas-liquid distinction.

For the gas bubble size adjustment it was shown that for small bubble diameter of 0.001 mm, phase segregation was hardly obtained. A bubble diameter of 0.1 mm or more gave a distinct gas-liquid interface at the outlet of the coil.

The practical experiments were conducted in a setup with 3 inch inner pipe diameter, curvature radius of 14.3 cm, pitch of 10 cm, and for various gas- and liquid flow rates. Figure 3.11 shows the observation sections before and after the helical coil. Photos documented the results of the experiments. The experiments were conducted using air and water flow. At the coil outlet (section C) a wavy stratified flow pattern was observed. The lower region of the pipe cross-section mainly contained liquid, the middle region had a layer of gas-liquid mixture, while the upper region mainly contained gas. The results from the experiments were similar to the results from the numerical simulation. The report concludes that the simulated and experimental results indicate that a helical coil *can* be used as a flow conditioner.

3.6.2 *Structure of air–water two-phase flow in helically coiled tubes*

The report *Structure of air–water two-phase flow in helically coiled tubes* by Murai et al. (2006) presents an experimental study of air-water flow in coiled pipes. The main goals of the study were to investigate the effect of centrifugal acceleration on flow regime and flow structure distribution. Figure 3.12 illustrates the complete experimental set up, consisting of a pipe with 20 mm inner diameter, curvature radius of 27.0 cm and 37.5 cm, and five number of loops. Total superficial velocities of up to 6 m/s were studied. A straight pipe section with equal dimensions was used to compare flow regime between coiled and straight pipes. Flow regime and flow structure interfaces were photographed with a high-speed video camera, capturing side- and top view of the pipe simultaneously.

Flow regime maps presented parts of the experimental results. It was found that the centrifugal force affected the flow regime transition lines compared to the straight pipe flow regime map.

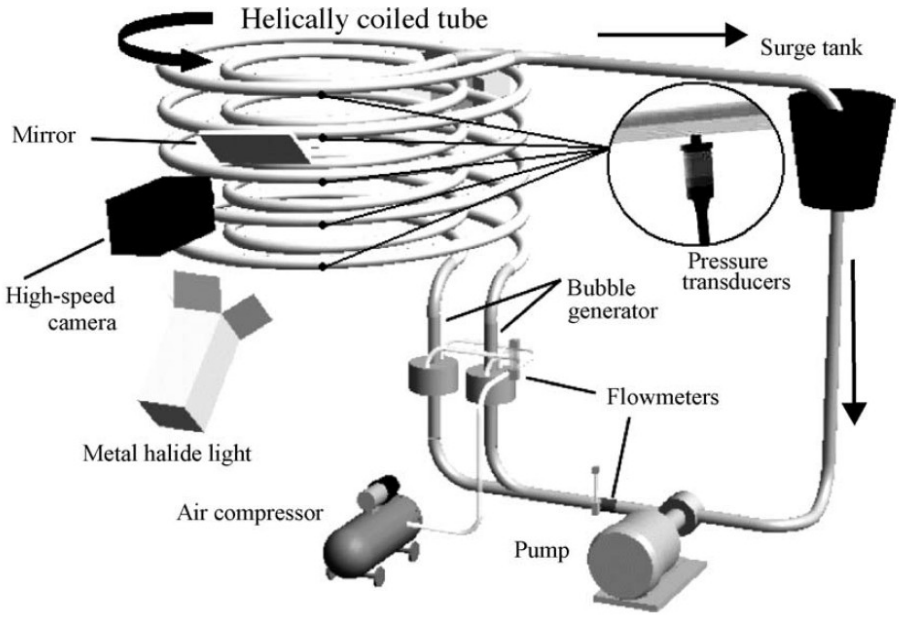

Figure 3.12: Experimental set up (Murai et al., 2006).

Figure 3.13 illustrates slightly elevated transition line between bubbly and plug flow (45°line) for increased curvatures. Murai et al. (2006) states that the reasons was due to enhanced bubble coalescence in the curved pipes, as a result of increased bubble collision frequency induced by secondary flow in the liquid phase. Additionally, it was observed that air bubbles accumulated in the inner region of the curved pipe also enhancing coalescence. This reduced the required axial flow length to achieve transition from bubbly to plug flow.

Other results from the study were presented in time-expansion images. This enabled to study the fluid distribution throughout one complete loop, as several sub-pictures with short time intervals were joined in one picture. For plug flow regime, the front part of air plugs pointed outwards through the loop, while the rear part of the plugs were located in the inner region. The reason was assumed to be that the highest axial velocity is biased to the outer half of the pipe cross-section because of secondary flow in the liquid part in front of the plug. Another observation was that the effect of increased liquid flow rate, or decreased curvature radius, shortened the interval distance between two air plugs. For cases with high total superficial velocity (>3 m/s), the air phase was mainly located in the inner pipe region due to the average static pressure gradient caused by the centrifugal force.

Analysis of phase velocities proved interesting results. For straight pipes, the gas phase has

similar -or higher- flow velocity than the total superficial velocity. For high velocities in curved pipe flow, the air phase accumulated in the inner region allowing the liquid phase to accelerate without obstruction of air bubbles in the outer region. This caused a negative slip effect by the air phase on the water phase.

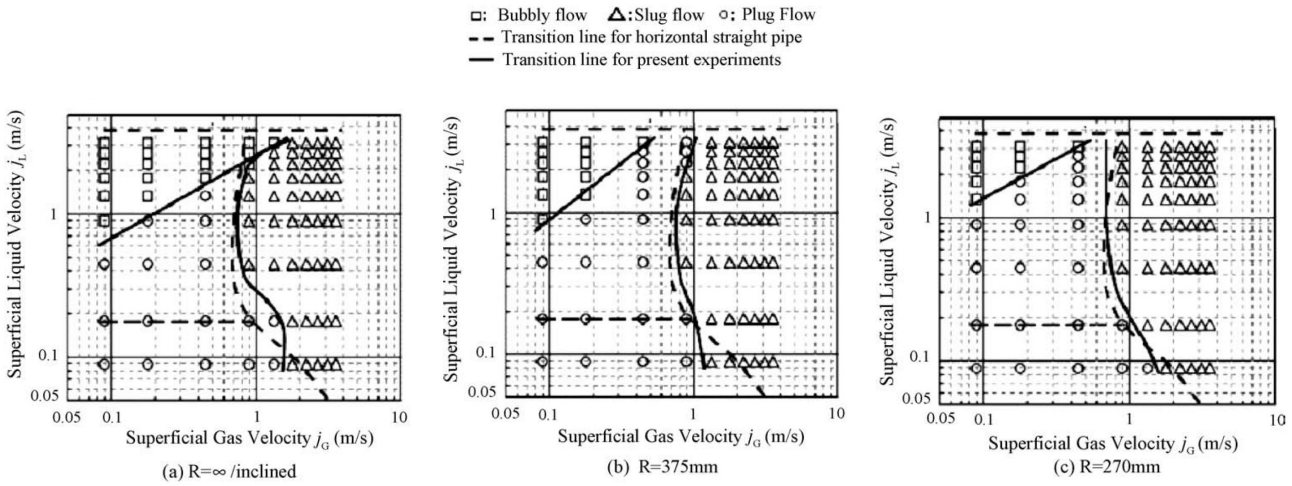

Figure 3.13: Flow regime maps for (a) straight inclined pipe, and helically coiled pipes with curvature radius of (b) 37.5 cm and (c) 27.0 cm (Murai et al., 2006).

3.6.3 *Gas-Non-Newtonian Liquid Two-Phase Flow in Helical Coils*

The publication *Gas-Non-Newtonian Liquid Two-Phase Flow in Helical Coils* by Mujawar and Rao (1981) presents an experimental study on flow patterns, holdup, and pressure drop. The experimental setup featured a pipe with 12.1 mm inner diameter, coiled at curvature radius of 8.2 cm, 12.7 cm, 30.5 cm, and 60.5 cm. The gas phase in the experiment was air, while the liquid phases were water and two aqueous polymer solutions. Gas superficial velocities were in the range 0.1-12 m/s, and liquid superficial velocities in the range 0.017-1.89 m/s.

For the interest of this report, the results of the flow pattern study are elaborated. The flow regimes observed for low and medium water rates with increasing air rate were elongated bubble, stratified, slug, and annular mist. For high liquid water rate with low to medium air rates, dispersed bubble and slug flow were observed. The stratified flow regime in straight pipes observed for low air and water rates, differed from the coiled pipe flow as it was affected by centrifugal forces, resulting in *"early onset of slug flow"*. In addition, Mujawar and Rao (1981) states

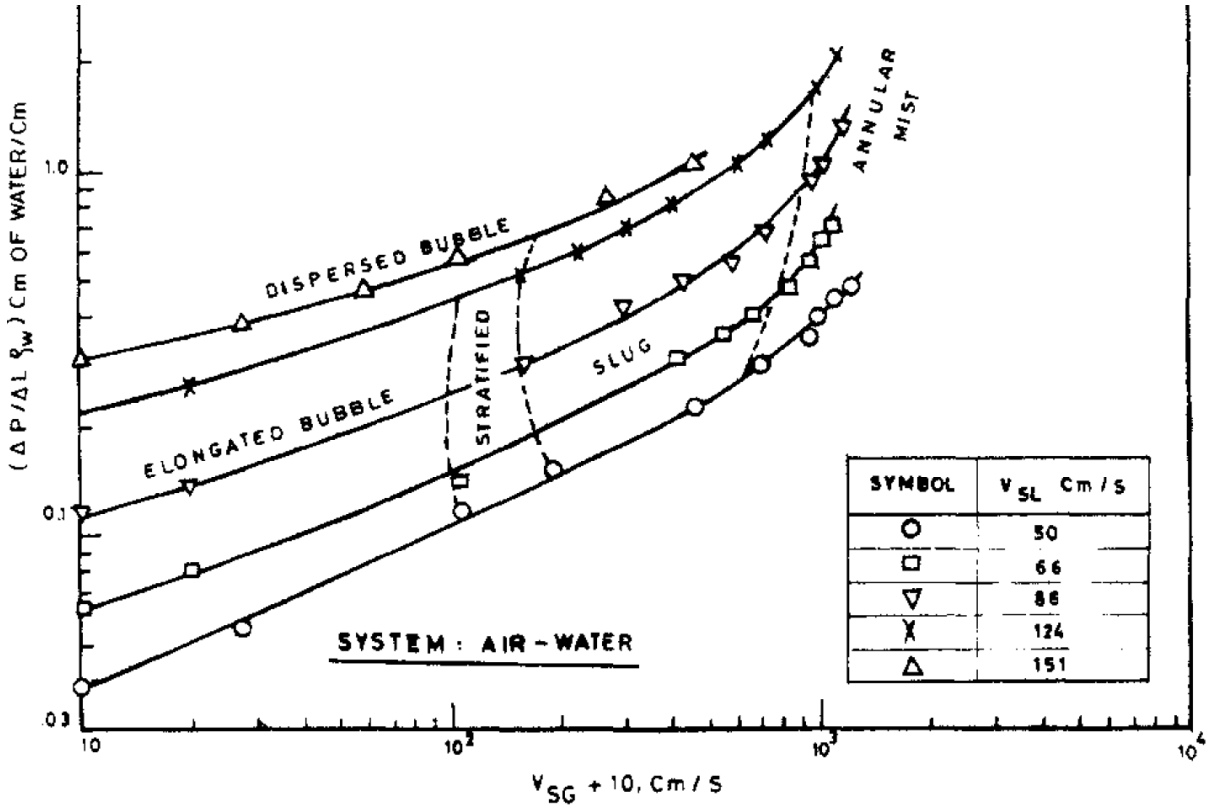

Figure 3.14: Flow regime map for helical coil with curvature radius of 8.2 cm. Excerpt of figure in publication by Mujawar and Rao (1981).

that *"the slug flow was found to be more dominant in the helical coils and the stratified flow was confined to a narrow gas rate range"*.

For the coil with 8.2 cm curvature radius and liquid flow velocity lower than 1.24 m/s, the air velocity range with stratified flow was approximately between 1.1-1.8 m/s. For air rates below this value, the flow regime had elongated bubbles. For liquid flow velocity of 1.51 m/s, the dispersed bubble flow developed to slug flow above approximately 1.8-1.9 m/s.

3.6.4 *Experimental Research and Numerical Simulation on Gas-Liquid Separation Performance at High Gas Void Fraction of Helically Coiled Tube Separator*

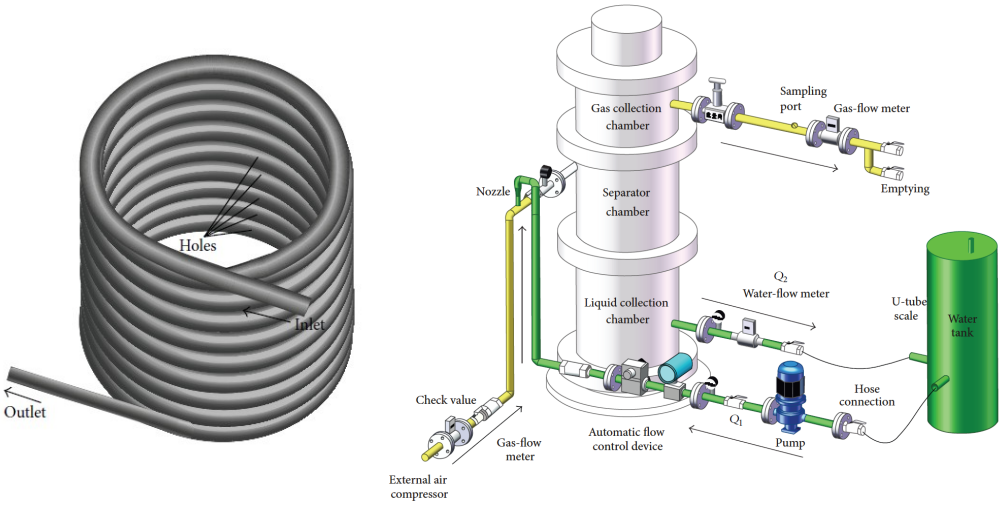

Figure 3.15: Helical pipe separator unit (Zhang et al., 2014).

Zhang et al. (2014) presents an experimental and numerical study of gas-liquid separation in helical coils, aimed to simulate separation of denser phases from wet natural gas. A nine-loop helically coiled pipe with inner diameter of 25 mm and a curvature radius of 15.0 cm was used. Figure 3.15 illustrates the helical coil and the experimental set up, also showing the downwards flow direction in the coil. Gas-phase drainage holes were made on the inner pipe region from the 5th loop of the coil. The holes diameters were 3 mm and they appeared at every quarter (90°) of each loop, located 3°above horizontal centre of the cross-section.

The simulated wet gas flow was made with compressed air flow and a nozzle for injection of atomised water. At the inlet of the separator the air-water mixture flow velocities ranged from 5-18 m/s, and air void fractions ranged from 88-97%.

Figure 3.16 illustrates the effect of inlet velocity and void fraction on the achieved separation efficiency. For constant void fractions and increasing flow velocity (left plot), an increase of separation efficiency evolves until 13 m/s. At this point, for void fraction of 93%, the highest efficiency of 95.2% was achieved. Increase of velocity from 13-15 m/s seemed to decrease the

efficiency, again followed by an increase of efficiency for velocities above 15 m/s. Zhang et al. (2014) explained this as the increase of velocity caused increase of centrifugal force, which enhances the separation effect. Simultaneously the increased velocity caused breakage of droplets, i.e. decrease of liquid droplet size, which decrease the efficiency.

For constant velocities and increasing void fraction (right plot), a similar efficiency pattern is observed. For all four velocities, the maximum efficiency is reached in the range 93-94% void fraction. Zhang et al. (2014) states that larger void fraction force liquid droplets toward the pipe wall, and forms a pure gas-core in the centre of the pipe, both enhancing the separation. Further increase of void fraction decrease the efficiency due to causing a liquid mist flow pattern, allowing the gas phase to extract liquid through the drainage holes.

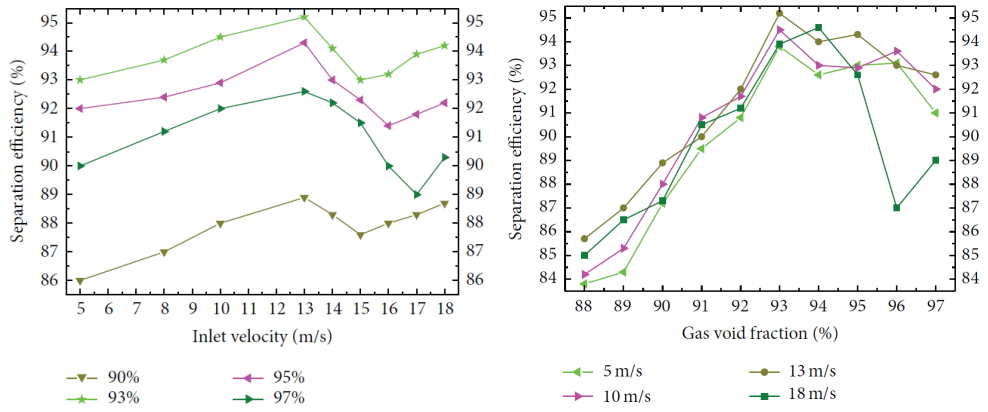

Figure 3.16: Effect of inlet flow velocity and void fraction on separation efficiency. The left plot illustrates the effect of increased flow velocity at four constant void fractions, the right plot illustrate the effect of increased void fraction at four constant inlet velocities (Zhang et al., 2014).

3.6.5 *An Investigation on Oil/Water Separation Mechanism inside Helical Pipes*

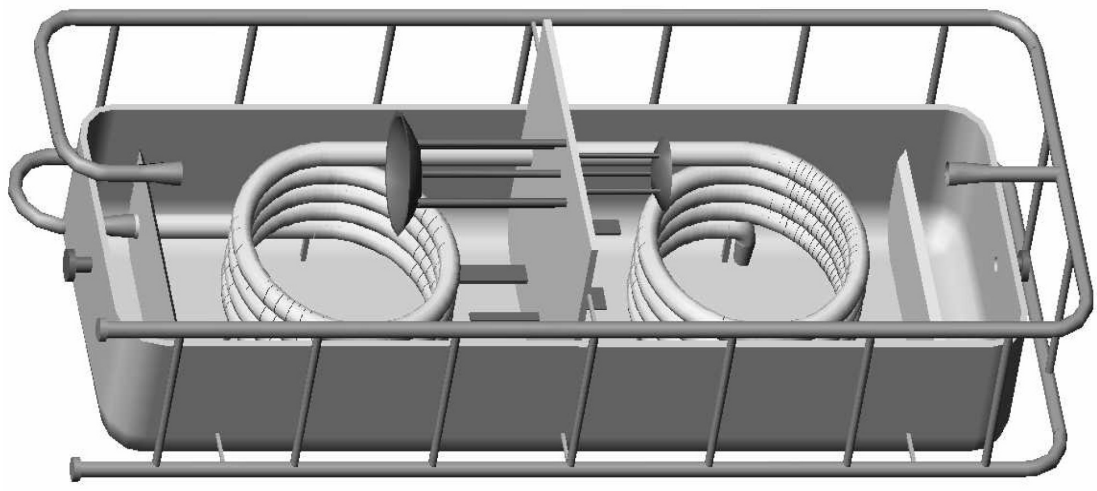

Figure 3.17: Helical pipe separator unit (Zhang et al., 2006).

The report *An Investigation on Oil/Water Separation Mechanism inside Helical Pipes* (Zhang et al., 2006) consider an oil-water separation unit as shown in Figure 3.17. The main component of the unit is a helical coil with several loops, featuring water drainage holes along the outer walls of the pipe. Numerical simulation was conducted with CFD-software, based on the Euler-Euler model and a discrete phase model. The water phase was considered as droplets in a primary phase of oil.

Two numerical simulation was conducted, the latter with improvements learnt from the first. The first simulation was performed without drainage holes. Results confirmed the effect of droplet size, where larger water droplets gave quicker phase segregation. For droplet diameter of 5 mm, high water fraction in the lower and outer part of the pipe was obtained after one loop. Additionally geometrical upgrades were made, including shorter curvature radius (40.0 cm to 15.0 cm) and smaller inner pipe diameter (40 mm to 22 mm).

The second simulation included 18 water drainage holes in the last three loops out of 15.5 loops. The drainage holes resulted in a change of oil volume fraction, from 44 % at coil inlet to 64 % at the coil outlet.

The practical experiment was conducted on two different coil geometries and two different

oil types. The first geometry had curvature radius of 40.0 cm and inner pipe diameter of 40 mm. The second had curvature radius of 15.0 cm and inner pipe diameter of 25 mm. The main difference of the two oil types was the viscosity being 20 cP and 70 cP, with respective densities of 836 kg/m^3 and 874 kg/m^3.

An important result from one of the experiments is that the low viscosity oil, in combination with high flow rate, had no separating effect. This indicates that a stable accumulation of water phase in the outer pipe section was not obtained, and not only water was drained. For the experiment with the same oil but smaller pipe diameter, higher flow velocity gave higher centrifugal force resulting in a water cut reduction of 22 %. As a comment on the experiments on the high viscosity oil, the report concludes that the number of drainage holes caused significant reduction of flow rate. Even though the water cut was reduced with approximately 80%, the flow rate at the outlet was far below an acceptable level.

3.6.6 *Apparatus and Method for Separating Water from Crude Oil*

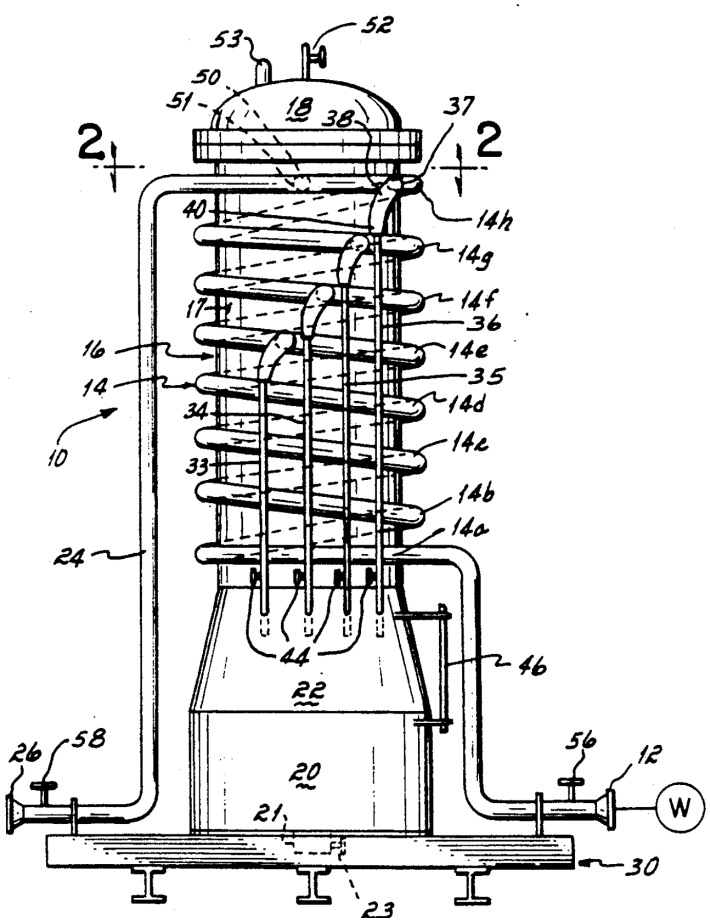

Figure 3.18: Apparatus for separating water from crude oil (Al-Yazdi, 1991)

The figure shows the complete idea of a vertical spiral separator unit. A flow containing water and oil, for example a well stream, can be led to the lower right inlet numbered 12 on the figure. The flow is led into several loops, going upwards in the helical coil. The upward configuration is said to enhance the separation efficiency, contrary to a downward configuration. As water droplets are continuously forced downward in the circular pipe cross-section, the droplets are swept along the pipe wall outwards and upwards when flowing in the coil. The total force on the fluid changes angle as the gravitational force is accompanied by the centrifugal. The centrifugal force will be strongest for the densest liquid. Accumulation of liquid with high density in the outer section of the pipe is obtained. This unit is designed with a helical coil of totally seven whole loops. The last four loops are meant to be equipped with drainage points at the outer section of the pipe, one for each loop. At the outlets, mainly the densest phase will be drained

from the coil and collected in the tank located in the centre of the coil structure. Fractions of the lighter phase collected in the tank will accumulate as an upper layer in the tank, caused by gravity settling. The light phase can be led through a return line from the upper region of the tank back into the coil pipe.

3.7 Discussion of the Helical Coil Principle

To obtain a compact separation system, the principle of utilising centrifugal forces is considered the most applicable. The efficiency of the gravity settling principle is dependent on large separator vessels due to the required residence time. The driving force achieved in a centrifugal separator is larger than the gravitational force, therefore reducing the required residence time and vessel size.

The compact separation system is convenient for topside facilities striving for limited space. For subsea installations, reducing the size of the system will lower the overall cost of the subsea station, allow for deeper water applications, and enable more agile interventions. However, Hannisdal et al. (2012) states that *"reducing the size of separators generally reduce the separation performance and the robustness to handle fluctuations in flow rate and composition"*. Compact separation system brings both advantages and challenges, which emphasise the need of further research and development of the technology.

The method of using helically coiled pipes for enhancing centrifugal forces is not commercially applied, but research and experiments show promising effects.

The optimal effect of introducing a multiphase flow to a coiled pipe would be to achieve a stable and layered phase distribution. It is critical to obtain a reliable phase distribution, enabling to separate or drain the different phases. da Mota and Pagano (2014) presented experimental results for air-water flow in a one-looped coil, showing a transition from bubbly to wavy stratified flow pattern. Murai et al. (2006) presented results on air-water flow in five-looped coils and observed accumulation of air bubbles in the inner region of the pipe. This proved that buoyant forces act on the bubbles and cause migration towards the centre of the coil. He further states that bubble coalescence is enhanced in curved pipe flow due to occurrence of secondary flow, which may explain the accelerated transition away from bubbly flow. However, both Murai

et al. (2006) and Mujawar and Rao (1981) report that the transition from bubbly flow patterns mainly result in plug or slug flow[2]. It seems as the flow regimes are dominated by the individual gas and liquid flow rates, but also depends on factors like coil radius, number of loops, and pipe diameter.

Regarding subsea applications, the cyclone separators are vessel-based systems and require more attention due to ambient pressure. The in-line systems are based on more robust T-pipe design, but still require internal swirl-elements and separation chambers. A helically coiled pipe would possess similar pressure containment capabilities as regular pipes, and does not require internal elements, making it more suitable for subsea installations. The coiled pipe itself would be the only required feature to achieve centrifugal forces and separation effects.

Existing centrifugal separators normally discharge the separated phases through individual pipe outlets for each phase. Discharge of phases in a helical coil is proved possible by drainage holes in the pipe wall. Zhang et al. (2006) performed experiments with oil-water flow, utilising coils with drainage holes in the outer pipe wall to discharge the denser water phase. The oil-water separation obtained maximum water cut reduction of 80%, but the amount of drainage holes caused substantial reduction in total flow rate. Zhang et al. (2014) performed experiments with air-water flow, at high void fraction, utilising coils with drainage holes in the inner pipe wall discharging the air. By tuning the air void fraction and total flow velocity, a separation efficiency of 95.2% was obtained.

Depending on the achievable effects in a helical coil, the practical application could be phase separation or flow conditioning. The project group desires to observe the coiled pipe flow phenomena, and study the possibilities of using a helical coil as a phase separator. Additionally, it is desired to investigate whether the air-water experiments can represent a full-scale hydrocarbon production scenario.

[2] Mujawar and Rao (1981) observed stratified flow pattern only for a narrow range of gas flow rate.

Chapter 4

Experimental Study

This chapter describes the laboratory experiments conducted in this project. The chapter includes description of the experimental set up, study of required coil geometry, how results were obtained, and details on the execution of the experiments. At last, the obtained results and effect of various parameters are discussed. A complete overview of measurements and observations are found in Appendix A.

4.1 Experimental Set Up

Simplification of the experimental set up was considered while putting the main goals in perspective. Configuration of a simple system included operation with one cohesive pipe that allowed for simple replacement to change pipe diameter, and modification of number of loops, and curvature radius. The helical coil section was required to be transparent such that identification of flow characteristics, and the flow development in the helical coil could be studied and documented. In order to fulfil these criteria the pipe had to be flexible and transparent. The simplest and cheapest solution was to use a PVC-hose for the experiments.

Tap water was used as water source, hence the water flow rate was limited by the performance of the tap water system. An air compressor system worked as the air source for the experiment. Separate pipes from the water and air sources were led to a commingling point, consisting of a T-pipe with two inlets, one for air and one for water. Each inlet was equipped with a control valve for flow regulation. Upstream the commingling point, the water flowed through

a 3/4 inch pipe and the compressed air flowed through a 1/2 inch pipe. These pipes were fixed without further adjustments. In the T-pipe, the two phases were commingled and a multiphase flow containing air and water was obtained. The commingled phases flowed from the T-pipe to the helically coiled pipe section. For most variations of flow rates, the flow regime upstream the helical coil was recognised as a bubbly flow.

To enhance the quality of the experiments and control the water and air flow rates, flow metering instruments were installed. A turbine meter was used to measure the water flow rate, and a mass flow meter was used to measure the air flow rate. The flow meters were installed upstream of each flow control valve at the T-pipe inlets.

The commingled phases flowed from the T-pipe outlet through the transparent PVC-pipe until it reached the helically coiled section. Approximately 30-40 cm upstream and downstream of the coiled section was fixed as straight pipe sections. From here, the two-phase stream went through about 10-12 m of pipe, and exited into a drainage pool.

The helical coil section was desired to enable quick and simple re-configuration. This was obtained by coiling the flexible PVC pipe around cylindrical objects for any number of loops. To fix the coil geometry for each configuration, tape and strips proved to be sufficient up to a certain level of air flow rate. High air flow rates caused heavily pulsating flow. The total length of the flexible pipe enabled to coil as many loops as desired around the objects. With this solution, different number of loops and curvature radii could be examined in a short amount of time.

4.2 Helical Coil Geometry

The helically coiled pipe section was required to apply a significant centrifugal force to the multiphase flow. From the equation of circular motion, the centrifugal acceleration is governed by tangential flow velocity, v, and the curvature radius, R, of the coil. Higher velocity and smaller radius cause higher centrifugal acceleration. Equation (4.1) is used to calculate the amount of centrifugal acceleration obtained by the different flow scenarios in terms of ratio to gravitational acceleration, g. Figure 4.1 illustrates the ideal helical coil geometry and the main dimensioning parameters.

$$a = \frac{v^2}{Rg} = \frac{Q^2}{A^2 Rg} \tag{4.1}$$

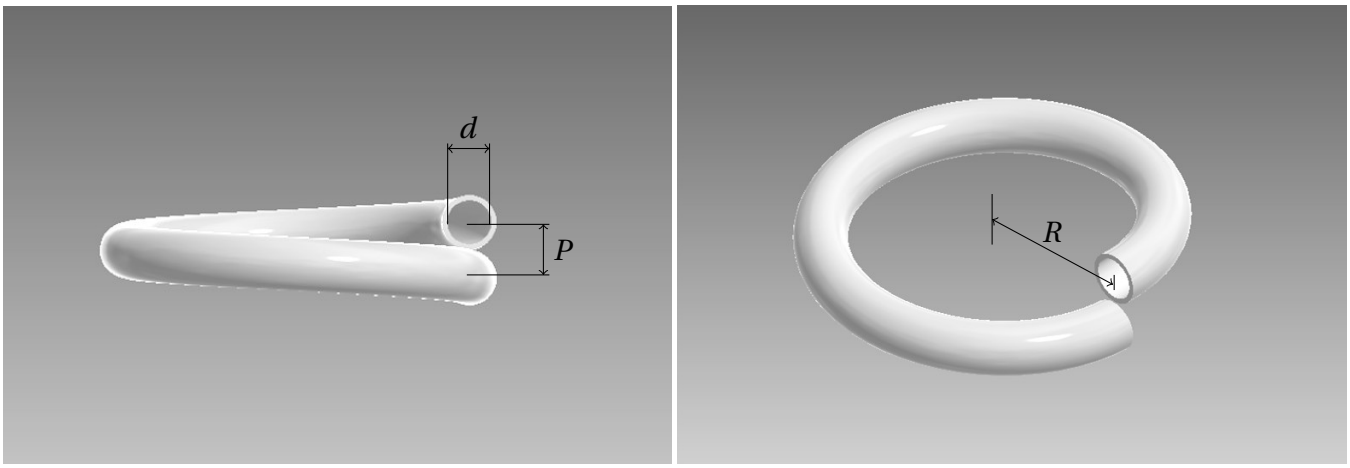

Figure 4.1: Illustration of parameters describing the helical coil geometry, where d is the inner diameter of the pipe, P is the pitch, and R is the curvature radius.

Table 4.1 shows theoretically obtainable centrifugal acceleration for three different pipe diameters, as a function of curvature radius and fluid flow rate. When selecting pipe diameter for the experiments, the limited flow rate from the tap water system had to be considered. As seen in Table 4.1, a 1 inch pipe diameter requires significantly larger flow rate than the smaller diameters to obtain high centrifugal acceleration. In order to reach an interesting amount of centrifugal acceleration, 3/4 and 1/2 inch pipes were selected. The obtainable higher levels of centrifugal acceleration for these diameters were assumed sufficient to give an indication of phase separation potential. A potential problem with the smaller diameter was thought to be the visibility of phase distribution.

Due to uncertainty of required centrifugal exposure time to achieve phase separation, adjustable number of loops in the helical coil was desired. The studies conducted by da Mota and Pagano (2014) and Zhang et al. (2006) indicated that phase separation effects could be observed within one loop, depending on density difference and droplet/bubble size of the phases. In the experiment of this report, the density difference was large (air and water) but droplet/bubble sizes were arbitrary. Hence the effect of various numbers of loops was studied. Another uncertainty was the effect of pitch length, but (da Mota and Pagano, 2014) stated that the pitch of the

Table 4.1: Table of obtainable centrifugal acceleration.

Pipe diameter	Curvature radius	Centrifugal acc. (g)			
		10 l/min	20 l/min	40 l/min	60 l/min
1/2"	0.05 m	3.5	14.1	56.5	127.0
	0.10 m	1.8	7.1	28.2	63.5
	0.15 m	1.2	4.7	18.8	42.3
3/4"	0.05 m	0.7	2.8	11.2	25.1
	0.10 m	0.3	1.4	5.6	12.5
	0.15 m	0.2	0.9	3.7	8.4
1"	0.05 m	0.2	0.9	3.5	7.9
	0.10 m	0.1	0.4	1.8	4.0
	0.15 m	0.1	0.3	1.2	2.6

helical coil had low influence on fluid behaviour. With this in mind, the solution to enable easy adjustment of number of loops in the experiments was to let each loop rest on the loop below. Then the pitch would equal the outer diameter of the pipe, and changing the number of loops could be done quickly without any additional adjustments.

To change the curvature radius during the experiments, different circular objects for which the pipe could be coiled around were required. Configuring the helical geometry in this manner was left to objects available. The main criteria for the elements were uniform cylindrical, or conical, outer shape, and if possible some weight for stability. Several randomly found objects appeared to fulfil the criteria, including plastic and metal trashcans, and smaller sized paint cans. Mainly three different objects were selected for the experiments, with curvature radius ranging from 4.9-18 cm.

4.3 Obtaining Data

The data from the experiments was obtained by observation and flow rate measurements. An overview of the data is found in Appendix A. Visual observations was logged by the project group during the experiments and captured with close-up photographs of the transparent pipe. The

photographs enabled to distinguish between the air and water phases inside the pipe, making it possible to observe potential phase segregation. To follow the flow regime development through the helical coil, photographs was taken at the straight pipe section upstream the helical coil, at 90°-, 180°-, and 270°angels of the helical coil, and at the straight pipe outlet downstream of the coil. When possible, the pictures were shot from side and top view of the current pipe section. This was not possible in the case of more than one loop due to the second loop overlap the previous and so on.

The camera used was a Canon EOS 650D with 18-55 mm lens and most pictures were captured with flash, 1/200 s shutter speed, and a resolution of 18 mega-pixels. The shutter speed of 1/200 s (5 ms) was sufficient to avoid motion blur in the pictures. Attempts with video recording of the flowing fluids were performed, but available video-equipment had maximum recording frequency of 120 frames per second. This was insufficient to follow the sudden change of motion in the water-air flow.

Measurement of water flow rate was performed with a turbine meter, installed in the water feed line upstream the commingling point of water and air. The working principle of the turbine meter is the transition of linear liquid motion to angular rotation of a rotor. The liquid acts on a freely spinning multi-bladed rotor inside the flow meter housing. The angular rotation velocity of the rotor is directly proportional to the volumetric flow rate (Liptak, 1993). RS Components delivered the turbine meter used in the experiments and details are found in Appendix A. The flow meter generated an output signal value in volts, which was converted to volumetric flow rate. The signal was read off with a connected multimeter, where the range 2-10 V corresponded to 0-100 l/min.

Measurement of air flow rate was performed with a thermal mass flow meter, installed in the air feed line upstream the commingling point. The working principle of the thermal mass meter is measurement of temperature difference between two heated resistance thermometer elements. As the air flow rate increases, the difference in temperature between the two elements increase (Bronkhorst High-Tech, a). Details on the mass meter is found in Appendix A. Similar to the turbine flow meter, a multimeter was connected to the mass meter to read off output signal voltage, which was converted to volumetric flow rate. The range 0-5 V corresponded to 0-30 l/min.

During the execution of experiments, each set of measured values and captured observations was logged and marked with the same time. This enabled post-experiment analysis between the different sets of measurements and observations.

4.4 Characterisation of Flow Regimes

Table 4.2: Flow regime characteristics for experiments

Flow regime types

Character	*Description*
B	Bubbly
B+	Bubbles coalesced (larger bubbles / small pockets)
P	Plug / transitional (large air pockets)
S	Slugs (very large air pockets, top to bottom of pipe)

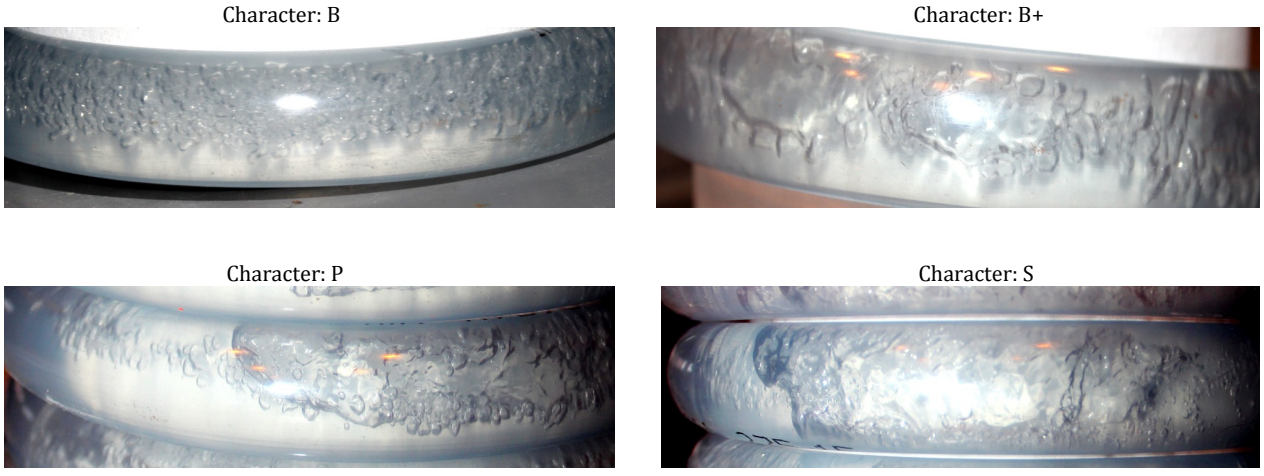

Figure 4.2: Flow regime characteristics

In order to give a simple description to every measurement during the experiments, they were given a character describing the flow regime. The different characterisations are shown in Table 4.2. Flow regime descriptions together with flow rate measurements was used to analyse the phase distribution for a variety of coil configurations and different flow rates.

Figure 4.2 refers to each flow regime character as captured in photographs during the experiments. Character B is clearly identified by a continuous steady flow with small air bubbles and evenly distributed throughout the loop. Character B+ describes a steady flow, but coalescing of air bubbles forms larger bubbles or small air pockets. The character P describes transition to unstable or pulsating flow, recognised with large air pockets forming plugs in the system. At last, character S describes heavy unstable flow with very large air pockets forming alternating air plugs and water slugs.

4.5 Execution of the Experimental Study

The first phase of the experiment regarded assembly of the system, testing, observation and adjustments in order to get familiar with the system. This included testing of camera settings and background to optimise documentation of the experiments. For all the different experiments, the flow regime upstream of the helical coil was recognised as bubbly flow.

The experiments started with a 3/4 inch pipe, as this was believed to show phase distribution in the coil better than smaller diameter pipes. Testing of this system gave results that were somewhat unexpected. The system experienced heavy pulsation when reaching a certain level of air flow rate. Above this level the flow characteristics became increasingly unstable, resulting in a slug-like flow. Stable flows were only obtainable for small amounts of air in the system. After an evaluation of this experiment the pipe diameter was reduced. The reason for unstable flow was thought to be low centrifugal acceleration, and the 3/4 inch pipe was difficult to coil around smaller curvature radii. The rest of the experiments were conducted with a 1/2 inch pipe, which had improved flexibility for coiling around smaller curvature radius and additional number of loops. The 1/2 inch pipe also ensured higher centrifugal acceleration, due to higher flow velocity, which hopefully enhanced the phase separation.

4.5.1 Ex.1 - 3/4 inch pipe and 18 cm curvature radius

The first experiment included a 3/4 inch transparent pipe helically coiled in one loop. Table 4.3 present the experimental results calculated from flow rate measurements for each phase. For all measurements the water flow valve was opened 100%, although the water flow rate was affected

Table 4.3: Experiment 1 - 3/4 inch pipe and 18 cm curvature radius

Experiment 1	ID	q_w	q_g	q_{tot}	α	a	Regime
	[-]	[l/min]	[l/min]	[l/min]	[-]	[g]	[-]
1 loop	1.1	51.88	0.00	51.88	0.000	5.2	-
	1.2	50.75	0.22	50.97	0.004	5.0	B+
	1.3	50.13	0.73	50.86	0.014	5.0	P
	1.4	49.81	1.95	51.76	0.038	5.2	S
	1.5	49.56	3.65	53.21	0.069	5.5	S
	1.6	49.50	7.04	56.54	0.124	6.2	S

as air was let into the system. When trying to add number of loops around lower curvature radii, the 3/4 inch pipe suffered deformation of cross-sectional geometry.

The 3/4 inch pipe ensured a high volumetric flow rate through the system, reaching 56.5 l/min. However, even at the highest total flow rate, the centrifugal acceleration reached only 6.2 g. This implied a smaller amount of separation force working on the flow through the helical coil. Explicitly, Table 4.3 expresses the separation quality in flow regime characteristics.

Throughout the observation of the experiment, the coil seemed weak towards air flow. Increasing the amount of air into the system soon showed problematic as bubbles easily coalesced into larger air pockets.

For an air flow rate as low as 0.22 l/min stable separation was achieved around the loop. As the air rate was increased to 0.73 l/min the flow became unstable, transforming to plug flow with larger air pockets. At 1.95 l/min, slug flow occurred after the first quarter of the loop. When reaching 3.65 l/min the flow had slug formation at inlet, throughout the coil, and after. Increasing the air flow further resulted in more intense and chaotic slug flow.

The execution of this experiment revealed relatively low centrifugal acceleration in the helical coil and low threshold against unstable flow characteristics. The flow regime evolved towards plug and slug flow even at low air rates, hence this system appeared to be unable to separate the two phases.

4.5.2 Ex.2 - 1/2 inch pipe and 16.1 cm curvature radius

Table 4.4: Experiment 2 - 1/2 inch pipe and 16.1 cm curvature radius

Experiment 2	ID [-]	q_w [l/min]	q_g [l/min]	q_{tot} [l/min]	α [-]	a [g]	Regime [-]
1 loop	2.1	32.63	0.00	32.63	0.000	11.6	-
	2.2	30.63	0.11	30.74	0.004	10.3	B
	2.3	26.88	1.38	28.26	0.049	8.7	B+
	2.4	25.00	2.74	27.74	0.099	8.4	P
	2.5	23.75	4.68	28.43	0.165	8.8	S
	2.6	23.13	8.20	31.33	0.262	10.7	S
3 loops	2.7	28.75	1.00	29.75	0.033	9.7	P
	2.8	25.63	4.40	30.03	0.147	9.9	S
6 loops	2.9	30.00	0.48	30.48	0.016	10.2	S

The reduction of pipe diameter from 3/4 to 1/2 inch increased the flow velocity and centrifugal acceleration. As seen in Table 4.4, the maximum total flow rate in this system was reduced with approximately 24 l/min compared with *Experiment 1*. The smaller diameter pipe enabled increased number of loops and to be coiled around lower curvature radius without significant deformation of the cross-section. The water control valve was 100% open throughout this experiment. The highest centrifugal acceleration achieved with multiphase flow was about 10.7 g, almost two times that in *Experiment 1*. Transition to unstable plug flow occurred at an air flow rate of 2.74 l/min, in the last quarter of the loop. Comparing this with *Experiment 1*, the amount of air should be in terms of void fraction due to different diameters and total flow rate. This proved that plug flow in this experiment appeared at almost 10%, compared to about 1.4% in *Experiment 1*.

Despite the improvement, plug and slug flow was still an issue when air flow rate exceeded 2.7 l/min. When increasing the number of loops in the coil from one to three, the threshold for appearance of plug flow was reduced to about 1 l/min, or 3.3% void fraction. Increasing the number of loops to six resulted in heavy slug flow in the coil already at air flow rate of 0.48

l/min, or 1.6% void fraction. Because of these observations, decreasing the curvature radius further was desirable to see if the separation effect could be improved.

This helical coil configuration proved some potential, as to be a more robust separation system. Causes are related to the reduction of pipe diameter, which increased the flow velocity and the centrifugal acceleration. Increasing number of loops in the helical coil resulted in slug flow at lower air flow rates than for one loop.

4.5.3 Ex.3 - 1/2 inch pipe and 8.6 cm curvature radius

Table 4.5: Experiment 3 - 1/2 inch pipe and 8.6 cm curvature radius

Experiment 3	ID	q_w	q_g	q_{tot}	α	a	Regime
	[-]	[l/min]	[l/min]	[l/min]	[-]	[g]	[-]
1 loop	3.1	32.63	0.00	32.63	0.000	21.8	-
	3.2	27.19	2.38	29.65	0.080	17.9	P
	3.3	23.75	7.31	31.06	0.235	19.7	S
3 loops	3.4	29.38	1.66	31.04	0.054	19.7	P
	3.5	25.13	4.40	29.53	0.149	17.8	S
6 loops	3.6	29.50	1.07	30.57	0.035	19.1	S
	3.7	27.50	2.44	29.94	0.082	18.3	S
	3.8	25.00	7.35	32.35	0.227	21.4	S

This experiment was conducted with 1/2 inch pipe and a curvature radius of 8.6 cm. The reduction of curvature radius from 16.1 cm in *Experiment 2*, approximately doubled the obtained centrifugal acceleration. Table 4.5 shows that the highest centrifugal acceleration for multiphase flow was 21.4 g. One, three and six loops in the helical coil were tested and the water valve opening was kept at 100% throughout the experiment.

For one loop coil at an air flow rate of 2.38 l/min, equal to a void fraction of 8%, initiation of unstable plug flow started in the last quarter of the loop. Despite the decrease of curvature radius, this experiment showed no significant improvements related to robustness against plug

and slug flow formation. The result of adding number of loops proved similar to *Experiment 2*, where plug and slug formation occurred at even lower air flow rates.

4.5.4 Ex.4 - ½ inch pipe and 4.9 cm curvature radius

For this experiment the curvature radius was reduced to 4.9 cm, achieving a maximum centrifugal force of 43.3 g. Contrary to the previous experiments, the water valve opening was not only set to 100%, but also three different levels below 100%. In this case the number of loops in the helical coil was fixed at one loop. Table 4.6 shows 27 measurements with different levels of water and air flow rate.

In the case of water flow at *Level 1* the system was especially sensitive to increase of air flow rate. The total flow rate at this level ranged from 12-18 l/min, hence the centrifugal acceleration was mainly between 6-7 g. At 1.9% air void fraction the flow became unstable, and a mixture of large bubbles and plug flow was observed. Initiation of slug flow occurred at 5% air void fraction. Further increase of air flow rate resulted in slug regime with heavy pulsation. In *Level 2*, the increased water flow rate indicated higher robustness against slug flow. The total flow rate was in the range 18-22 l/min, with a corresponding centrifugal acceleration range of 12-17 g. Transition from bubbly to plug flow occurred at 3.9% air void fraction. Plug flow was dominating until an air flow rate of 3.84 l/min, equal to a void fraction of 19.1%, where the observations proved transition to slug flow regime.

In *Level 3*, the further increased water flow rate indicated an even more robust system. Total flow rate in this case ranged from 24-27 l/min. Stable bubbly flow was sustained at 4% air void fraction, while an increase to 8% void fraction caused transition to plug flow. Transition from plug to slug flow regime seemed to occur at about 26% void fraction.

In *Level 4*, the water control valve was fully open, and this appeared to be the most robust system. The total water flow rate was in the range 29-35 l/min, giving centrifugal acceleration between 32-43 g. A stable bubbly flow regime was sustained up to 5% air void fraction where initiation of plug flow was observed. Plug flow regime was dominating from 7-28% air void fraction. At about 33% void fraction a transition from plug to slug flow was observed at the outlet section of the coil.

Table 4.6: Experiment 4 - 1/2 inch pipe and 4.9 cm curvature radius

Experiment 4	ID [-]	q_w [l/min]	q_g [l/min]	q_{tot} [l/min]	α [-]	a [g]	Regime [-]
W(100%)	4.1	32.13	0.00	32.13	0.000	37.3	-
1 loop Level 1	4.2	12.63	0.24	12.87	0.019	6.0	B+/P
	4.3	12.38	0.66	13.04	0.051	6.1	S
	4.4	12.00	1.68	13.68	0.123	6.8	S
	4.5	11.38	2.28	13.66	0.167	6.7	S
	4.6	10.75	7.62	18.37	0.415	12.2	S
1 loop Level 2	4.7	18.75	0.12	18.87	0.006	12.9	B+
	4.8	17.88	0.72	18.60	0.039	12.5	P
	4.9	17.50	1.02	18.52	0.055	12.4	P
	4.10	16.63	2.28	18.91	0.121	12.9	P
	4.11	16.25	3.84	20.09	0.191	14.6	P/S
	4.12	15.25	6.48	21.73	0.298	17.1	S
1 loop Level 3	4.13	24.50	0.36	24.86	0.014	22.3	B+
	4.14	22.88	0.96	23.84	0.040	20.5	B+
	4.15	22.50	1.92	24.42	0.079	21.5	P
	4.16	21.00	4.20	25.20	0.167	22.9	P
	4.17	20.63	5.58	26.21	0.213	24.8	P
	4.18	20.25	7.14	27.39	0.261	27.1	P/S
1 loop Level 4 (100%)	4.19	30.25	0.36	30.61	0.012	33.8	B+
	4.20	28.13	1.62	29.75	0.054	32.0	B+/P
	4.21	27.25	2.28	29.53	0.077	31.5	P
	4.22	26.50	3.48	29.98	0.116	32.5	P
	4.23	26.00	4.98	30.98	0.161	34.7	P
	4.24	24.88	6.24	31.12	0.201	35.0	P
	4.25	24.38	7.89	32.27	0.245	37.6	P
	4.26	24.00	9.18	33.18	0.277	39.8	P
	4.27	23.19	11.43	34.62	0.330	43.3	S

This experiment revealed the importance of liquid flow rate in the multiphase flow system. Measurement 4.2 achieved tendencies to plug flow already at void fraction of 1.9%. However, gradually as the water valve was opened to 100%, the system did not experience slug flow until 33% air void fraction.

4.5.5 Ex.5 - ½ inch pipe and 4.9 cm curvature radius

Table 4.7: Experiment 5 - ½ inch pipe and 4.9 cm curvature radius

Experiment 5	ID [-]	q_w [l/min]	q_g [l/min]	q_{tot} [l/min]	α [-]	a [g]	Regime [-]
3 loops	5.1	30.88	0.42	31.30	0.013	35.4	B+
	5.2	28.94	0.99	29.93	0.033	32.4	P
	5.3	27.81	2.58	30.39	0.085	33.4	P
	5.4	26.50	4.08	30.58	0.133	33.8	P
6 loops	5.5	32.63	0.00	32.63	0.000	38.4	-
	5.6	30.38	0.68	31.06	0.022	34.8	P
	5.7	29.81	0.69	30.50	0.023	33.6	P
	5.8	28.63	1.59	30.22	0.053	33.0	P
	5.9	27.38	3.12	30.50	0.102	33.6	P
	5.10	26.63	3.86	30.49	0.127	33.6	S

This experiment was similar to *Experiment 4* besides the use of more than one loop. Table 4.7 shows the various measurements with three and six loops, and the water valve control fully open. As the previous experiments indicated, adding several loops to the coil resulted in transition from bubbly to plug and slug flow at lower air rates.

The three loop coil obtained plug flow at 3% air void fraction. No transition from plug to slug flow was experienced up to 13% void fraction.

With the six-loop coil, a stable bubbly flow was hard to achieve as the transition to plug flow occurred already at 2% void fraction. Transition from plug to slug flow initiated when reaching

13% air void fraction.

This experiment was mainly affected by heavy pulsating plug and slug flow occurring at low air rates. Because of the pulsation the helical pipe system itself became unstable, and testing of higher air rates did not seem useful.

4.6 Effects of coil configurations and flow rates

This section discusses the measurements and observations obtained during the experiments. The main focus is the flow behaviour and distribution of phases in the helical coil. The experiments were conducted for several helical coil configurations and various flow rates. The configuration parameters of interest are assumed to be the number of loops, the curvature radius, and the inside diameter of the pipe.

4.6.1 Effect of number of loops

The effect of number of loops on flow regime in the helical coil is discussed. To find potential effects of number of loops, other parameters that can affect flow regime have to be fixed. In this case the pipe diameter was 1/2 inch, the curvature radius 4.9 cm, and the water valve was fully open for all the studied measurements. Besides the number of loops, air flow rate was the only variable parameter. The pictures from the experiments were examined for each level of air flow rate, and the flow regime in the helical coil was studied. The approximate location of where transition from stable -smoothly distributed- bubbly flow to unstable bubbly-, plug-, or slug flow appears was obtained. The reason for not using bubbly, plug, or slug as the only flow regime indicators was due to the difference in flow behaviour from one loop coil to three and six loop coils. In the one loop coil, plug or slug flow was not possible to recognise, even for high air flow rates. In the three and six loops coils, deviations from stable bubbly flow was recognised as transition to plug and slug flow, as explained in Table 4.2. The difference between stable and unstable bubble flow distribution for the one loop coils are shown in Figure 4.3. The location of regime transition for the studied measurements are illustrated in Figure 4.4. Be aware of the different numbers of measurements -and different air flow rates- for each loop number.

Figure 4.4 clearly shows that one loop can take higher air flow rate than three and six loops

Figure 4.3: Flow regime in one loop coil. Left picture shows stable bubbly flow with smooth bubble distribution. Right picture shows unstable bubbly flow with irregular bubble distribution.

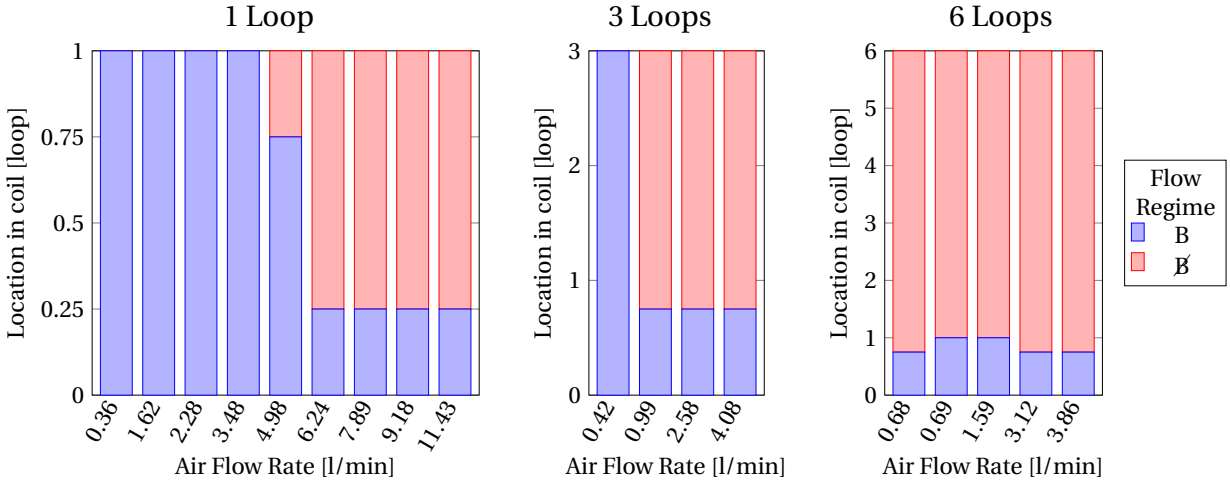

Figure 4.4: Effect of number of loops and increasing air flow rate in coils with curvature radius 4.9 cm and 1/2 inch diameter. Blue colour indicates stable bubbly flow. Red colour indicates unstable bubbly, plug, or slug flow.

without experiencing unstable flow. For one loop, unstable flow occurred for air flow rate somewhat above 3.5 l/min. The air flow range between 3.5-6.2 l/min seemed to move the point of instability from the last quarter to the first quarter of one loop. Further increase of air flow rate, above 6.2 l/min, did not seem to move the point earlier than the first quarter.

For three loops, unstable flow occurred for air flow rates above 0.4 l/min. The range of initiation of unstable flow was between 0.4-1.0 l/min. For rates above 1.0 l/min the location of instability appeared in the third quarter of the first loop.

For six loops, unstable flow occurred within the last quarter of the first loop for all measurements, even down to the lowest of 0.68 l/min. Stable flow through the coil was not achieved. Another experiment with six loops was studied for comparison, experiment 2.9 with curvature radius of 16.1 cm. This coil experienced initiation of unstable flow in the 4th loop at air flow rate

of 0.48 l/min. It was therefore considered likely that for air flow rates lower than 0.68 l/min one would observe initiation further downstream in the coil.

Despite the inability to determine accurately at which air flow rates the transition of flow regime occurred, the trend in Figure 4.4 is clear. Increased number of loops, giving increased coil length, lowered the limiting air flow rate for unstable flow.

A result of increased number of loops is the increased duration of which the flow is affected by centrifugal forces. The average duration for one fluid particle in each helical coil was 0.075 s, 0.23 s, and 0.46 s, for 1, 3, and 6 loops, respectively. The durations are calculated based on total superficial velocity, which was about 4 m/s for all the measurements in Figure 4.4. The prolonged duration in the coil may enable increased magnitude of secondary flow, as it requires some length to become fully developed. One important observation that disprove the reasoning above is the fact that despite increased number of loops, Figure 4.4 shows that the initiation of unstable flow occurs within the very first loop. Hence the fluids duration in the different coils - until instability occurs- are very similar, just at different air flow rates. An alternative explanation is proposed: increased number of loops, giving longer curved pipe length, causes an increase of total axial pressure gradient for the coil. This increases the local pressure in front of -and inside- the coil, which may enhance coalescing of air bubbles.

4.6.2 Effect of curvature radius

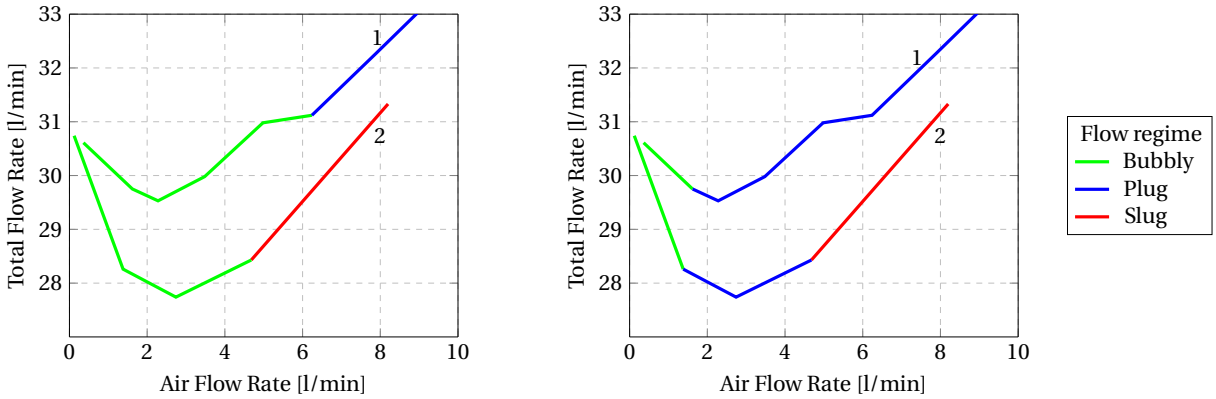

(a) Effect of curvature radius in the helical coil.

(b) Effect of curvature radius at the outlet of the helical coil.

Figure 4.5: Effect of curvature radius on flow regime in the coil and at the outlet of the coil. Curve 1 = 4.9 cm, and Curve 2 = 16.1 cm

The variation in curvature radius had an influence on the flow regime in the helical coil system. The diagrams below display the effect between two different curvature radii 4.9 cm and 16.1 cm. Both graphs represents the 1/2 inch pipe and one loop with the water control valve fully open. The graphs are plotted for total flow rate versus air flow rate. The flow characteristics are expressed throughout the plotted curves, where each colour represents a different flow regime.

Figure 4.5a and 4.5b shows deviation between the two plotted curves, both for total flow rate and flow regime. Curve 1, with curvature radius 4.9 cm, seems to resist the transition from bubbly to intermittent flow better than curve 2, as it occurs at a slightly higher air rate. In addition, curve 1 does not experience transition to slug flow within the tested air flow rates. In curve 2, with curvature radius 16.1 cm, transition from bubbly, or plug, to slug flow occurs for air flow rate of 4.6 l/min. The lowest curvature radius appears to enhance the robustness towards slug flow. One of the main differences between the curves is the centrifugal force, where curve 1 obtains 32-40 g and curve 2 obtains between 8-12 g.

The distinctions between the flow rates of the two graphs are assumed to be a result of pressure loss differences. As explained in section 2.8, and stated by White (2011), *"The separation and secondary flow losses decrease with R/d, while the Moody losses increase because the bend length increases"*. This indicates that the total losses, like the increased moody-friction losses for curve 2, exceeds the separation[1] - and secondary flow losses in curve 1. The cause is assumed to be that the length of curve 2 was approximately 100 cm, and curve 1 was only 30 cm.

The effect of decreasing the curvature radii is a significantly larger centrifugal acceleration. This implies a stronger separation impact on the two-phase flow. A shorter length of curvature decreases the total friction losses, giving higher flow rate. Despite that the magnitude of secondary flow essentially is larger in curve 1, due to its short curvature, curve 1 is still more resistant to slug flow. This could be explained by the results from Vashisth and Nigam (2009), where shorter curvature radii seemed to require longer developing length for the secondary flow, hence the secondary flow might not reach its full strength.

[1] Separation losses means that the fluid tend to flow away from the inner pipe wall, as a result of the sudden curvature, causing a low pressure drag zone

4.6.3 Effect of pipe diameter

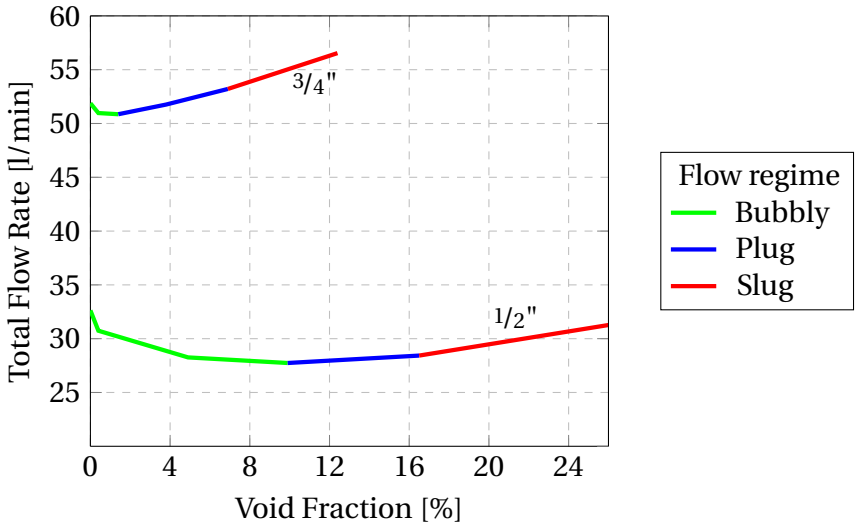

Figure 4.6: Effect of pipe diameter on flow regime in helical coil. Pipe diameter 3/4 inch, R = 18 cm, δ = 0.05. Pipe diameter 1/2 inch, R = 17.6 cm, δ = 0.04.

The effect of pipe diameter on flow regime is discussed. The experiments were performed with 1/2 and 3/4 inch diameters. The 3/4 inch pipe was tested with one loop coil, curvature radius of 18 cm, curvature ratio of 0.05, and fully open water valve. The most comparable 1/2 inch pipe coil configuration was with one loop coil, curvature radius of 17.6 cm due to the smaller pipe diameter, curvature ratio of 0.04, and fully open water valve. Figure 4.6 shows the helical coil flow regime for each pipe diameter as a function of increased void fraction. The 3/4 inch pipe experienced transition from bubbly to plug flow between 0.4-1.4% void fraction, corresponding to an air flow rate of 0.2-0.7 l/min. Increasing the void fraction further to about 7% resulted in slug flow. The 1/2 inch pipe experienced transition from bubbly to plug flow between 5-10% void fraction, corresponding to 1.4-2.7 l/min air flow rate. Plug to slug flow transition occurred within 16% void fraction.

There is a clear difference in flow regime transitions between the two pipe diameters. The 3/4 inch pipe has a short range of stable bubbly flow, and a low tolerance for increased air fraction, compared to the 1/2 inch pipe. An important issue as a result of diameter differences is the total fluid velocity, which is between 3.0-3.3 m/s for the 3/4 inch and between 3.7-4.3 m/s for the 1/2 inch. The difference in velocities correspond to centrifugal acceleration of 5-6 g in the 3/4

inch pipe, and 8-11 g in the 1/2 inch pipe. This gives reason to believe that higher centrifugal acceleration prolong the region with bubbly flow.

Due to only testing two different pipe diameters, and the unequal velocities and geometry, the effect of pipe diameter cannot be determined with certainty. Hence the effect of pipe diameter on flow regime in helical coils needs more comprehensive research.

4.6.4 Effect of air and water flow rates

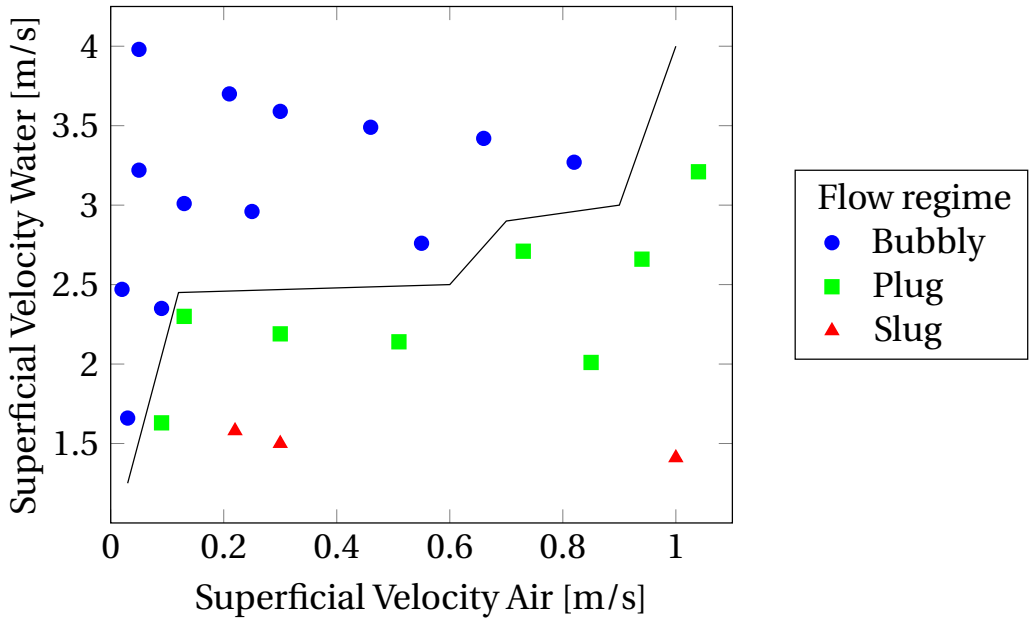

Figure 4.7: Effect of water and air superficial velocities on flow regime in one loop helical coil, with curvature radius 4.9 cm.

To study the flow regime in the coils for a wider range of water flow rates, a set of experiments were conducted with partly open water flow valve. The experiments were done with 1/2 inch pipe in a one loop coil with curvature radius of 4.9 cm. The process of obtaining measurements started with the air flow valve closed and adjusting the water flow rate to a certain level below maximum. When water flow rate was stabilised, the air flow valve was opened step by step. For each step of increased air flow rate, both flow rates and flow regime in the coil was logged. A total of three initial water flow rates below maximum were assessed. The results are presented in Figure 4.7, showing the flow regimes at various air-water velocities. The black line highlights the transition from bubbly to plug flow.

As Figure 4.7 illustrates, higher water flow rates can reduce occurrence of plug or slug flow at increasing air rates. At high water rates, the void fraction is low and the centrifugal forces are high. At low water rates the void fraction increases, and the centrifugal force decreases, which seem to strengthen occurrence of plug and slug flow.

4.6.5 Effect of helical coil orientation and geometry

Vertical and horizontal helical coil orientation were tested. Horizontal orientation was tested with inlet and outlet at upper and lower position. For the upper position, air was below water when reaching the coil outlet. At this point the gravitational forces overcame the centrifugal, bringing the air above the water phase. For the lower position, the air and water phase was distributed according to gravitational forces, when the centrifugal force subsided. Changing the orientation of the coil did not seem to affect the flow regime. The effect of coil orientation was examined visually, thus no specific remarks were achieved.

Cylindrical and conical helical coil geometry was briefly examined. An experiment was conducted with a six-loop coil and radii ranging from 17 cm to 15.7 cm. The changing radius did not seem to affect the flow behaviour. It is assumed that a larger change of radius is required to influence the flow. Again, the experiment was based on visual observation.

4.7 Discussion of Experimental Results

The experimental part of this report was aimed towards the study of utilising helically coiled pipes as a potential separator, or flow conditioner. The conducted experiments contained variations in flow rates, number of loops, curvature radii, and pipe diameters, in addition to the orientation and geometry of the helical coil. The study was based on flow regime behaviour, and phase distribution through the system. This section will discuss the applicability of the technique, and factors that would enable it to become successful.

For the helical coil principle to become an adequate phase separator, or flow conditioner, it would have to posses certain capabilities. The forces introduced in the coil would have to enable a separation mechanism on a multiphase flow, resulting in a distinct and layered phase distribution. It is essential to achieve a stable phase distribution in the system, allowing sepa-

ration of the different phases. To be a flow conditioner, the helical coil is required to affect the flow regime by reducing intermittent flow, or contribute in achieving other desired influences.

4.7.1 Occurrence of intermittent flow regimes

The governing issue with the air-water flow was the occurrence of intermittent flow regimes inside the coiled section. Murai et al. (2006) stated that the accumulation of bubbles in the inner pipe region allowed the liquid phase to accelerate without obstruction in the outer region, such that air had a negative slip effect on the water phase. This could be an explanation of the increased, and accelerated, occurrence of slug flow in curved pipes compared to straight pipes. Adding to the statement above, it was believed that if the water phase travels faster than air in the loop, the flow resistance downstream of the coil would counteract the acceleration, causing local water accumulation inside the coil, and result in formation of water slugs.

An alternative explanation to the phenomena was that a larger frictional force acts on the water phase in the outer pipe region inside the coil, reducing the water phase velocity. This could cause water build-up similar to the reasoning above, with the difference that it is a result of increased pipe wall friction.

The basic mechanism behind accelerated occurrence of intermittent flow in curved pipes is not further assessed in this thesis.

4.7.2 Factors influencing the flow regime

The flow characteristics in the helical coil were dependent on a combination of factors. The flow regime had a tendency to develop from bubbly to plug, or slug, as a result of increasing the air flow rate. For low water rates, even slightly increased air rates caused intermittent flow. At high water rates, a bubbly flow with stable phase distribution was maintained even for relatively high air rates. This effect is assumed to be because low water rates imply higher void fractions and lower centrifugal force because of reduced total flow velocity.

The effect of reducing the pipe diameter was a lower total flow rate, but increased total flow velocity. This significantly increased the limit of void fraction where bubbly flow developed to plug flow. The increased velocity, giving higher centrifugal force, seemed to be the main rea-

son for improving the flow characteristics. However, the effect of pipe diameter is considered uncertain due to the simplicity of this comparison.

Lowering the curvature radius, increasing the centrifugal force, improved the robustness against slug flow at high void fraction. The lowered curvature radius reduces the coil length, which seemed to slightly increase the flow velocity, indicating decrease of frictional pressure loss.

Adding number of loops, extending the coil length, increased the occurrence of plug and slug flow. The extended coil length caused higher frictional pressure loss, but also prolonged the residence time where centrifugal forces act on the phases. It is assumed that the higher frictional pressure loss enhance liquid hold-up, which could accelerate occurrence of plug and slug flow.

The coil configurations that essentially would give a larger magnitude of secondary flow were short curvature radii and high flow velocity. One would expect that secondary flow cause mixing of fluids and disturbs the phase distribution, but this was not observed in these experiments. A possible explanation is that the secondary flow effects are too weak to overcome the phase distribution caused by density difference of air and water, and large centrifugal forces. If this is true, the secondary flow could become a problem for multiphase flows with small density differences, as water and oil.

4.7.3 Methods for separating the phases

Different methods to separate one of the phases from the coil were considered during the experiments. Previous studies have utilised small drainage holes at the outer pipe wall for water drainage (Zhang et al., 2006), and inner pipe wall for air drainage (Zhang et al., 2014). These studies presented coils with several loops where a number of drainage holes gradually released one of the phases. Drainage holes seem applicable for the experiments in this project that achieved stable distribution of air bubbles, i.e. the one-loop coil experiments. The one loop coil has shorter coil length, depending on its curvature radius, and would require efficient draining. This could be solved with larger holes at short intervals.

The ideal position to drain from appears to be around the first half of the loop. This section is generally characterised with a stable distribution of bubbly flow at the inner region, even for

a wide range of void fractions. Initiation of plug or slug flow usually forms at later stages in the loop, which would complicate drainage.

For the drainage hole solution to handle variation in void fraction, and reduce unintended phase drainage, the holes opening should be adjustable. It is also proposed that the alignment of drainage holes could be angled rather than perpendicular to the axial flow direction. This may reduce pressure loss and disturbance of the main flow.

Other proposed solutions to separate the phases are splitting of the coiled pipe flow. The splitting could be based on a converter from single-to-double pipe, e.g. Y-pipe. The splitting should be in the coiled section, or immediately downstream, ensuring that the wanted phase distribution is lead into each pipe. This solution would require a device that adjusts the amount of gas and liquid that is lead into each pipe. Larger centrifugal forces are believed to vertically align the gas-liquid interface inside the coil, defending a vertically oriented internal flow splitter.

To enhance the ability to handle varieties in gas-liquid ratio, solutions to measure the void fraction in the coil are proposed. One solution is based on installing a slightly angled flap located in the inner pipe region. The flap is preloaded, moving away from the pipe wall. It is forced towards the pipe wall at zero void fraction, because liquid inertia overcomes the preload. When gas void fraction increases, and gas accumulates at the inner region, the flap would move towards the centre of the pipe following the liquid interface. The flap position would then represent gas-liquid distribution inside the pipe for bubbly and stratified flows.

Murai et al. (2006) installed a pressure sensor in the bottom inner region of the coiled pipe to study pressure fluctuations. The results showed pressure variations depending on the instant occurrence of passing liquid slugs and air plugs. This brings the idea of using pressure sensors at several circumferential positions to estimate both flow regime and phase distribution.

4.7.4 Applicability as a flow conditioner

For the helical coil to operate as a flow conditioner, the flow regime achieved downstream of the coil is important. For most of the experiments, the flow regime that developed inside the coil was also observed downstream of the coil. However, images of the flow regime in a low curvature radius coil with one loop indicated a transition of flow regime at the shift from curved to straight pipe. A bubbly flow regime was seen throughout the coil, and images proved bubbly

flow regime at 3/4 of the loop. Still, images of the coil outlet showed instant occurrence of air plugs. A possible explanation is that despite the accumulation of bubbles in the inner region, which together with secondary flow effects is believed to accelerate bubble coalescence (Murai et al., 2006), the bubbles are somewhat protected by the cross-sectional pressure difference from the inner to outer pipe region. The lower pressure in the inner region could therefore prevent coalescence, but when the pressure difference disappears, as the pipe turns straight, the accumulated bubbles collapse and coalesce.

da Mota and Pagano (2014) achieved a wavy stratified flow downstream of a one loop coil with bubbly inlet flow, indicating potential as flow conditioner. The main difference from da Mota and Pagano (2014), was the 3 inch internal pipe diameter, compared to 1/2 inch in this project. A stratified flow regime was never observed in the 1/2 inch pipe, and most of the results showed bubbly inlet flow developing to intermittent flow regimes. The reason for not achieving stratified flow in the 1/2 inch experiments is assumed to be that the air bubbles only migrate within the water phase, having no free surface (air-water interface) to exit. In da Mota and Pagano (2014) one could observe a bubbly water phase *and* an air void above the water, at the coil inlet. Inside the coil the centrifugal force cause migration of air bubbles towards the air void, allowing the bubbles to exit the liquid phase, resulting in a stratified flow.

This brings doubt to the applicability as a flow conditioner, and emphasise the need for further research on the effect of pipe diameter.

4.7.5 Applicability for the helical coil principle

The helical coil experiments revealed abilities that could make it applicable as a type of phase separator. The experiments reached high centrifugal forces, drawing similarities towards cyclone separators. The convenient geometry makes it especially suitable for subsea deep-water developments. The configurations of the influencing factors will need to be assessed in order to obtain the ideal flow regime for separation, or flow conditioner purposes. Thus, the helical coil technology seems to prove its potential of becoming a phase separator, although further research is required to avoid flow regime complications.

The experimental results indicate challenges of using the helical coil for separation purposes. This is due to difficulties of achieving stable phase distribution and separating the phases

efficiently from one another. However, the project group assume that for optimisation of the coil configuration, the technology could be utilised as a coarse separator.

For flow conditioner purposes, the technology could be localised before a separator, or riser base entrance. This could ideally eliminate heavy intermittent flow occurrences at process facilities. The experiments indicated that the coil did not improve intermittent flow. In fact, the coil mainly developed occurrence of plug and slug flow, from bubbly flow.

4.7.6 Limitations and uncertainties

The piping in the experiments were transparent PVC pipes. The experience was that after some usage it had a tendency of losing its transparency. In addition, the PVC pipe hardened and became less flexible, causing difficulties handling and forming the system geometry. At several occasions the pipe cracked as a result of wear.

The control valve regulators for air and water at the T-piece were sensitive, making it hard to regulate a desirable flow. This caused irregular intervals between measurements. During testing, the flow rates had a tendency to vary, increasing and decreasing, causing unstable readings. This was due to instabilities in the compressed air system.

The pipe section between the T-piece and the helical coil was not fixed as a straight pipe. This may have affected the inlet flow characteristics, even though it was mostly similar to a bubbly flow. Ideally, this part of the system should be fixed in a straight line of a certain length, ensuring fully developed flow.

The simplicity of using a PVC pipe and coiling around cylindrical objects naturally caused some irregularities to the coil geometry. The internal cross-section could become slightly deformed, and gradient and pitch of each loop could vary.

Chapter 5

Level of Similitude between Experiments and Full-Scale Flows

This chapter discuss the level of similitude between the experiments in Chapter 4 and full-scale hydrocarbon production scenarios. The similarities are examined based on superficial velocities, and obtaining geometric, kinematic, and dynamic similitude. The main focus was to compare between the 1/2 inch experimental pipe and a hypothetical 6 inch full-scale pipe. The flow is compared to a full-scale hydrocarbon flow, both at standard and non-standard pressure and temperature.

5.1 Superficial Velocity

In this section the superficial velocity is used as a similarity parameter between the experimental water-air flow, and a hypothetical full scale oil-gas flow. The basic assumption of the comparison is that the superficial velocities of liquid and gas in a full-scale pipe, are set equal to the superficial velocities for water and air in the experiment. The calculated full-scale flow rates for liquid and gas was then assumed to be "field condition" volumetric flow rates. To convert the field flow rates to standard condition flow rates, a hydrocarbon composition[1] was selected and inserted in the software *Hysys*. The reason for selecting a condensate composition was because it has low viscosity and could behave more similar to water. Pressure and temperature was set

[1] Condensate composition. See Appendix C for specifications

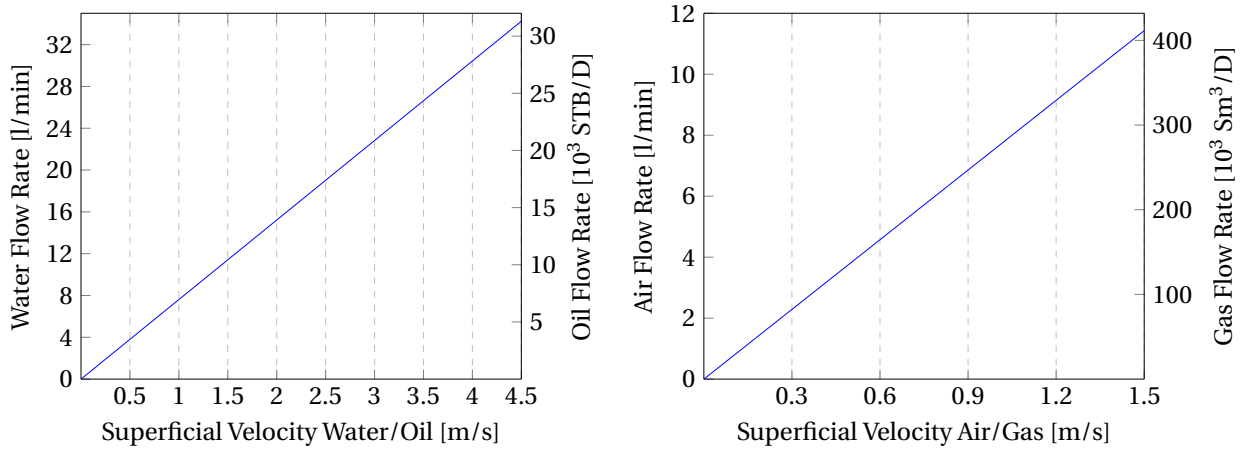

(a) Relation between experimental water flow and a full-scale oil flow.

(b) Relation between experimental air flow and a full-scale gas flow.

Figure 5.1: Comparison between experimental flow rates in a 1/2 inch pipe and full-scale flow rates in a 6 inch pipe, for equal superficial velocities.

to field conditions (100 bara and 100 °C) and to standard conditions (1.01 bara and 15 °C). The software calculated the volumetric differences between standard and field conditions, which was expressed by a volumetric *flow ratio* with dimensions Sm^3/m^3, for each phase. The flow ratio of the liquid phase equals the reciprocal of the *oil formation volume factor*.

Since the comparison converts field condition flow rates to standard condition flow rates by use of one specific hydrocarbon composition the comparison is limited to represent this specific composition only. As most of the experiments were performed with 1/2 inch pipe, the comparison regards this pipe diameter only. In other words, variation in pressure and temperature at field conditions are not evaluated.

Assuming equal superficial velocities, the relationship between water flow rate in the 1/2 inch pipe and full-scale oil flow rate in a 6 inch pipe is shown in Figure 5.1a. The highest measured water flow rate during the experiments was 32.6 l/min, which corresponded to a full-scale oil flow rate of about 30 000 STB/D[2]. For the same water flow rate, but increasing the hypothetical full-scale pipe diameter to 8, 10, or 12 inch, results in oil flow rates of about 52 900, 82 700, and 120 000 STB/D, respectively.

The relationship between air flow rate and full-scale gas flow rate is shown in Figure 5.1b. The highest measured air flow rate was 11.4 l/min, which corresponded to a full-scale gas flow

[2]Stock Tank Barrels per Day

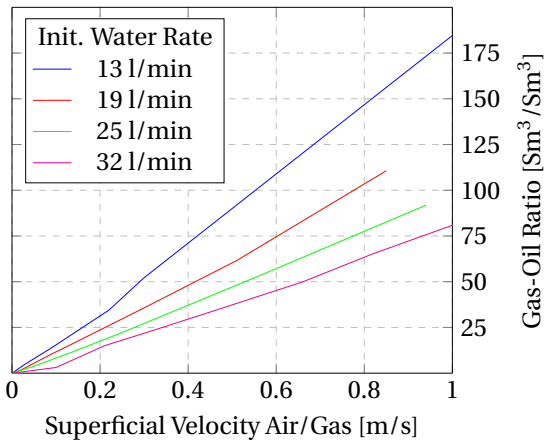

(a) Relation between experiment superficial velocity of air and calculated full-scale GOR.

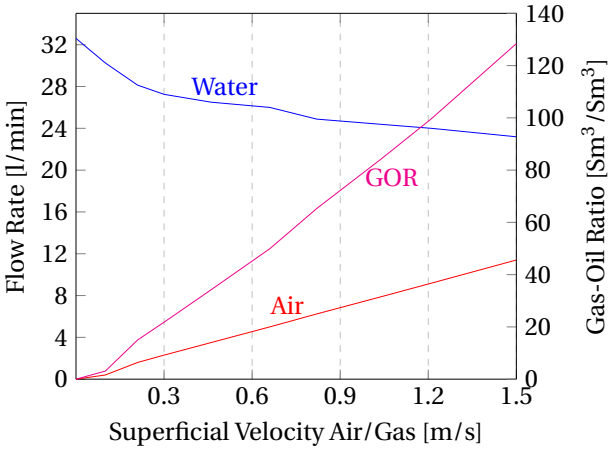

(b) Relation between experiment water and air flow rates and calculated full-scale GOR.

Figure 5.2: Comparison of experiment flow rates to full-scale GOR.

rate of about 430 000 Sm^3/D.

The relationships shown in Figure 5.1a and 5.1b are useful to find full-scale flow rates for each phase individually. As most of the experiments regard various levels of water and air flow combined, it was of interest to present the hypothetical full-scale flow in terms of a GOR[3]. The GOR relationship is dependent of both air and water flow rate. The experiments were conducted such that an initial single-phase water flow rate was obtained, then followed by increasing the air flow rate gradually. It was observed that the water flow rate decreased as a result of increasing the air rate. The range of GOR obtained during the experiments, at different initial water flow rates, are shown in Figure 5.2a.

Figure 5.2b illustrates the effect of increasing air flow rate, reducing the water flow rate, and the GOR. It shows that the initial decrease in water flow rate is nonlinear. A probable explanation is that for low air rates, the water flow must accelerate the air injected at the commingling point.

A remark on the comparison of volumetric flow rates, is that the experiment did not seem to be limited by the flow performance in the 1/2 inch pipe. The highest rates of both water and air corresponded to relatively high, but realistic, full-scale flow rates. Depending on the trustworthiness of this comparison, it can be used to map within which flow rates, and GOR, a full-scale helical coiled pipe may be successfully utilised.

[3]Gas-Oil-Ratio

5.2 Geometric Similarity

Geometric similarity between a model and a prototype (full-scale) is achieved when all body dimensions have equal linear length scale ratio (White, 2011). For flow in a circular pipe conduit, the inner pipe diameter yields to be the first dimension to scale. Considering a 1/2 inch pipe and a 6 inch pipe, saying λ is the dimensionless length scale ratio, then λ can be obtained as shown in Equation (5.1).

$$\lambda = \frac{d_m}{d_p} = \frac{0.5"}{6"} = \frac{1}{12} \tag{5.1}$$

Based on the selected full-scale pipe diameter, the calculated scale ratio λ yields that the model is 1/12 of the full-scale pipe. Assuming the pipe is coiled in one helical loop, the same scale ratio is used to find the dimensions of the full-scale loop. The full-scale curvature radius of the 4.9 cm radius from the experiment is calculated in Equation (5.2), resulting in a radius of about 0.6 m. Table 5.1 show all experimental coil radii converted to full-scale curvature radii, based on the assumption of 6 inch pipe diameter.

$$R_p = \frac{R_m}{\lambda} = \frac{0.049 \text{ m}}{12^{-1}} = 0.59 \text{ m} \tag{5.2}$$

Table 5.1: Experimental curvature radii and curvature ratios converted to geometrically similar full-scale curvatures for 6 inch pipes.

Experiment			Full-scale	
d	R	δ	d	R
[inch]	[m]	[-]	[inch]	[m]
0.5	0.049	0.130	6	0.59
0.5	0.086	0.074	6	1.03
0.5	0.161	0.039	6	1.95

The full-scale coil radii range between 0.6-2 m. Experimental results in chapter 4 indicated best potential for low radii and one loop coils.

5.3 Kinematic Similarity

White (2011) states that to achieve kinematic similarity the model and prototype must have the same length scale ratio, *and* the same time scale ratio. This results in having the same velocity scale ratio. Having equal length scale ratios require geometric similarity. A time scale ratio must be defined dependent on the type of flow.

Both White (2011) and Chanson (2004) agree that frictionless free-surface flows obtain kinematic similarity with *Froude similitude*, i.e. equal Froude numbers. This is because gravitational effects usually dominate free-surface flows..

White (2011) states that frictionless flows with no free surface only require to be related by a length scale ratio, and an independent time scale ratio. However, he adds that if viscosity, surface tension, or compressibility has significant effects, kinematic similarity may require dynamic similarity. Chanson (2004) states that fully enclosed flows usually are modelled based on *Reynolds similitude*, because viscous effects on pipe walls are dominating.

Based on the reasoning above, the fully enclosed flow velocity scale ratio for achievement of kinematic similarity is defined by Equation (5.3), as given by Chanson (2004). Note that $L_r = L_p/L_m$.

$$V_r = \frac{1}{L_r} \cdot \frac{\mu_r}{\rho_r} = \frac{L_m}{L_p} \cdot \frac{\mu_r}{\rho_r} \tag{5.3}$$

For simplicity, the velocity scale ratio between single-phase experimental water flow and single-phase oil flow velocity is considered. For oil with field condition properties, the ratio becomes as calculated in Equation (5.4).

$$V_r = \frac{1}{12} \cdot \frac{\left(\frac{0.21}{1}\right)}{\left(\frac{581}{998}\right)} = 0.03 \tag{5.4}$$

For a water flow velocity of 4.3 m/s, the field condition oil velocity becomes 0.13 m/s, corresponding to a flow rate of 141 l/min in a 6 inch pipe. For the same oil with standard condition properties, density 724 kg/m^3 and viscosity 0.8 cP, the velocity scale ratio becomes 0.09. This gives an oil velocity of 0.39 m/s, corresponding to 423 l/min.

By assuming single-phase liquid flow, the coiled pipe flows was regarded as no free surface flows. However, there are uncertainties related to whether a multiphase pipe flow with a gas-liquid interface should be treated as a no free surface or a free-surface flow. It is believed that for small diameter pipes, as the 1/2 inch in the experiments, gravitational forces can be overrun by viscous effects or surface tension effects. However, moderately increased pipe diameters with closer to 50/50 gas-liquid distribution, may increase the effect of gravity on different-density liquids. For curved pipe flows with significant centrifugal forces, it seems possible that the flow could be treated as gravity-dominated flows, and hence Froude similitude could be included in the study.

5.4 Dynamic Similarity

In the kinematic similarity section it was understood that in some cases achievement of kinematic similarity is dependent on dynamic considerations, and could require dynamic similarity White (2011). This section elaborates requirements for dynamic similarity.

White (2011) states that to achieve dynamic similarity, geometric similarity must be ensured. Then, dynamic similarities, together with kinematic similarity, are obtained for the following flow types and requirements. *Compressible flow* requires equal Reynolds number, Mach number, and specific-heat ratio. *Incompressible flow with no free surface* requires equal Reynolds number. *Incompressible free-surface flow* requires equal Reynolds number, Froude number, and possibly Weber number and cavitation number.

Chanson (2004) states that for fully enclosed pipe flows, Reynolds similitude is the general requirement because viscous effects on pipe walls are dominating. He adds that the flow resistance, i.e. pressure loss due to pipe roughness, should be equal, and this can be ensured by equal Reynolds number or knowing that both model and prototype flows are fully turbulent. The importance of having a fully turbulent model flow, if the full-scale model is fully turbulent, is highlighted as critical.

Despite the focus on equal Reynolds number, White (2011) further states that true dynamic similarity of free-surface flows is often not achievable. This happens because Froude number equality constrains the length and velocity with the scale ratio, λ. Then to achieve true Reynolds

similitude, it may require differences in fluid properties that none or few actual fluids possess. Since Froude number is the dominating parameter for free-surface flows, inequality of Reynolds number must be accepted. Actually, White (2011) states that the Reynolds number achieved in a model can be smaller than the full-scale by a factor of 10-1000.

The statements above indicate that the requirement of exactly equal Reynolds number for a model and prototype, sometimes have to be disregarded. The following sections discuss dynamic similarities between single-phase water flow and full-scale single-phase oil flows.

As the Reynolds number in the experiments are generally lower than full-scale Reynolds numbers, the similarity study utilise the highest values that was obtained in the experiment. For the cases of multiphase flow, the Reynolds number is calculated based on average density and viscosity, causing low values of Reynolds number. Therefore, this section considers liquid flow only.

Reynolds similitude between water and oil with field condition properties

The 1/2 inch pipe with single-phase water flow rate of 32.6 l/min, and flow velocity of 4.3 m/s, reached a Reynolds number of approximately 54 500. It was assumed that the full-scale oil flow required the exact same Reynolds number, and that oil flow velocity was the only variable parameter. Equation (5.5) shows the calculation, resulting in a velocity of 0.13 m/s. Note that this velocity is equal to the velocity achieved for kinematic similarity in the previous section.

The relation between the obtainable experimental water flow rate, and the required oil flow rate achieving same Reynolds number, is illustrated in Figure 5.3. The required oil flow rate in terms of STB/D, is to get an impression of what production rate the in-field Reynolds similitude would cause. Conversion from field flow rate to standard flow rate is shown in Equation (5.6), utilising the flow ratio (0.7) found by Hysys.

The maximum water flow rate of 32.6 l/min was found equal to a production rate of approximately 900 STB/D. This is considered a very low full-scale rate, and does not seem to be representative for a typical 6 inch pipe flow. Table 5.2 shows the oil properties at field and standard conditions.

$$\frac{\rho_w \overline{v}_e d_e}{\mu_w} = \frac{\rho_{oil} \overline{v}_{fs} d_{fs}}{\mu_{oil}} \quad \Rightarrow \quad \overline{v}_{fs} = 4.3 \ {}^{m}/_{\mathrm{s}} \cdot \left(\frac{998}{581}\right) \cdot \left(\frac{0.5}{6}\right) \cdot \left(\frac{0.21}{1.0}\right) \approx 0.13 \ {}^{m}/_{\mathrm{s}} \tag{5.5}$$

$$q_{o,Std} = q_{oil} \cdot \frac{0.7 \cdot 86400}{0.159} \approx 900 \ {}^{STB}/_{\mathrm{D}} \tag{5.6}$$

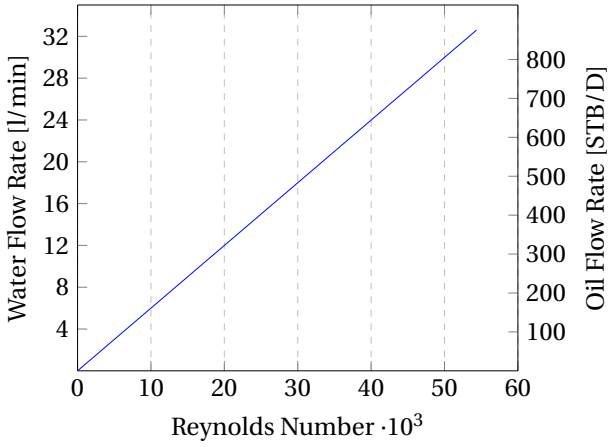

Figure 5.3: Reynolds number relationship between water and oil with field properties.

Table 5.2: Water and oil properties.

	Water	Oil (Std.)	Oil (Field)	Unit
d	0.5	6	6	[inch]
ρ	998	724	581	$[kg/m^3]$
μ	1.0	0.8	0.21	[cP]
p	1	1	100	[bara]
T	15	15	100	[°C]

Reynolds similitude between water and oil with standard condition properties

To see the effect of changing the full-scale fluid properties, the same procedure of requiring equal Reynolds number is performed for oil at standard conditions. Equation (5.7) shows that the higher density and viscosity of the oil result in a velocity that is closer to the experimental. Equation (5.8) calculates the corresponding flow rate, and converts (without flow ratio) the flow rate to production rate in terms of STB/D, for comparison with the previous section.

$$\overline{v}_{fs} = 4.3 \cdot \left(\frac{998}{724}\right) \cdot \left(\frac{0.5}{6}\right) \cdot \left(\frac{0.8}{1.0}\right) \approx 0.40 \ {}^{m}/_{\mathrm{s}} \tag{5.7}$$

$$q_{o,Std} = 0.40 {}^{m}/_{\mathrm{s}} \cdot A_{fs} = 0.0073 {}^{m^3}/_{\mathrm{s}} \ = 3965 \ {}^{STB}/_{\mathrm{D}} \tag{5.8}$$

The result is an approximate production rate of 3965 STB/D. This rate is considered more representative of typical full-scale production rates. This indicates that the experiment does not represent volatile -low viscosity- oil at high pressure and temperature.

Dean number as similarity requirement for curved pipe flow

The Reynolds number describes fluid force ratios, inertial and viscous, for straight pipe flows. In the case of curved pipe flows, the Dean number includes curvature effects by describing force ratio between inertial, viscous, and centrifugal forces. The Dean number is calculated by multiplying Reynolds number with the square root of the curvature ratio, defined in Equation (5.9). Uncertainties exist to whether the Dean number can be a parameter of similitude for curved pipe flows. This issue is not elaborated in this thesis, but the publication by Cieĺ et al. (2012) found that the Dean number could be a parameter for laminar flows within limited ranges of Dean number and curvature ratios.

$$De = \sqrt{\delta} \times Re \tag{5.9}$$

The importance on having geometric similarity from the previous sections, are adapted into this section. Hence a requirement for a model and full-scale helical coil is having equal curvature ratios, ensuring geometric similarity. This requirement actually imply that Dean similarity is dependent of Reynolds similarity, because the root-term in Equation (5.9) cannot change.

Table 5.3 presents important parameters and results for different similarity calculations. The *experiment*-column contains the reference parameters used to calculate the full-scale scenarios. The two first full-scale columns show examples of Dean/Reynolds-similarity for oil flow with field and standard condition properties. The next columns show alternative similarity calculations, based on flow velocity (as in section 5.1), and centrifugal force as similarity parameters.

The cases where true dynamic similarity is achieved, the reduced flow velocity cause insignificant centrifugal force. The case with flow velocity as similarity parameter, cause a centrifugal force of 3.2 g, and the Reynolds numbers are off by a factor of 33. The last case with centrifugal force as similarity parameter requires a flow velocity of 14.9 m/s to obtain 38.5 g, and the Reynolds numbers are off by a factor of 115.

Table 5.3: Full-scale flow velocity, flow rate, Reynolds number, Dean number, and centrifugal force, calculated for different oil properties and different similarity parameters.

	Experiment	Full-scale				Units
		Field	Standard	Field	Field	
d	0.5	6	6	6	6	[inch]
R	0.049	0.59	0.59	0.59	0.59	[m]
δ	0.13	0.13	0.13	0.13	0.13	-
ρ	998	581	724	581	581	[kg/m3]
μ	1.00	0.21	0.8	0.21	0.21	[kg/m3]
v	4.3	0.13	0.40	4.3*	14.9	[m/s]
q	32.6	141	423	4 706	16 338	[l/min]
Reynolds	54 500	54 500*	54 500*	1 813 052	6 294 086	-
Dean	19 650	19 650	19 650	651 571	2 269 365	-
Centr. force	38.5	0.003	0.027	3.2	38.5*	[g]

*Similarity parameter in current column.

5.5 Discussion of Similarities

In the superficial velocity section, the water and air flow rates was converted to full-scale oil and gas flow rates in a 6 inch pipe. The highest experimental flow rate of water was estimated to a full-scale oil flow rate of 30 000 STB/D, which is considered a significant value. Normally, single wells does not produce more than 10 000 STB/D, hence the full-scale oil rate could represent a pipe with commingled well streams.

The highest air flow rate, in combination with water flow, was estimated to a full-scale gas production rate of about 430 000 Sm^3/D. The calculated GOR for this measurement was about 130 Sm^3/Sm^3, while the largest GOR in the experiment was estimated to about 180 Sm^3/Sm^3. Both values of GOR is in the range of a typical black oil (Jahn et al., 2008).

Geometric similarity between the different experimental helical coil curvatures and 6 inch full-scale coils was studied. The experimental curvature radii ranged from 4.9-18.0 cm, which corresponded to full-scale coil curvature radii in the range 0.6-2.0 m. The lower bound radii were

considered relatively small in size, and possibly beneficial compared with typical gravitational separation systems.

Since kinematic similarity preferably was achieved based on dynamic considerations, the main focus was set on achievement of dynamic similarity. This required equal Reynolds number between the experiment and full-scale scenario. To reduce complexity of the study, single-phase liquid flow was assumed. For oil properties at field conditions, the flow velocity required to achieve similarity was 0.13 m/s, corresponding to a production rate of 900 STB/D. For standard condition oil, i.e. increased density and viscosity, required flow velocity became 0.40 m/s, corresponding 3900 STB/D. This was considered comparable to a single well production rate.

For flow in curved pipes and helical coils the Dean number was assumed the similarity parameter, and geometric similarity was fulfilled by equal curvature ratios between experiments and full-scale. This implied that Reynolds similitude was required to achieve equal Dean numbers. Dependent on oil properties, the results was flow velocities of 0.13 and 0.40 m/s in a coil with curvature radius of 0.6 m, creating insignificant centrifugal forces. As an alternative, the flow velocity were set as similarity parameter, causing centrifugal force of 3.2 g, and Reynolds number was off by a factor of 33. At last, centrifugal force was set as similarity parameter, requiring a full-scale flow velocity of 14.9 m/s, implying a very high flow rate, and Reynolds number off by a factor of 115.

It was understood that true dynamic similarity with exact Reynolds number similitude was rarely achievable (White, 2011). Thus, the cases where Reynolds numbers are off are not necessarily incomparable. It was also discussed that for very small pipe diameters, viscous- and surface tension effects could overrun the gravitational and centrifugal forces. To avoid or reduce the issues above, one can select experimental fluids with other properties, and increase experimental dimensions, enhancing the level of similitude with full-scale hydrocarbon flows.

Uncertainty regarding whether a multiphase pipe flow was to be considered a no free surface flow, or a free surface flow was discussed. It is recommended for further work to investigate this issue, as this can improve comparability of future experiments with full-scale scenarios.

Chapter 6

Conclusion and Recommendations for Further Work

The need for more compact separation systems in the petroleum industry formed the background for this thesis. An analysis of separation systems and an experimental study of air-water flow in helically coiled pipes were conducted. The main goal of the experimental study was to investigate separation capabilities for helical coils.

The flow behaviour inside the helical coils was photographed for a variety of coil configurations and air-water flow rates. The flow regime at coil inlet was mainly recognised as a bubbly flow, independent of air flow rate. However, inside the coiled pipe, air flow rates above certain values developed intermittent flow regimes as plug and slug flow. Adjustment of coil configurations revealed effects on the flow development. When adding numbers of loops in the coil, intermittent flow regimes occurred at lower air flow rates. When shortening the curvature radii, intermittent flow regimes occurred only for higher air flow rates.

The study in Chapter 3 indicated that most of the existing compact separation systems utilise the centrifugal principle. The motivation to investigate applicability of helically coiled pipes as separators was enhanced. Indications on abilities to achieve phase separation and influence flow behaviour in a helical coil, seemed promising for development of compact separation systems. Compact separators were found convenient for topside facilities with limited space, and for deep-water subsea developments affected with high ambient pressure. The experiments in chapter 4 revealed that for certain coil configurations and flow rates a favourable phase distribu-

tion could be achieved. The combination of one loop and short curvature radii, both reducing total coil length, seemed to achieve more stable phase distributions. This was assumed to be a result of lowered friction loss and higher centrifugal force. A different observation was that for moderate to high air rates, one could experience instant transition from bubbly to intermittent flow immediately downstream the coil outlet. This indicated that despite maintaining favourable phase distribution in the coiled pipe, the distribution may not sustain downstream of the coil. This could reduce the helical coils potential for flow conditioning. Chapter 5 discussed the level of similitude between the experiment and full-scale scenarios. Geometric similarity between the smallest experimental coil and a full-scale 6 inch pipe diameter, gave a reasonably compact coil diameter of 1.2 m. The experimental water flow was compared with a full-scale condensate flow. The condensate required a very low flow velocity to achieve dynamic similarity (equal fluid force ratios). In addition, it was found that the experimental flow could show misleading behaviour, as viscous- and surface tension effects become significant for small diameter pipes.

Results from the experiment may have been affected by inaccuracies. The range of achievable liquid flow rates was limited by the tap water system used as liquid source. Sensitive flow control valves combined with instabilities in the compressed air system made accurate flow rate adjustments difficult. The use of flexible pipes gave geometrical inaccuracies due to deformation of cross-sectional area. Logging of flow rates and flow regime imaging were performed with a time span up to one minute, reducing the accuracy between measurements and images in the analysis. The small scale of the experiment in addition to the difference in fluid properties and pressure-temperature conditions reduced the comparability with genuine hydrocarbon productions.

The experimental study gave indications on separation capabilities, as achievement of stable phase distribution was possible for certain coil configurations and flow rates. However, the narrow operating range, and possible errors in the experiment, brought uncertainties to whether a full-scale helical coil could achieve phase separation. Thus, the experimental study could neither approve nor disprove the applicability of helically coiled pipes as phase separators. The work in this thesis indicate both promising capabilities and significant challenges, hence the helical coil principle needs continued and more comprehensive research.

The study towards a possible helical coil separation system is at an early stage, and further research and work is required to get a fundamental understanding of the principle. Recommendations for further work are based on what was not conducted, or sufficiently examined. The short-term recommendations are meant for enhancing the understanding of the helical coil principle. The long-term recommendations are dependent of proved separation abilities.

Short-term

- Study the effect of different pipe diameters, with focus on achieving stratified flow regime
- Study the required magnitude of centrifugal forces to ensure stable phase distribution
- Study the effect of coil axis orientation. Find optimal orientation or whether the orientation could be optional
- Study the effect of progressively decreasing or increasing curvature radius along the loop. This could cause a smoother transition into or out of the coil, and affect flow behaviour
- Investigate methods of decreasing intermittent flow development in coil or coil outlet, e.g. pipe internals or avoiding abrupt straightening at outlet
- Study the effect of non-circular cross-sectional pipes with the helical coil principle, e.g. elliptical, triangular, rectangular, or other geometries thought to be beneficial. This could affect the secondary flow and phase distribution in the coil
- Utilise fluids that improve similarities to hydrocarbon flows
- Increase the experimental dimensions to improve similarity with larger scale flows, especially because of scale-effects induced by viscous forces and surface tension

Long-term

- Investigate techniques to efficiently separate one phase out of the main flow from the helically coiled pipes
- Investigate if the principle can sufficiently separate liquid-liquid phases, aimed towards achieving oil-water separation
- Large or full-scale experiments

Bibliography

1. Al-Yazdi, A. (1991). Apparatus and method for separating water from crude oil. https://www.google.no/patents/US5004552 [2015-02-27].

2. Balachandran, P. (2006). *Fundamentals of compressible fluid dynamics*. PHI Learning Pvt. Ltd.

3. Berger, S., Talbot, L., and Yao, L. (1983). Flow in curved pipes. *Annual review of fluid mechanics*, 15(1):461–512.

4. Chanson, H. (2004). *Hydraulics of open channel flow*. Butterworth-Heinemann.

5. CieĹ, K., Piechna, A., et al. (2012). Can the dean number alone characterize flow similarity in differently bent tubes? *Journal of Fluids Engineering*, 134(5):051205.

6. da Mota, F. R. and Pagano, D. J. (2014). Simulation and experimental study of phase segregation in helical pipes: A new method for flow conditioning. *Flow Measurement and Instrumentation*, 35(March):99–108.

7. Falcone, G., Hewitt, G., and Alimonti, C. (2009). *Multiphase flow metering: principles and applications*, volume 54. Elsevier.

8. Hannisdal, A., Westra, R., Akdim, M. R., Bymaster, A., Grave, E., Teng, D., et al. (2012). Compact separation technologies and their applicability for subsea field development in deep water. *OTC*, 23223.

9. Hoffmann, A., Stein, L., and Bradshaw, P. (2003). Gas cyclones and swirl tubes: Principles, design and operation. *Applied Mechanics Reviews*, 56:28.

10. Holdich, R. G. (2002). *Fundamentals of particle technology*. Midland Information Technology and Publishing.

11. Jahn, F., Cook, M., and Graham, M. (2008). *Hydrocarbon Exploration & Production*, volume 55. Elsevier.

12. Kidnay, A. J., Parrish, W. R., and McCartney, D. G. (2011). *Fundamentals of natural gas processing*, volume 218. CRC Press.

13. Liptak, B. G. (1993). *Flow measurement*. CRC Press.

14. Massey, B. S. and Ward-Smith, J. (1998). *Mechanics of fluids*, volume 1. CRC Press.

15. Mujawar, B. and Rao, M. R. (1981). Gas-non-newtonian liquid two-phase flow in helical coils. *Industrial & Engineering Chemistry Process Design and Development*, 20(2):391–397.

16. Murai, Y., Yoshikawa, S., Toda, S.-i., Ishikawa, M.-a., and Yamamoto, F. (2006). Structure of air–water two-phase flow in helically coiled tubes. *Nuclear engineering and design*, 236(1):94–106.

17. Palmer, A. C. and King, R. A. (2008). *Subsea Pipeline Engineering*, volume 2. PennWell Books.

18. Stewart, M. and Arnold, K. (2008). *Gas-liquid and Liquid-liquid Separators*. Gulf Professional Publishing.

19. ASCOM Separation. *ASCOM Spherical Separator Subsea*, http://www.ascomseparation.com/technology-and-products/advanced-separation-technology/subsea-processing-%E2%80%93-deepwater-solutions, [2015-03-15].

20. Bronkhorst High-Tech. *Thermal mass flow measurement*, http://www.bronkhorst.com/en/products/theory/thermal_mass_flow_measurement/, [2015-03-18].

21. Bronkhorst High-Tech. *EX-FLOW*, http://www.bronkhorst.com/files/downloads/brochures/exflow_leaflet.pdf, [2015-03-18].

22. FMC Technologies. (2009). *InLine DeWaterer*. http://www.fmctechnologies.com/en/SeparationSystems/Technologies/InLineTechnologies/InLineLiquidLiquidSeparation/InLineDeWaterer.aspx, [2015-02-10].

23. FMC Technologies. (2011), *CDS-Gasunie Cyclone Scrubber*, http://www.fmctechnologies.com/en/SeparationSystems/Technologies/HighPerformanceInternals/CDSGasUnie.aspx, [2015-02-22].

24. RS Components. (1994), *Combined Liquid Flow Transducer/Transmitter*, http://docs-europe.electrocomponents.com/webdocs/001a/0900766b8001aea1.pdf, [2015-03-18].

25. Twister BV. *Twister® Supersonic Separator*, http://twisterbv.com/products-services/twister-supersonic-separator/how-it-works/, [2015-02-22].

26. Truesdell, L. and Adler, R. (1970). Numerical treatment of fully developed laminar flow in helically coiled tubes. *AIChE Journal*, 16(6):1010–1015.

27. Vashisth, S. and Nigam, K. (2009). Prediction of flow profiles and interfacial phenomena for two-phase flow in coiled tubes. *Chemical Engineering and Processing: Process Intensification*, 48(1):452–463.

28. Vogel, S. (1996). *Life in moving fluids: the physical biology of flow*. Princeton University Press.

29. White, F. (2011). *Fluid Mechanics*. McGraw-Hill series in mechanical engineering. McGraw Hill.

30. Yamaguchi, H. (2008). *Engineering fluid mechanics*, volume 85. Springer.

31. Zamir, M. and Zamir, M. (2000). *The physics of pulsatile flow*. Springer.

32. Zhang, J., Jun, G., Gong, D.-t., Wang, L.-y., Chi, T., and Zheng, Z.-c. (2006). An investigation on oil/water separation mechanism inside helical pipes. *Journal of Hydrodynamics, Ser. B*, 18(3):343–347.

33. Zhang, Y., Guo, C., Hou, H., and Xue, G. (2014). Experimental research and numerical simulation on gas-liquid separation performance at high gas void fraction of helically coiled tube separator. *International Journal of Chemical Engineering*, 2014.

Appendix A - Experimental Data

This appendix presents the experimental excel tables, which documents every measured experiment conducted. The table lists measurements for water and air rates, and their calculated details. The multiphase flow is further calculated from the measurements. In addition, the characteristic of the flow regime at inlet, inside, and outlet of the helical coil is documented.

Ex. 1 - ¾" pipe				WATER				AIR			MULTIPHASE								OTHER			
R[m] / δ	0,180	0,053		Turbine meter				Air flow meter									0,05					
-	Flow	Time	ID	Flow rate	Mass flow	Superficial velocity	Vol.frac	Flow rate	Mass flow	Superficial velocity	Vol.frac	Flow rate	Mass flow	Total superf. velocity	Density	Viscosity	Re	De	Centri. acc.	Flow in	Flow coil	Flow out
	-	hh:mm	[-]	[l/min]	[kg/s]	[m/s]	[-]	[l/min]	[kg/s]	[m/s]	[-]	[l/min]	[kg/s]	[m/s]	[kg/m³]	[cP]	[-]	[-]	[g]			
	W(100%)	14:13	1.1	**51,88**	0,863	3,03	1,00	**0,00**	0,E+00	0,00	0,00	**51,88**	0,86	3,03	998,0	1,000	57 670	13 284	5,2			
	W & A	14:16	1.2	**50,75**	0,844	2,97	1,00	**0,22**	5,E-06	0,01	0,00	**50,97**	0,84	2,98	993,6	1,000	56 435	12 999	5,0	B	B +	B+
	W & A	14:22	1.3	**50,13**	0,834	2,93	0,99	**0,73**	1,E-05	0,04	0,01	**50,86**	0,83	2,97	983,7	0,999	55 775	12 847	5,0	B+	P	P
1 Loop	W & A	14:29	1.4	**49,81**	0,829	2,91	0,96	**1,95**	4,E-05	0,11	0,04	**51,76**	0,83	3,03	960,4	0,998	55 512	12 787	5,2	B+/P	P	S
	W & A	14:38	1.5	**49,56**	0,824	2,90	0,93	**3,65**	7,E-05	0,21	0,07	**53,21**	0,82	3,11	929,6	0,996	55 351	12 750	5,5	P	P/S	S
	W & A	14:48	1.6	**49,50**	0,823	2,89	0,88	**7,04**	1,E-04	0,41	0,12	**56,54**	0,82	3,31	874,0	0,991	55 515	12 787	6,2	P	S	S

Ex. 2 - ½" Pipe				WATER				AIR			MULTIPHASE								OTHER			
R[m] / δ	0,161	0,039		Turbine meter				Air flow meter									0,04					
-	Flow	Time	ID	Flow rate	Mass flow	Superficial velocity	Vol.frac	Flow rate	Mass flow	Superficial velocity	Vol.frac	Flow rate	Mass flow	Total superf. velocity	Density	Viscosity	Re	De	Centri. acc.	Flow in	Flow coil	Flow out
	-	hh:mm	[-]	[l/min]	[kg/s]	[m/s]	[-]	[l/min]	[kg/s]	[m/s]	[-]	[l/min]	[kg/s]	[m/s]	[kg/m³]	[cP]	[-]	[-]	[g]			
	W(100%)	12:22	2.1	**32,63**	0,543	4,29	1,00	**0,00**	0,E+00	0,00	0,00	**32,63**	0,54	4,29	998,0	1,000	54 405	10 793	11,6			
	W & A	12:29	2.2	**30,63**	0,509	4,03	1,00	**0,11**	2,E-06	0,02	0,00	**30,74**	0,51	4,04	994,3	1,000	51 081	10 134	10,3	B	B	B
	W & A	12:36	2.3	**26,88**	0,447	3,54	0,95	**1,38**	3,E-05	0,18	0,05	**28,26**	0,45	3,72	949,2	0,997	44 959	8 919	8,7	B	B	B+
1 Loop	W & A	12:43	2.4	**25,00**	0,416	3,29	0,90	**2,74**	6,E-05	0,36	0,10	**27,74**	0,42	3,65	899,7	0,993	41 972	8 327	8,4	B+	B+	P
	W & A	13:18	2.5	**23,75**	0,395	3,12	0,84	**4,68**	1,E-04	0,62	0,16	**28,43**	0,40	3,74	834,0	0,988	40 088	7 953	8,8	B+	S*	S*
	W & A	13:24	2.6	**23,13**	0,385	3,04	0,74	**8,20**	2,E-04	1,08	0,26	**31,33**	0,38	4,12	737,1	0,979	39 410	7 818	10,7	B/P	S+	S+
3 Loops	W & A	13:30	2.7	**28,75**	0,478	3,78	0,97	**1,00**	2,E-05	0,13	0,03	**29,75**	0,48	3,91	964,6	0,998	48 046	9 531	9,7	B	P	P
	W & A	13:52	2.8	**25,63**	0,426	3,37	0,85	**4,40**	9,E-05	0,58	0,15	**30,03**	0,43	3,95	851,8	0,990	43 187	8 567	9,9	B+	P	S
6 Loops	W & A	14:06	2.9	**30,00**	0,499	3,95	0,98	**0,48**	1,E-05	0,06	0,02	**30,48**	0,50	4,01	982,3	0,999	50 077	9 934	10,2	B	P	S

Ex. 3 - ½" Pipe				WATER				AIR			MULTIPHASE								OTHER			
R[m] / δ	0,086	0,074		Turbine meter				Air flow meter									0,07					
-	Flow	Time	ID	Flow rate	Mass flow	Superficial velocity	Vol.frac	Flow rate	Mass flow	Superficial velocity	Vol.frac	Flow rate	Mass flow	Total superf. velocity	Density	Viscosity	Re	De	Centri. acc.	Flow in	Flow coil	Flow out
	-	hh:mm	[-]	[l/min]	[kg/s]	[m/s]	[-]	[l/min]	[kg/s]	[m/s]	[-]	[l/min]	[kg/s]	[m/s]	[kg/m³]	[cP]	[-]	[-]	[g]			
	W(100%)	12:22	3.1	**32,63**	0,543	4,29	1,00	**0,00**	0,E+00	0,00	0,00	**32,63**	0,54	4,29	998,0	1,000	54 405	14 753	21,8			
1 Loop	W & A	14:29	3.2	**27,19**	0,452	3,58	0,92	**2,38**	5,E-05	0,31	0,08	**29,56**	0,45	3,89	917,9	0,995	45 583	12 361	17,9	B	B+	P
	W & A	14:38	3.3	**23,75**	0,395	3,12	0,76	**7,31**	1,E-04	0,96	0,24	**31,06**	0,40	4,09	763,4	0,982	40 361	10 945	19,7	B+	P	S
3 Loops	W & A	14:52	3.4	**29,38**	0,489	3,86	0,95	**1,66**	3,E-05	0,22	0,05	**31,04**	0,49	4,08	944,6	0,997	49 157	13 330	19,7	B	P	P
	W & A	15:08	3.5	**25,13**	0,418	3,31	0,85	**4,40**	9,E-05	0,58	0,15	**29,53**	0,42	3,88	849,4	0,989	42 353	11 485	17,8	B+	S	S
6 Loops	W & A	15:14	3.6	**29,50**	0,491	3,88	0,97	**1,07**	2,E-05	0,14	0,03	**30,57**	0,49	4,02	963,2	0,998	49 304	13 370	19,1	B	S	S
	W & A	15:17	3.7	**27,50**	0,457	3,62	0,92	**2,44**	5,E-05	0,32	0,08	**29,94**	0,46	3,94	916,6	0,995	46 111	12 504	18,3	B+	S	S
	W & A	15:19	3.8	**25,00**	0,416	3,29	0,77	**7,35**	1,E-04	0,97	0,23	**32,35**	0,42	4,26	771,6	0,982	42 449	11 511	21,4	B+	S	S+

Ex. 4 - ½" pipe				WATER			AIR			MULTIPHASE								OTHER			
R[m] / δ	0,049	0,130		Turbine meter			Air flow meter									0,13					
-	Flow -	Time hh:mm	ID [-]	Flow rate [l/min]	Mass flow [kg/s]	Superficial velocity [m/s]	Vol.frac [-]	Flow rate [l/min]	Mass flow [kg/s]	Superficial velocity [m/s]	Vol.frac [-]	Flow rate [l/min]	Mass flow [kg/s]	Total superf. velocity [m/s]	Density [kg/m³]	Viscosity [cP]	Re [-]	De [-]	Centri. acc. [g]	Flow in	Flow coil	Flow out
	W(100%)	11:27	4.1	**32,13**	0,534	4,23	1,00	**0,00**	0,E+00	0,00	0,00	**32,13**	0,53	4,23	998,0	1,000	53 571	19 314	37,3			
	W & A	11:36	4.2	**12,63**	0,210	1,66	0,98	**0,24**	5,E-06	0,03	0,02	**12,87**	0,21	1,69	979,4	0,999	21 078	7 599	6,0	B	B+	B+/P
	W & A	11:43	4.3	**12,38**	0,206	1,63	0,95	**0,66**	1,E-05	0,09	0,05	**13,04**	0,21	1,71	947,5	0,997	20 704	7 465	6,1	B+	P	S
1 Loop(Level 1)	W & A	11:48	4.4	**12,00**	0,200	1,58	0,88	**1,68**	3,E-05	0,22	0,12	**13,68**	0,20	1,80	875,6	0,992	20 185	7 277	6,8	P	S	S
	W & A	11:56	4.5	**11,38**	0,189	1,50	0,83	**2,28**	5,E-05	0,30	0,17	**13,66**	0,19	1,80	831,6	0,988	19 204	6 924	6,7	P	S	S
	W & A	11:59	4.6	**10,75**	0,179	1,41	0,59	**7,62**	2,E-04	1,00	0,41	**18,37**	0,18	2,42	584,5	0,959	18 714	6 747	12,2	S	S	S
	W & A	12:06	4.7	**18,75**	0,312	2,47	0,99	**0,12**	2,E-06	0,02	0,01	**18,87**	0,31	2,48	991,7	1,000	31 279	11 278	12,9	B	B	B+
	W & A	12:21*	4.8	**17,88**	0,297	2,35	0,96	**0,72**	1,E-05	0,09	0,04	**18,60**	0,30	2,45	959,4	0,998	29 882	10 774	12,5	B	B+	P
1 Loop(Level 2)	W & A	12:13*	4.9	**17,50**	0,291	2,30	0,94	**1,02**	2,E-05	0,13	0,06	**18,52**	0,29	2,44	943,1	0,996	29 288	10 560	12,4	B+	P	P
	W & A	12:26	4.10	**16,63**	0,277	2,19	0,88	**2,28**	5,E-05	0,30	0,12	**18,91**	0,28	2,49	877,8	0,992	27 959	10 080	12,9	P	P	P
	W & A	12:33	4.11	**16,25**	0,270	2,14	0,81	**3,84**	8,E-05	0,51	0,19	**20,09**	0,27	2,64	807,5	0,986	27 495	9 913	14,6	P	P	P/S
	W & A	12:36	4.12	**15,25**	0,254	2,01	0,70	**6,48**	1,E-04	0,85	0,30	**21,73**	0,25	2,86	700,8	0,975	26 100	9 410	17,1	P	P	S
	W & A	12:44	4.13	**24,50**	0,408	3,22	0,99	**0,36**	7,E-06	0,05	0,01	**24,86**	0,41	3,27	983,6	0,999	40 893	14 744	22,3	B	B+	B+
	W & A	12:47	4.14	**22,88**	0,380	3,01	0,96	**0,96**	2,E-05	0,13	0,04	**23,84**	0,38	3,14	957,9	0,997	38 245	13 789	20,5	B	B+	B+
1 Loop(Level 3)	W & A	12:50	4.15	**22,50**	0,374	2,96	0,92	**1,92**	4,E-05	0,25	0,08	**24,42**	0,37	3,21	919,6	0,995	37 719	13 599	21,5	B	B+	P
	W & A	12:53	4.16	**21,00**	0,349	2,76	0,83	**4,20**	9,E-05	0,55	0,17	**25,20**	0,35	3,32	831,9	0,988	35 453	12 782	22,9	B+	B+	P
	W & A	12:56	4.17	**20,63**	0,343	2,71	0,79	**5,58**	1,E-04	0,73	0,21	**26,21**	0,34	3,45	785,8	0,984	34 971	12 608	24,8	B+	P	P
	W & A	13:07	4.18	**20,25**	0,337	2,66	0,74	**7,14**	1,E-04	0,94	0,26	**27,39**	0,34	3,60	738,2	0,979	34 507	12 441	27,1	B+/P	P	P/S
	W & A	14:09	4.19	**30,25**	0,503	3,98	0,99	**0,36**	7,E-06	0,05	0,01	**30,61**	0,50	4,03	986,3	0,999	50 481	18 201	33,8	B	B+	B+
	W & A	14:12	4.20	**28,13**	0,468	3,70	0,95	**1,62**	3,E-05	0,21	0,05	**29,75**	0,47	3,91	943,7	0,997	47 068	16 970	32,0	B	B+	B+/P
	W & A	14:15	4.21	**27,25**	0,453	3,59	0,92	**2,28**	5,E-05	0,30	0,08	**29,53**	0,45	3,89	921,0	0,995	45 677	16 468	31,5	B	B+	P
	W & A	14:18	4.22	**26,50**	0,441	3,49	0,88	**3,48**	7,E-05	0,46	0,12	**29,98**	0,44	3,94	882,3	0,992	44 551	16 062	32,5	B	B+	P
1 Loops(Level 4)	W & A	14:22	4.23	**26,00**	0,432	3,42	0,84	**4,98**	1,E-04	0,66	0,16	**30,98**	0,43	4,08	837,8	0,988	43 872	15 818	34,7	B	B+	P
	W & A	14:28	4.24	**24,88**	0,414	3,27	0,80	**6,24**	1,E-04	0,82	0,20	**31,12**	0,41	4,09	798,1	0,985	42 126	15 188	35,0	B	B+	P
	W & A	14:30	4.25	**24,38**	0,405	3,21	0,76	**7,89**	2,E-04	1,04	0,24	**32,27**	0,41	4,25	754,3	0,981	41 463	14 949	37,6	B/B+	P	P
	W & A	14:32	4.26	**24,00**	0,399	3,16	0,72	**9,18**	2,E-04	1,21	0,28	**33,18**	0,40	4,37	722,2	0,977	40 971	14 772	39,8	B+	P	P
	W & A	14:36	4.27	**23,19**	0,386	3,05	0,67	**11,43**	2,E-04	1,50	0,33	**34,62**	0,39	4,55	668,9	0,971	39 849	14 367	43,3	B+/P	P	S

Ex. 5 - ½" pipe				WATER			AIR			MULTIPHASE								OTHER			
R[m] / δ	0,049	0,130		Turbine meter			Air flow meter									0,13					
-	Flow -	Time hh:mm	ID [-]	Flow rate [l/min]	Mass flow [kg/s]	Superficial velocity [m/s]	Vol.frac [-]	Flow rate [l/min]	Mass flow [kg/s]	Superficial velocity [m/s]	Vol.frac [-]	Flow rate [l/min]	Mass flow [kg/s]	Total superf. velocity [m/s]	Density [kg/m³]	Viscosity [cP]	Re [-]	De [-]	Centri. acc. [g]	Flow in	Flow coil	Flow out
	W & A	15:23*	5.1	**30,88**	0,514	4,06	0,99	**0,42**	9,E-06	0,06	0,01	**31,30**	0,51	4,12	984,6	0,999	51 530	18 579	35,4	B	B+	B+
3 Loops	W & A	15:20*	5.2	**28,94**	0,481	3,81	0,97	**0,99**	2,E-05	0,13	0,03	**29,93**	0,48	3,94	965,0	0,998	48 358	17 435	32,4	B	B+/P	P
	W & A	15:18*	5.3	**27,81**	0,463	3,66	0,92	**2,58**	5,E-05	0,34	0,08	**30,39**	0,46	4,00	913,4	0,994	46 646	16 818	33,4	B	P	P
	W & A	15:28	5.4	**26,50**	0,441	3,49	0,87	**4,08**	8,E-05	0,54	0,13	**30,58**	0,44	4,02	865,0	0,991	44 613	16 085	33,8	B	P	P
	W(100%)	12:22	5.5	**32,63**	0,543	4,29	1,00	**0,00**	0,E+00	0,00	0,00	**32,63**	0,54	4,29	998,0	1,000	54 405	19 615	38,4			
	W & A	15:28	5.6	**30,38**	0,505	4,00	0,98	**0,68**	1,E-05	0,09	0,02	**31,06**	0,51	4,09	976,2	0,999	50 723	18 288	34,8	B	P	P
6 Loops	W & A	15:32	5.7	**29,81**	0,496	3,92	0,98	**0,69**	1,E-05	0,09	0,02	**30,50**	0,50	4,01	975,5	0,999	49 786	17 950	33,6	B	P	P
	W & A	15:35	5.8	**28,63**	0,476	3,77	0,95	**1,59**	3,E-05	0,21	0,05	**30,22**	0,48	3,98	945,5	0,997	47 899	17 269	33,0	B	P	P
	W & A	15:39	5.9	**27,38**	0,455	3,60	0,90	**3,12**	6,E-05	0,41	0,10	**30,50**	0,46	4,01	896,0	0,993	45 972	16 575	33,6	B	P	P
	W & A	15:38	5.10	**26,63**	0,443	3,50	0,87	**3,86**	8,E-05	0,51	0,13	**30,49**	0,44	4,01	871,7	0,991	44 799	16 152	33,6	B+	P/S	S

Experimental Data - 2

Appendix B - Flow Meters

This appendix presents data sheets on the flow meters used to measure air and water flow rates during the experiments.

Combined Liquid Flow Transducer/Transmitter

Stock No. 257-026 (Type One)
Stock No. 285-790 (Type Two)

General

These two sturdy turbine flow sensors are designed to operate with most liquids. Two types are available with type one combining a 4-20mA flow transmitter within the same housing. The output signal of this device is 4-20mA, proportional to the flow. The unit is supplied factory calibrated to 4-100 l/minute but may be field calibrated as follows:-

a) Set system to zero flow and connect a multimeter between terminals 1 (+20mA) and ⏚ (0mA).

b) Adjust zero pot to read 4mA on meter.

c) Set system to full flow with multimeter still connected as (a) above. (Max. flow = 150 l/minute).

d) Adjust span pot to read 20mA on meter.

Type two provides a pulse output proportional to flow rate. This is factory calibrated (2 l/m-150 l/min.) and is not user adjustable.

WARNING

This product contains components manufactured from glass filled polyester and borosilicate glass. Although robustly constructed and rigorously tested, we recommend the following precautions are taken:-

1. DO NOT over-tighten pipe fittings (Max. Torque 60Nm).
2. Only use pipe fittings and sealing methods recommended for use with the End Couplings provided.

2a. DO NOT use tapered male pipe fittings.

3. Although it should not be necessary, P.T.F.E. tape may be used, but must not be allowed to enter pipework.
4. Support pipework and mount the unit in such a way as to minimise side loading, mechanical shock loads and vibrations etc.
5. In use the glass body of this meter is subjected to pressure and must under NO circumstances be subjected to physical abuse.
6. DO NOT use if any form of damage occurs, or is suspected to have occurred during handling or installation.
7. Protect from frost.
8. This unit is intended for permanent installation and should not be used for temporary applications.

Maximum working temperature +80°C (+60° with water). Maximum working pressure 10 bar.

Technical Specification

Construction	
Body	Polyester
Glasstube	Borasilicone
Seals	Nitrile
Washers and shaft	Stainless steel
Rotor and locator	Acetal
Rotor tips	Stainless steel
Calibration (Type 1)	4-100 l/min. on water ┐ as 4mA - 0 l/min ┘ factory 20mA - 100 l/min ┘ set
Type 2 'K' factors	Oil - 51.14 pulses per litre Water - 44.25 pulses per litre
Maximum flow rate (field calibration)	150 l/min
Maximum working pressure	10 bar Oil/Water
Minimum flow indication	2 l/m (Max 150 l/m)
Temperature range	5 to 80°C Oil 5 to 60°C Water
Accuracy	±2%
Connections	1" BSP Parallel threads
Electrical details	Supply 24V ⎓
Output (type 1)	4-20mA
(type 2)	Pulsed
Pulse output connections	
Pin 1	+ve o/p
Pin 2	+ve supply
Pin 3	-ve o/p (not shown on diagram)
Pin 4	Earth (-ve supply)

Figure 1.

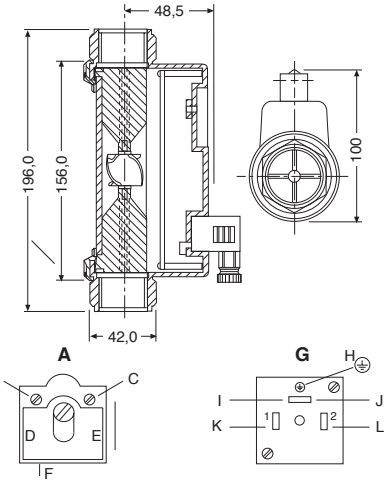

A = Flow setup
B = Set full flow to 20mA
C = Set zero flow
D = Span
E = Zero
F = Slider

G = Plug wiring
H = Earth
I = 0mA
J = 0v power
K = +20mA
L = +24V power

Turbine flow meter datasheet, Type One (RS Components)

EX-FLOW

Ex-Proof (ATEX II 2 G) Mass Flow Meters and Controllers for Gases

> Introduction

Bronkhorst High-Tech B.V., the European market leader in thermal Mass Flow Meters/Controllers and Electronic Pressure Controllers, has many years experience in designing and manufacturing precise and reliable measurement and control devices. With a wide range of instruments, Bronkhorst High-Tech offers innovative solutions for many different applications in many different markets. The instruments are made to customers' specification, in various styles, suitable for use in laboratory, industrial environment, hazardous areas, semiconductor or analytical installations.

> EX-FLOW series for hazardous areas

The Mass Flow Meters of the EX-FLOW series are of rugged design for gas flow applications in hazardous environments. The intrinsically safe measuring head is tested according to ATEX 95 Directive 94/9/EC and approved under EC-Type Examination Number: KEMA 01ATEX1172, protection II 2 G Ex ib IIC T4 Gb. This stands for:

II 2 G	= ATEX group and category
Ex ib IIC T4	= CENELEC marking
ib	= intrinsically safe Zone 1
IIC	= highest gas group with a minimum ignition energy of 20 µJ, with gases such as acetylene or hydrogen
T4	= max. surface temperature of 135°C
Gb	= IEC equipment protection level

The housing of the electronics compartment is rated to IP65. Mass Flow Meters can be supplied in ranges starting from 0,16…8 ml_n/min up to 11000 m^3_n/h air-equivalent, with pressure rating between vacuum and 700 bar. In combination with control valves, either integrated or separate, Mass Flow Controllers can be offered up to 10…500 m^3_n/h air-equivalent.

> Mass Flow Controllers for every application

The control valve can be furnished as an integral part of an EX-FLOW MFC, or as a separate component. It is a proportional, electromagnetic control valve with fast and smooth control characteristics. With reference to the specific field of application there are different series of control valves. There is a standard direct acting valve for common applications, a pilot operated valve for high flow rates and the so-called Vary-P valve with a pressure rating of 400 or 700 bar, that can cope with up to 400 bar ΔP. These valves will be equipped with explosion proof certified coils. There are two options:

Coil XB: protection II 1 G Ex ia IIC T6
protection II 1 D Ex ta IIIC T80°C

Coil XC: protection II 2 G Ex eb IIC T4
protection II 2 D Ex tb IIIC T130°C

The electrical connection of flow meter and control valve to the safe E-7000 readout system (located in the safe zone) is achieved via separate cables. The readout system contains a controller function pc-board to complete the control loop.

> General EX-FLOW features

- ATEX approval Cat.2, Zone 1
- weatherproof IP65 housing
- flow ranges from 0,16…8 ml_n/min up to 220…11000 m^3_n/h
- optional: low-ΔP versions up to 4…200 l_n/min
- pressure ratings up to 700 bar

> Fields of application

- Process gas measurement or control in (petro-) chemical industries
- Fuel cell technology
- Gas distribution systems
- Hydrogenation processes
- Gas consumption measurement for internal accounting
- Heating or biogas production

Bronkhorst®
HIGH-TECH

Air mass flow meter datasheet page 1, (Bronkhorst High-Tech, b)

> Technical specifications

Measurement / control system

Accuracy (incl. linearity)	: standard: ±1% FS;
(based on actual calibration)	other on request
	(for flow > 1000 m^3_n/h contact factory)
Turndown	: 1 : 50 (2 … 100%)
Repeatability	: < ±0,2% Rd
Time constant	: 5 seconds
Operating temperature	: EX-FLOW sensor: -10…+70°C;
	XB-coil: -40…+ 65°C
	XC-coil: -40…+ 65°C
Temperature sensitivity	: zero: < ±0,05% FS/°C;
	span: < ±0,05% Rd/°C
Leak integrity	: tested < 2 x 10^{-9} mbar l/s He
Attitude sensitivity	: max. error at 90° off horizontal 0,2%
	at 1 bar, typical N2
Warm-up time	: 30 min. for optimum accuracy;
	2 min for accuracy ± 2% FS

Mechanical parts

Material (wetted parts)	: stainless steel 316L or comparable
Process connections	: compression type or face seal couplings;
	wafer type on series F-106;
	DIN or ANSI flanges on series F-107
Seals	: standard: Viton®
	options: EPDM, FFKM (Kalrez®)
Ingress protection (housing)	: IP65

Electrical properties

Signal circuit	: in type of explosion protection intrinsic
	safety Ex ib IIC, only for connection to a
	certified intrinsically safe circuit with the
	following maximum values:
	Ui = 28 V, Ii = 98 mA, Pi = 686 mW
	The effective internal capacitance between:
	Terminals 1 and 3: Ci = 1 nF;
	Terminals 2 and housing: Ci = 120 nF;
	Effective internal inductance: Li = 0,3 mH
Output signal	: 15…20 mA (linear)
	Terminal connection, cable gland M16x1,5
XB-coil	: Coil voltage max. 28 V/110mA;
	295 Ohm at 20°C, cable gland PG9
XC-coil	: Coil voltage max. 24 V;
	65 Ohm at 20°C, cable gland M16x1,5;
	Pmax = 9W at 20°C

Technical specifications subject to change without notice.

Related drawing 9.27.002K. No modifications permitted without approval of authorised person.

> Models and flow ranges (based on Air)

Mass Flow Meters (MFM); PN100 (pressure rating 100 bar)

Model	min. flow	max. flow
F-110CX	0,16…8 ml_n/min	0,2…10 ml_n/min
F-111BX	0,2…10 ml_n/min	0,4…20 l_n/min
F-111AX	0,1…5 l_n/min	2…100 l_n/min
F-112AX	0,2…10 l_n/min	5…250 l_n/min
F-113AX	2…100 l_n/min	25…1250 l_n/min
F-116AX	0,4…20 m^3_n/h	4…200 m^3_n/h
F-116BX	1…50 m^3_n/h	10…500 m^3_n/h

For ranges of 200, 400 or 700 bar rated MFMs please contact factory

High-Flow MFMs; PN10 / PN16 / PN25 / PN40 / PN100

Model	min. flow	max. flow
F-106AX/F-107AX/F-117AX	0,4…20 m^3_n/h	4…200 m^3_n/h
F-106BX/F-107BX/F-117BX	1…50 m^3_n/h	10…500 m^3_n/h
F-106CX/F-107CX/F-117CX	2…100 m^3_n/h	20…1000 m^3_n/h
F-106DX/F-107DX/F-117DX	3,6…180 m^3_n/h	36…1800 m^3_n/h
F-106EX	8…400 m^3_n/h	80…4000 m^3_n/h
F-106FX	14…700 m^3_n/h	140…7000 m^3_n/h
F-106GX	22…1100 m^3_n/h	220…11000 m^3_n/h

Mass Flow Controllers (MFC); PN64 / PN100

Model	min. flow	max. flow
F-200CX/F-210CX	0,2…10 ml_n/min	0,2…10 ml_n/min
F-201CX/F-211CX	0,22…11 ml_n/min	0,4…20 l_n/min
F-201AX/F-211AX	0,1…5 l_n/min	2…100 l_n/min
F-202AX/F-212AX	0,2…10 l_n/min	5…250 l_n/min
F-203AX/F-213AX	2…100 l_n/min	25…1250 l_n/min
F-206AX/F-216AX	0,4…20 m^3_n/h	4…200 m^3_n/h
F-206BX/F-216BX	1…50 m^3_n/h	10…500 m^3_n/h

Contact factory for max. Kv-values (depending of coil type)

MFCs for high-pressure / high-ΔP applications; PN400

Model	min. flow	max. flow
F-230MX	0,2…10 ml_n/min	10…500 ml_n/min
F-231MX	10…500 ml_n/min	0,2…10 l_n/min
F-232MX	0,2…10 l_n/min	2…100 l_n/min

For ranges of 700 bar rated MFCs please contact factory

F-106AX Ex-proof Mass Flow Meter for high flow ranges

Bronkhorst®
HIGH-TECH

Nijverheidsstraat 1a, NL-7261 AK Ruurlo The Netherlands
T +31(0)573 45 88 00 F +31(0)573 45 88 08 I www.bronkhorst.com E info@bronkhorst.com

ISO 9001 ISO 14001

Air mass flow meter datasheet page 2, (Bronkhorst High-Tech, b)

Appendix C - Hydrocarbon Composition

This appendix presents the hydrocarbon composition and fluid properties of the hypothetical full-scale flow in chapter 5.

Component	Mole Fractions	Vapour Phase	Liquid Phase
Nitrogen	0,004	0,014	0,004
CO2	0,001	0,001	0,001
Methane	0,432	0,903	0,429
Ethane	0,047	0,045	0,047
Propane	0,030	0,016	0,030
i-Butane	0,015	0,005	0,015
n-Butane	0,009	0,003	0,009
22-Mpropane	0,000	0,000	0,000
i-Pentane	0,008	0,002	0,008
n-Pentane	0,005	0,001	0,005
n-Hexane	0,018	0,002	0,018
n-Heptane	0,041	0,002	0,041
n-Octane	0,050	0,002	0,050
n-Nonane	0,038	0,001	0,038
n-Decane	0,301	0,004	0,304
Total	1,000	1,000	1,000

Fluid Properties	Stream 1	Vapour Phase	Liquid Phase	Stream 1	Vapour Phase	Liquid Phase
Pressure[bara]	100	-	-	1,01325	-	-
Temperature[C]	100	-	-	15	-	-
Mass Density [kg/m3]	396,65	71,30	580,61	5,61	0,92	723,98
Viscosity [cP]		0,02	0,21		0,01	0,79
Phase Fraction [Act. Vol. Basis]	0,36	0,36	0,64	0,99	0,99	0,01
Phase Fraction [Mass Basis]	0,06	0,06	0,94	0,16	0,16	0,84